IMPROVEMENT ON THE MECHANICAL PROPERTIES OF BORON SUBOXIDE (B_6O) BASED COMPOSITES USING OTHER COMPOUNDS AS SECOND PHASE.

OLUWAGBENGA TEMIDAYO JOHNSON

A dissertation submitted to the Faculty of Engineering and the Built Environment, University of the Witwatersrand, Johannesburg, in fulfillment of the requirements for the degree of Master of Science in Engineering.

Johannesburg, 2008.

DECLARATION

I declare that this dissertation is my own unaided work. It is being submitted for the degree of Master of Science in Engineering to the University of the Witwatersrand, Johannesburg. It has not been submitted before for any degree or examination to any other university.

……...

Oluwagbenga Temidayo, JOHNSON

……. Day of …….. Year ……

ABSTRACT

The problem of low fracture toughness and the difficulties to densify has delayed the application of B_6O materials as superhard materials in the industry. Therefore, in this work, effort has been directed towards improving the fracture toughness and densification of these materials by incorporating suitable secondary phases and tailoring the microstructure to the desired properties.

Boron suboxide (B_6O) powder was synthesized from the reaction of amorphous boron and boric acid powders. The synthesized B_6O powder was hot pressed at 1900^oC and 50MPa. In addition to the pure B_6O material, composites with transition metals, transition metal oxides, transition metal borides and rare-earth metal oxides were prepared at 1850^oC. The microstructure, phase composition and properties of resulting materials were investigated.

A boride secondary phase was formed after sintering. Materials with densities higher than 95% theoretical density were achieved for the composites. Although the pure B_6O sample was brittle, fracture toughness of 7.6±1.1 MPam$^{0.5}$ was obtained for the B_6O+FeB composite.

This study gives a basis for optimizing the sintering additives with potentials for improving the hardness and fracture toughness of B_6O materials.

DEDICATION

I will bless the name of the Lord at all times; his praise shall continually be in my mouth, I sought the Lord; He heard me and delivered me from all my fears. For thou has been strength to the needy in his distress, a refuge and a shadow from the heat.

Indeed no man can choose the womb through which he comes to the world but every man can choose the tomb where he will be laid. If I could make a choice of the womb however, I would choose the same through which I came. This work is dedicated to my parents: Late Mr. Adetula & Mrs. Rachel Johnson. *For their love, care and understanding.*

.

ACKNOWLEDGEMENTS

Trust in the Lord with all your heart, and lean not on your own understanding; in all your ways acknowledge Him, and He shall direct your paths. To God is all the glory for the great things he has done for me. I have the greatest pleasure to express my profound gratitude and appreciations to the following persons who have contributed in one way or the other to the success of the study;

Professor I. Sigalas: For being the great facilitator and the channel through whom God used to make me undertake and complete this study at WITS University. Thanks for your fatherly love, financial assistance, moral support, effective supervision, words of encouragement and mentorship.

Dr. M. Herrmann: For efficient, expertise and useful comments, love and co-operations during the laboratory work, and the effective writing skills learned from you.

Dr. P.A Olubambi: I share my dream of academic greatness with you seven years ago, and you believed it. You spoke of my dream to the kings, and today it is a reality! I have realized that man can only give awards, but only God rewards adequately. God will reward you.

I wish to appreciate **Mr. K. Katuku** for his assistance in getting good SEM images, **Mr. A. Andrews** for his contribution to knowledge.

I sincerely and deeply appreciate the efforts and love of Pastor Gbenga Ojo, Pastor Titilayo Ojo, Pastor Mike, Pastor E.A. Adeyemi, Pastor Peter Ayodeji, Pastor Bode Akindele, Dr. D.K. Olukoya and Bro Gbile Akanni for impacting my life so much.

Special thanks to all my senior friends; Mrs. F. Omoya, Mr. James Adewunmi, Mr. Afolabi, Mr. & Mrs. Adeleke, Mr. Akinyemi, Mr. David, Mr. Chris Idibie, Mrs. Abe, Mrs. Olubambi, Mr. Ogunniyi, Mr. Bada, Mr. Saka, Mr. Albert and the Ilemobades for the sweet fellowship, love, courage, prayers, words of exhortations and encouragements. You really made me feel at home during my study.

The list of my friends is unending; postgraduate students in the School of Chemical and Metallurgical Engineering, DFC members, SWGC members, Genius camp tutorial college, Periscope Academy, Universal Success Academy (USA), NCCF Obudu, RCF FUTA and so on. Truly, a man's friend gives an indication of his end!

My profound gratitude goes to the family of Arowolo, Abikenlu, Omitogun, Badru, Aregbesola and Ogunmuyiwa including Uncle Bash for their encouragement and support in all areas. The prayers of my brother and sister: Rotimi and Shade Johnson are not forgotten. It has been highly helpful. The members of the Area Family; Enoch Ogunmuyiwa , Modupe Dosunmu, Bukky Asiru & Titilayo Adebere always constant.

Finally, the support of the DST/NRF Centre of Excellence in Strong Materials (CoE-SM), Financial Aid Office of the University of the Witwatersrand and Element Six (Pty) Ltd – Diamond Research Laboratory towards this research is hereby acknowledged.

TABLE OF CONTENTS

LIST OF FIGURES

LIST OF TABLES

LIST OF SYMBOLS

SEM	=	Scanning Electron Microscopy
EDX	=	Energy Dispersive X-ray Spectroscopy
TEM	=	Transition Electron Microscopy
XRD	=	X-ray diffraction
ICSD	=	International Centre for Diffraction Data
ICP-OES	=	Inductively coupled plasma optical emission spectroscopy
Hv	=	Vickers hardness
K_{IC}	=	Fracture toughness
GPa	=	GigaPascal
MPa	=	MegaPascal
hr(s)	=	hour(s)
min(s)	=	minute(s)
μm	=	micrometers
wt%	=	Weight percent
^{o}C	=	degrees Celsius
K	=	degrees Kelvin

CHAPTER ONE

1.0 INTRODUCTION

Superhard materials are usually composed of light elements such as boron, carbon, nitrogen and oxygen. The intrinsically strong and directional covalent bonds of these light elements lead to tight, three-dimensional networks with extreme resistance to external shear (Duanwei *et al.,* 2002). This structure creates a unique combination of properties including low density, high hardness, high chemical stability and excellent wear resistance, which allows these materials to find extensive use as nozzles, pump impellers, grinding wheels, drill bit components, abrasives and cutting tools. Potential industrial applications have in recent years brought about intense studies of the physical and chemical properties of these materials.

Only diamond and cubic boron nitride have been used in the industry as superhard materials, due to their great hardness and structural stability when subjected to extreme external load. However, the application of diamond is somewhat limited at high temperatures owing to its instability, for example, as cutting tool for steel (Zerr, 2000). Also, as the temperature increases, diamond and cBN weaken due to the onset of the transformation to the graphite structure as well as due to diffusion wear. Furthermore, the dominant methods for the industrial synthesis of diamond and cBN materials require high pressures and temperatures, which render their manufacturing expensive and limit the sizes and geometric forms possible.

Boron suboxide (B_6O) has been of considerable scientific interest because it displays a range of outstanding physical and chemical properties. Recent investigation indicates that boron suboxide qualifies as a superhard phase, having an average Vickers hardness of 45 GPa (100g load) comparable to that of diamond (H_V = 70-100GPa) and cubic boron nitride (H_V = 60 GPa) (Zhongwu *et al*., 2005, Itoh *et al*., 1998). In addition to this hardness, the fracture toughness of this material (B_6O single crystal) was found to be 4.5 MPa.$m^{1/2}$, which approaches that of single crystal diamond at 5 MPa.$m^{1/2}$ (Duanwei *et al.,* 2002) and is significantly better than that of single crystal cubic boron nitride at 2.8 MPa.$m^{1/2}$ (Brookes, 1986).

These properties proved that this material (B_6O) is a good candidate for cutting tool and other applications where abrasive wear resistance is important. Moreover, unlike both diamond and cBN, boron suboxide (B_6O) bulk powders may be produced without the need for high pressures using cheap starting materials (boron and boron oxide) (Duanwei *et al.,* 2002). For these reasons and because of the need to replace or complement expensive diamond and cubic born nitride in many other applications, boron suboxide has been of technological interest.

1.1 JUSTIFICATION OF THE STUDY

B_6O powder can be produced at low pressure in an argon atmosphere by reducing B_2O_3 with B or by oxidation of boron with zinc oxide or other oxidants. However, it has been established that boron suboxide powders formed at or near ambient pressures are generally oxygen deficient (B_6O_x, $x<0.9$). They also have poor crystallinity and very small grain sizes. High pressure applied during the synthesis of B_6O can significantly increase the crystallinity, oxygen stiochiometry, and crystal size of the materials produced (Hubert *et al*., 1998).

In addition, it is very difficult to sinter B_6O powders to full density, but a careful selection of additives in combination with controlled sintering conditions could result in the production of B_6O materials having unique combination of mechanical properties for industrial applications. Hot pressed B_6O materials have not produced a combination of good mechanical properties, having hardness values between 30 and 38 GPa (Holcombe *et al*., 1972; Goosey, 1974; Bairamashvili *et al*., 1979), but the fracture toughness measurements were not reported. Promising mechanical properties, especially fracture toughness, for hot pressed B_6O materials, have only been reported by Kayhan *et al*. (1999). This author made sintered B_6O compacts under *vacuum* through hot pressing and found good hardness (37 GPa) and fracture toughness (6.2 $MPa.m^{1/2}$) values but the samples had a high amount of porosity (7.5 or more), which resulted in materials with low strength values [50-80MPa]. Also, the diameter for the notch used to measure the fracture toughness was 0.4mm, which renders the values reported for that property very suspect.

Studies were made by Itoh *et al*. (2000) to improve the mechanical properties of B_6O materials by introducing other hard materials, like B_4C and c-BN as a binder in the materials. Maximum micro hardness $Hv_{0.1}$ of 46 GPa was obtained from B_6O-30vol% B_4C sintered composite under the sintering conditions of 4 GPa, 1700^oC and 20 minutes. The fracture toughness was approximately 1 $MPa.m^{1/2}$. The fracture toughness of the B_6O-x-cBN composites increased as the cBN content increased; the maximum fracture toughness (1.5-1.8 $MPa.m^{1/2}$) was observed for x=40-60 vol%. Slight crack deflection along the B_6O-cBN grain boundary contributed to the increase of this property.

The composition of the grain boundary phase and the grain sizes of the phases in the sintered material are the main features in the microstructure that influence the mechanical properties of the material, especially fracture toughness. The presence of secondary phases in the sintered compacts allows the activation of toughening mechanisms such as crack bridging and crack deflection. This is assumed to occur because of mismatch in thermal expansion between the grain boundary phases and the B_6O phases, which places the grain boundary and the grains under residual stress (Shabalala T.C (2007), Peterson, I.M. and Tien, T.Y (1995)). In some of the B_6O sintered composites investigated, the sintering additives acted as liquid phase at sintering temperature which could have an added the advantage of lowering the sintering temperature, rate of grain growth and the cost of production and hence a finer grain size could be obtained. This results in a material with higher hardness, strength and wears resistance (Shabalala T.C (2007), Kayhan *et al*. (1999)). This research work is therefore aimed at improving the mechanical

properties, especially fracture toughness of B_6O-based composites by incorporating suitable secondary phases.

1.2 AIM AND OBJECTIVES

The primary aim of this research work is to produce hard and tough B_6O-based materials using different compounds from Fe-Cr-Co-B-O systems and rare- earth metal oxides (Sc_2O_3, La_2O_3 and Yb_2O_3) as the secondary phases. The aim would be achieved through the following objectives:

1. Synthesizing and characterising submicron boron suboxide powder.
2. Sintering and densifying submicron boron suboxide powder with and without additives using hot pressing technique.
3. Evaluating the mechanical properties of B_6O-based composites in terms of hardness and fracture toughness of the micrometer grained-sized materials.

1.3 SCOPE OF RESEARCH

The approach to this work involves using the benefit of existing technology in the literature to synthesize B_6O powder by mixing amorphous boron (B) and boric acid (H_3BO_3) at a suitable molar ratio, and heating in a tube furnace under argon atmosphere. The synthesized powder will then be milled into the submicron grain size and characterized in terms of phase composition, particle size distribution and grain morphology. B_6O materials will be made by mixing different additives in the form of Fe, FeO, FeB, Cr, CrO_3, Co, Sc_2O_3, La_2O_3 and Yb_2O_3 with B_6O powder. The pure B_6O powder as well as mixed powders will then be characterized and hot pressed. The

sintered compacts and composites will be analyzed in terms of densification, phase composition, microstructure as well as mechanical properties.

1.4 CONTRIBUTION TO KNOWLEDGE

The research studies into the improvement on the mechanical properties of boron suboxide (B_6O) based composites using transition metal compounds as secondary phase using the proposed methodology are expected to:

1. Provide information on the hardness-to-toughness relationship of B_6O-based composites.
2. Provide information on the suitability of these sintering additives in the stability of B_6O-based composites.
3. Provide information on the toughening mechanism of B_6O-based composites when second, minority phases are present.
4. Enhance the potential for industrial applicability of B_6O-based materials.

1.5 STRUCTURE OF THE DISSERTATION

A literature review of the work done on potential superhard compounds, followed by the latest studies on the *structure, synthesis, properties and applications of* Boron suboxide (B_6O), while concluding on the toughening mechanism of ceramic material is presented in **Chapter Two**.

Chapter three gives a detailed discussion of the starting materials used, together with experimental equipments and techniques.

In **chapter four** the results of all the experimental work and analysis carried out are given. The relationship between the microstructure and properties of the produced B_6O materials is discussed in **chapter five**, including the comparison to B_6O materials fabricated in other studies.

The dissertation ends in **chapter six** with the conclusions drawn from the work and stating recommendations for future work.

CHAPTER TWO

2.0 LITERATURE REVIEW

The search for superhard materials is driven by both the scientific curiosity of researchers to explore the possibilities of synthesizing a material whose hardness could approach or even exceed that of diamond and the technical importance of hard and superhard materials for wear resistant applications such as machine cutting tools and wear parts.

The aim of this literature survey is to give a review on the progress made on the development of synthetic superhard material with more attention given to Boron suboxide (B_6O). The review will first highlight the work done on potential superhard compounds, followed by the latest work done on the *structure, synthesis, properties and applications of* Boron suboxide (B_6O), while concluding on the toughening mechanism of ceramic material.

2.1 POTENTIAL SUPER HARD COMPOUNDS

Superhard materials are always required in modern technology because of their high hardness and mechanical/ chemical stability particularly when used as cutting tools, dies, molds or protective coatings. The higher the mechanical properties of the work piece materials become, the harder the tools for cutting them should be (Hideaki Itoh, 2004). This relationship accelerates the demand to develop new superhard materials, which can be used under severe working conditions at high cutting speeds, high temperatures and highly corrosive environments.

Hardness is related to permanent plastic deformation after indentation. Many phenomena are involved in this process: resistance to the volume compression produced by the pressure created by the indenter, resistance to shear deformation, resistance to plastic yield due to the production and motion of dislocations. These different types of resistance to deformation indicate the conditions that a material must fulfill to be hard. The material must first support the volume decrease created by the applied load. This is equivalent to stating that the bulk modulus (the inverse of the compressibility) should be high. The next condition is that a stress in a given direction should not be transmitted along a different direction: therefore the shear modulus must also be high (Jean-Michel & Julian Haines, 1997). These two conditions have guided the choice for selecting potential hard materials and in particular, the search for high bulk modulus compounds.

Potential hard materials are composed of atoms linked by short bonds, which correspond to small atoms of the light elements: B, C, N, O, and Si. The shortest bond found in a solid network is the C-C bond in diamond; shorter bonds are found in isolated molecules, which are linked by weak Vander Waals interactions to form solids, which have very low bulk moduli and are not hard. The next shortest bond is B-N and, actually, cubic boron nitride is the second- hardest material known.

Up to the present, much attention has been focused on the C-N bond which is slightly shorter than the C-C bond in diamond. Over the past several years, the search for C_3N_4 has been conducted, fueled by theoretical prediction (Cohen *et al.,* 1997) which were initially based on the analogy with the known homologue β-Si_3N_4 (Cote M and Cohen

M.L, 1997, Teter D.M and Hemley M.J 1996, Sung C.M and Sung M, 1996). The calculated bulk moduli of hypothetical carbon nitride phases including β-C_3N_4 are close to that of diamond and may exceed its value. This is not true for their shear moduli and hardness because their properties deviate from the optimum found for diamond in all respects. There have been reports of the preparation of thin films containing β-C_3N_4 (Chen *et al.,* 1997). Nanoindentation tests have been performed on non-stoichiometric carbon nitride films and carbon nitride/TiN composite coatings yielding hardness values of 8-35 GPa and 45-50 GPa (Li *et al.,* 1995), respectively. It should be noted that these materials are much more difficult to prepare than diamond and would pose the problem of carbide formation and nitrogen dissolution into the work piece if they were to be used to machine ferrous metals.

Considering the Si-O bond, this is slightly longer than the C-C bond in diamond. Many compounds with Si-O bonds are known; in particular silica (SiO_2) with its numerous polymorphs in which the Si-O bonds are 1.61Å long. These compounds have low bulk moduli and are not hard because their structures are made up of corner-linked SiO_4 tetrahedra which can easily tilt. However, these tetrahedral considered alone are very hard: from single-crystal diffraction studies, it was concluded that the trihedral bulk modulus of SiO_4 was higher than 400 GPa (Hazen R.M and Finger L.W 1982). Above 9 GPa, a high- pressure phase of silica is obtained, stishovite; it is about 60% more compact than quartz due to a dense packing of octahedra: the arrangement of the oxygen atoms around a silicon atom has changed at the transition from a tetrahedron with four oxygen nearest neighbours around the silicon atom to an octahedron with six oxygen

nearest neighbours. Recent indentation hardness tests showed stishovite has the highest hardness, H= 33 GPa (load not stated) (Leger *et al.,* 1996) of any well –characterized oxide, the hardness of corundum being only 21 GPa.

In 1999, a new high-pressure phase of silicon nitride having a cubic spinel structure, denoted as $\gamma - Si_3N_4$ or $c - Si_3N_4$, was first synthesized (Zerr et al., 1999). It was reported that $c - Si_3N_4$ shows excellent thermal (meta) stability in air, which is superior to that of other superhard materials, such as diamond, c-BN, c-BC_2N, SiO_2-stishovite, B_4C, or B_6O. The vickers hardness of $c - Si_3N_4$ sintered in a multianvil apparatus was reported to be between 33 and 37 GPa, which approaches that of SiO_2-stishovite but is significantly below that of diamond and c-BN.

Other possible candidates for compounds harder than diamond are the carbides of titanium and silicon. Under normal conditions, TiC and SiC are already hard (H=26 and 28 GPa, respectively). A transition to a more compact structure under high pressure was observed in SiC (Yoshida *et al.,* 1993). This cubic, NaCl-type structure with silicon and carbon in sixfold coordination, could thus be superhard. The major drawback is that the transition occurs at a very high pressure of above 100 GPa.

Solid materials composed of light elements such as B, C, N and O are known to have superhardness, and more superhard and tough materials are expected to be synthesized by their combinations. Fig 2.1 illustrates a map of such materials in the phase diagram of the B-C-N-O system. Boron-rich materials, B_4C, B_6O and B_6P have bulk moduli of close to

200 GPa. All these boron compounds are in fact built from boron icosahedra, as in elemental boron, with a few additional intericosahedral chain atoms, and their hardness of about 29-30 GPa is similar to that of pure boron.

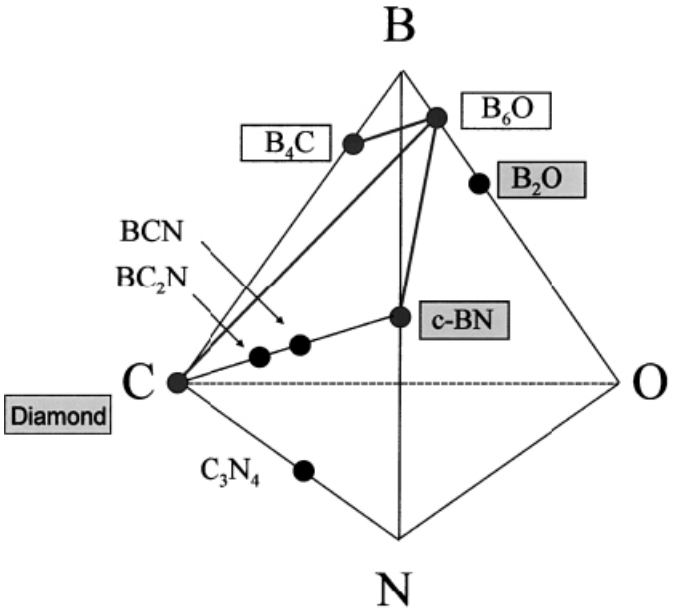

***Fig2. 1**: Map of superhard materials in the phase diagram of the B-C-N-O system.*
(Hideaki Itoh, 2004).

The first report of the deposition of the ternary BC_xN_y films by thermal CVD was by Badzian *et al.*, (1988) who also used microwave plasma for this process and obtained deposits with a cubic modification as was seen by x-ray diffraction achieving hardness between 4 and 33 GPa depending on the deposition conditions. More recently Riedel *et al.,* (1999) prepared superhard BC_4N coatings by plasma CVD from single source organometallic precursors, pyridine borane ($C_5H_5NBH_3$) and triazaborabicyclodecane [$BN_3H_2(CH_2)_6$]. The highest hardness of 64 GPa, which was reported by these researchers, clearly shows that the B-C-N triangle is worthy of further detailed study.

Solozhenko *et al.,* (2001) synthesized cubic BC_2N phase with diamond-like structure at pressures above 18 GPa and temperatures higher than 2200K using a laser heated diamond-anvil cell (DAC) and a multi- anvil press. The lattice parameter of c-BC_2N determined by these authors at ambient conditions was 3.642(2) Å, which is larger than those of diamond and c-BN. Vickers hardness measurement of c-BC_2N under a load of 2N was reported to be 76GPa, which is higher than that of c-BN single crystal and rivals that of diamond.

Dubrovinskaia *et al.,* (2007) reported on the synthesis of unique superhard aggregated boron nitride nanocomposites (ABNNCs) showing the enhancement of hardness up to 100% in comparison with single crystal c-BN. Such a great hardness (85 GPa) was explained to be the unique combination of two factors: (1) nanosize effect, which restricts dislocation propagation through the material, and (2) two-phase composition on nano-and subnanometer scales, which, due to the quantum confinement, increases hardness of individual crystallites. It makes ABNNC the first non-carbon-based bulk material with hardness higher than that of PCD and approaching that of single crystal and nanocrystalline diamonds and aggregated diamond nanorods.

Badzian *et al.*, (1988) reported on superhard boron suboxide $B_{22}O$ which "easily wore the (001) surface of diamond and scratched the (111) face. The material was prepared by solid-state reaction from a stoichiometric mixture of boron and B_2O_3 at 1600-2000^oC. The reported hardness was about 60 GPa.

Stoichiometric high-pressure-temperature phases of B_2O have been prepared and described by Hall and Compton (1965) and Endo *et al.,* (1987). In the former study, a graphite-like B_2O compound was synthesized by the reduction of B_2O_3 with B or Li and by the oxidation of B with $KClO_3$. The preparation was carried out within the pressure and temperature ranges of 5.0 GPa to 7.5 GPa and 1200^o to 1800^{o}C. The B_2O synthesis of Endo *et. al.,* (1987) was carried out by reacting BP with oxygen derived from the thermal decomposition of CrO_3 to CrO_2 at pressures of 3.5 to 5.5 GPa in the temperature range 1000^o to 1200^{o}C. The recovered B_2O high-pressure phase appeared to have a diamond-like structure and was characterized by Vickers microhardness (100-g load) of 40.5 GPa.

Recently, a microhardness of 45 GPa (100g load) was measured for boron suboxide single crystals, which is closely rivaling that of cubic boron nitride (Duanwei *et al.,* 2002). In addition to this hardness, the fracture toughness of this material (B_6O single crystal) was found to be 4.5 $MPam^{0.5}$. These properties proved that this material (B_6O) is a good candidate for cutting tool and other applications where abrasive wear resistance is a desirable property.

2.2 BORON SUBOXIDE COMPOUNDS

Boron normally has a valence of 3 and reacts with oxygen to form boron oxide having the stoichiometric formula B_2O_3. Under suitable conditions, boron may react with oxygen and forms compounds in which boron exhibits a valence less than 3. Powders of nominal compositions B_2O, B_3O, B_4O, B_6O, B_7O, B_8O, $B_{10}O$, $B_{12}O$,$B_{13}O_2$, $B_{15}O$, $B_{18}O$, $B_{20}O$ and

$B_{22}O$ have been reported as being formed by reacting elemental boron (B) with boron oxide (B_2O_3) under suitably high pressure and temperature conditions (Hayashi *et al.,* 1992).

Boron suboxide, B_7O, was first reported by Weintraub (1909), who prepared this material by the reduction of B_2O_3 and determined its composition by chemical analysis. Pasternak (1959) and Holcombe (1972) further confirm the existence of this compound by reducing zinc oxide with boron at a temperature adequate to effect the reduction reaction. After this, B_2O with a diamond-like structure was synthesized through the reaction of BP with oxygen, which was supplied by the thermal decomposition of CrO_3 into CrO_2 (Endo *et al.,* 1987, Hall and Compton 1965). Other boron suboxides; $B_{13}O_2$ (Kharlamov *et al.*, 2002), $B_{12}O_2$ (Brodhag and Thevenot 1986, Rizzo *et al,* 1960), $B_{13}O$ (Novak 1972) $B_{22}O$ (Badzian *et al.*, 1988) were synthesized by chemists, but firmly established formulae and structures were still lacking up until 1990s. After Badzian *et al.*, (1988) pointed out that boron suboxide can be a superhard material, scientists began to pay more attention to these borides.

Boron suboxide (B_6O), with high hardness, was for the first time prepared by Badzian in 1988. After synthesizing B_6O by means of reactive hot pressing of boron and B_2O_3, he melted the suboxide in an induction furnace, in an inert atmosphere of argon, and characterized its structure and properties. The melted material was found to be black in colour with polycrystalline morphology. X-ray diffraction analysis performed on the melt showed the crystallographic structure of the grains to resemble β-rhombohedral boron.

2.2.1. STRUCTURE OF BORON SUBOXIDE

Boron and boron rich compounds are attractive systems because of their unique structure, high hardness, high melting point and low density values. Their strong and short covalent bonding provides the basis for a wide range of distinctive refractory, thermoelectric and optical properties.

Boron, which has a valence of 3, exhibits a number of different compositions and structures arising from the specific electronic nature of its atom. Unpaired electrons possessing three bonding functions provide the possibility of forming a series of electronic configurations of different stabilities. The most important and the most common is the icosahedron (a regular polyhedron with 20 triangular faces), formed from 12 B atoms, which exhibits cubic symmetry (G. L. Gal'Chenko *et al*., 1977).

In addition to the crystalline forms of α and β rhombohedral and α and β tetrahedral boron, an amorphous form also exists. The temperature, pressure and reactants present during formation determine which phase will result. Each phase exhibits different chemical and physical characteristics. Amorphous boron, which is deposited at low temperatures, tends to be fine-grained and most reactive. As the temperature rises during deposition, the first crystalline material to form is α-rhombohedral followed by the formation of β-rhombohedral. Tetragonal modifications are generally formed at intermediate temperatures when impurities are present (G. L. Gal'Chenko *et al*., 1977).

Thermodynamically, the most stable form of boron is its β-rhombohedral phase, which possesses a complicated but loosely packed crystal structure composed of B_{12} icosahedra

(Badzian *et al.*, 1988). Studies have been performed for the densification of this stable but loosely packed structure and up until now only one approach, based on the creation of interstitial structures (and consequent formation of interstitial bonds), has been found successful (Badzian *et al.*, 1988). Oxygen atoms dissolving in this electron deficient β-rhombohedral boron structure can be considered a good example for this type (interstitial) of bond formation (Kayhan and Inal, 1999).

The structure of boron suboxide (B_6O) is built of eight icosahedra at the apexes of the rhombohedral unit cell (space group $R\bar{3}m$) (H. Hubert *et al.,* 1998, Duanwei *et al.,* 2002). The structure can be viewed as a distorted cubic close packing (ccp) of B_{12} icosahedra. Two oxygen atoms are located in the interstices along the [111] direction (fig 2.2). The O-O distance of 0.307nm precludes direct O-O bonding (M. Kobayashi *et al.,* 1993).

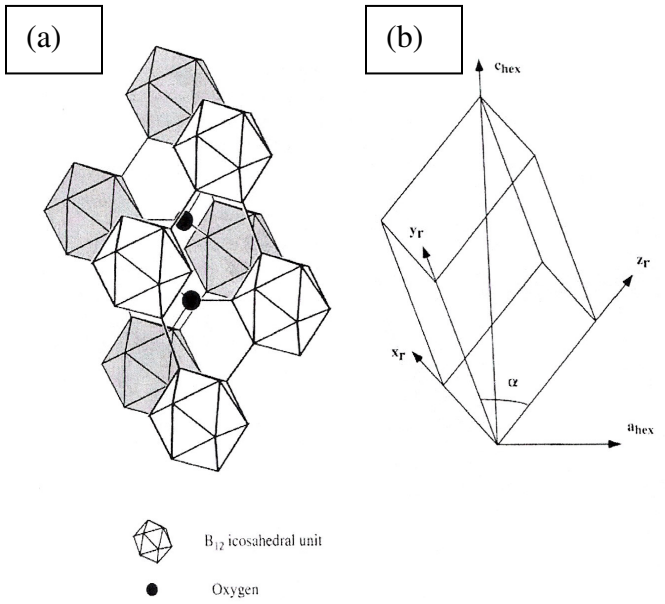

Fig2. 2*: (a) The structure of nominal B_6O with space group $R\bar{3}m$, derived from the α-rhombohedral structure of elemental boron with eight (slightly distorted) B_{12} icosahedra at the apices of the rhombohedral unit cell.*

*(b) An outline of the rhombohedral unit cell with the rhombohedral (x_r, y_r, z_r) and hexagonal (c_{hex}, a_{hex}) axes shown. The base of the rhombohedron defines a tetrahedral figure in which the angle α may be distorted from the ideal value (70.5^o), depending upon the ratio c_{hex}: a_{hex} (*H. Hubert *et al.,* 1998*).*

2.2.2 SYNTHESIS OF BORON SUBOXIDE

Though several techniques have been previously employed for producing boron suboxide, there are two (2) general methods which have gained wide application:

Firstly, the high temperature solid-liquid reaction shown below between amorphous boron (B) and boric oxide (B_2O_3), under argon atmosphere at different temperatures ranging from 1100°C to 2200°C with reaction time between 1 to about 12 hours results in

the formation of boron suboxide (H. Itoh *et al.*, 1998, H. Hubert *et al.*, 1998, F. Goosey 1974, I. O. Kayhan and O. T. Inal 1999, T. Lundstrom and Y.G. Andreev, 1996, D. He *et al*., 2002, T. Lundstrom, 1997)

$$16B_{(S)} + B_2O_{3(L)} \rightarrow 3B_6O_{(S)} \qquad \text{..... (2.1)}$$

The molar ratio of B: B_2O_3= 16:1.03 is used with a slight excess amount of B_2O_3 in comparison with the molar ratio of the stoichiometric reaction, to compensate for the small amount of B_2O_3 that evaporate during the synthesis. Furthermore, while the B_2O_3 starting material is assumed to be essentially pure, it has been found that if the elemental boron used as starting material is less than 95% pure, a B_6O material which is harder than previously reported in the literature can be formed (Hayashi *et al.,* 1992). They claimed that the impure B contained about 6% Mg, which serves as sintering aid for the B_6O and improves the hardness of the final material. An alternative method of producing B_6O of high hardness is to use pure raw materials and separately add a suitable quantity of the desired sintering aid. Other materials such as Ca and Y (Hayashi *et al.,* 1992) are also expected to act as sintering aids.

Secondly, boron suboxide powder may be produced by the reduction of metal oxides, usually ZnO (Holcombe, Jr. *et al*., 1972, C. Brodhag and F. Thevenot 1986, X. Liu *et al.,* 1995) or other oxidants like MgO, SnO, CdO, In_2O_3, CuO and $Li_{12}B_4O_7$ (T. Lundstrom and Y.G. Andreev, 1996) with boron under argon atmosphere to a temperature range of 1200^{o}C- 1600^{o}C. The chemistry of the reaction is generally given as:

$$B + MO \rightarrow B_X O + M \quad \text{.................................... (2.2)}$$

Liu *et al.,* (1995) synthesized boron suboxide B_7O by the oxidation of boron with an excess of zinc oxide ZnO under a pressure of 3.5 GPa and a temperature of 1200^oC, according to the following reaction;

$$7B + ZnO \rightarrow B_7O + Zn \quad \text{............................. (2.3)}$$

It was observed that this route produces a single phase product of B_7O, as compared with other routes which give a mixture of boron suboxide B_7O with either boron or boron oxide B_2O_3. Also, the zinc (melting point of 419^oC) produced in the course of synthesis is beneficial in bringing about the complete solid state reaction. Although there are many oxidizing agents used in high pressure and high temperature experiments, such as CrO_3, $KClO_3$, MgO, Ga_2O_3 etc., these authors chose ZnO to avoid working with a gas at high pressure and high temperature.

$$4CrO_3 \rightarrow 2Cr_2O_3 + 3O_2 \uparrow \quad \text{............................ (2.4)}$$

$$2KClO_3 \rightarrow 2KCl + 3O_2 \uparrow \quad \text{........................... (2.5)}$$

With each of these procedures there are attendant shortcomings or drawbacks which detract from the usefulness of the procedure in the production of B_6O. For example, one of the more successful procedures involves the reduction of molten B_2O_3 with boron, but the high volatilization and vapour pressure of this oxide at the reaction temperatures of 1200^0- 1500^{0}C respectively increase the likelihood of producing non-stoichiometric B_6O. Also, the molten B_2O_3 reacts with the metal or ceramic reaction vessel and thereby contaminates the B_6O. With respect to other known procedures, the reduction of B_2O_3

with magnesium produces a solid solution of magnesium boride contaminants in the suboxide while the reduction of magnesium oxide with boron produces only a relatively small yield of B_6O.

In U.S. Patent No. 3,816,516 (Goosey), a method of fabricating boron suboxide products is disclosed. According to this patent, a mixture of elemental boron and boron oxide is cold pressed in a tantalum lined metal die. After the pressure on the compacted mixture was released, it was coated with a mixture of boron nitride and boron oxide, and was subjected to a second pressing step while heating at a temperature sufficient to melt the boron oxide in the compacted mixture. This was followed by a cooling step and another hot pressing step. The boron suboxide product made by this method was reported as being smooth, sound article, free of flaws and contaminations, and suitable for a variety of applications, e.g., cutting tools, ceramic bearings, and grinding media. Upon, analysis, the boron suboxide product gave 80.1*wt%* boron and 19.9*wt%* oxygen which corresponds to the stiochiometry of B_6O.

2.2.2.1 LOW PRESSURE- HIGH TEMPERATURE TECHNIQUE

Although the synthesis of boron suboxide (B_6O) at or near ambient pressure comes with the advantage of reduced cost of production and avoids the risk of working with gases at high pressure, it leaves an open the possibility of forming a non-stoichiometric B_6O compound, generally oxygen deficient (B_6O_x, $x < 0.9$) and having poor crystallinity and very small grain size (less than 5 μm). Hence, the chemical formula for boron suboxide

was commonly expressed as B_6O_x, where $x \leq 1$. (Duanwei *et al.,* (2002), P.F McMillan *et al*., (1999), L.A.J Garvie *et al.,* (1997)).

Studies were made by M.Olofsson and T. Lundstrom (1997) to understand the synthesis and structure of this non-stoichiometric B_6O. The powder was synthesized from a mixture of amorphous boron or α-rhombohedral boron and B_2O_3 in excess. They found that the use of α- boron resulted in a more completely crystallized boron suboxide, which was utilized to study the homogeneity range of the suboxide in the temperature range 1250°C- 1450°C. The oxygen content of solid was determined from Rietvelt analysis of X-ray powder diffraction intensities. These authors claim that the oxygen concentration in solid B_6O decreases with temperature in the range 1250°C- 1450°C as anticipated (Fig 2.3). The cell dimensions, occupancy of the 6c position by oxygen and some interatomic distances are shown Table 2.1 for materials prepared at different temperatures and presumably not too far from equilibrium. At temperatures lower than 1250°C it was progressively more difficult to reach equilibrium, since the reaction rate decreases.

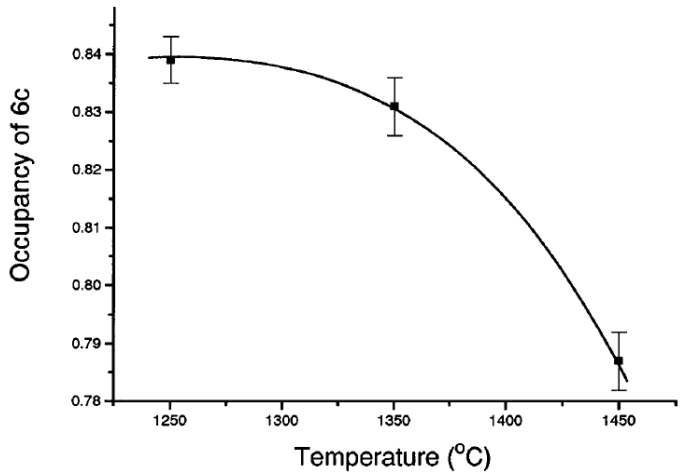

Fig2. 3: *Oxygen content (occupancy of position 6c) of B_6O vs. temperature*. (Olofsson and Lundstrom (1997)

They concluded that stoichiometric B_6O cannot be prepared using oxygen at ambient pressure. The cell dimensions of B_6O material reported at high pressure/ high temperature conditions were a = 5.435Å and c = 12.415 Å, (X.Y. Liu et al., 1995) which was substantially larger than the values shown in Table 2.1.

Table 2.1: *Crystallographic Data for Boron suboxide sample*

Sample, comp.	*a* axis (Å)	*c* axis (Å)	Temp. (°C)	Occup. of pos. 6*c*	Dist. (Å) O(1)–O(1)	Dist. (Å) O(1)–3B(1)
B_6O_{1-x}						
I, $B_6O_{0.79}$	5.3824(4)	12.322(1)	1450	0.787(5)	3.007(5)	1.463(1)
II, $B_6O_{0.83}$	5.3761(7)	12.326(3)	1350	0.831(5)	3.025(5)	1.476(1)
III, $B_6O_{0.84}$	5.3774(7)	12.322(3)	1250	0.839(4)	3.004(5)	1.476(1)

Lundstrom and Andreev (1996) also confirmed in their earlier work that B_6O contained a high concentration of vacancies at the oxygen positions, with compositions ranging from $B_6O_{0.72}$ to $B_6O_{0.86}$. The consistency of this result might be difficult because of the variation of the B source for sample I, II and III and the difference in the temperature conditions used.

2.2.2.2 HIGH PRESSURE- HIGH TEMPERATURE TECHNIQUE

With the goal of synthesizing boron suboxide with improved purity, crystallinity and less oxygen- deficiency (i.e., closer to the nominal B_6O composition), scientist began to explore the high pressure technique.

H. Hubert *et al.,* (1998), synthesized B_6O at high pressure and high temperature using a Walker-type multianvil apparatus. The pressure medium consisted of a cast MgO octahedron and force was applied by eight tungsten carbide cubes with corners truncated

to triangular faces. The cell assembly is illustrated in fig 2.4. Amorphous boron (B) was mixed with B_2O_3 and the samples were pressurized between 1 to 10 GPa at 1200^oC - 1800^oC.

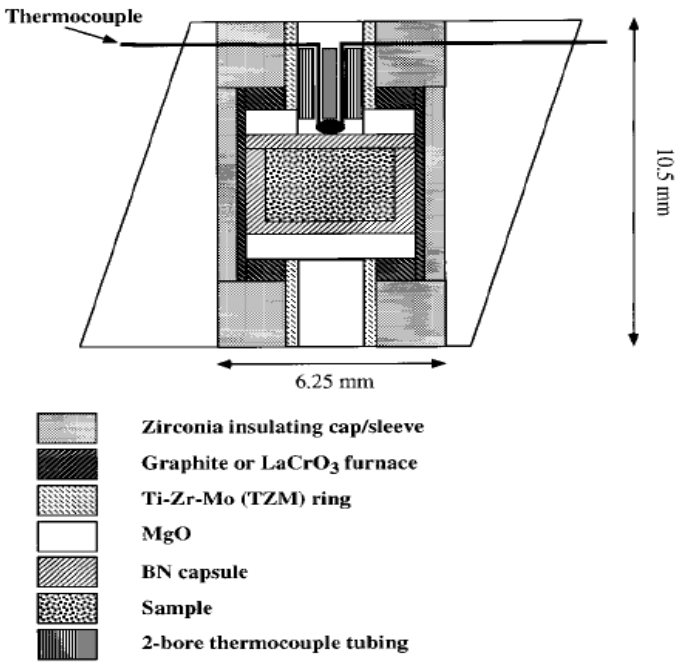

Fig2. 4: *Cell assembly containing the B and B_2O_3 mixture, used for the synthesis of B_6O at high pressure. This assembly is placed at the center of MgO octahedron to which pressure is applied isostatically.* (H. Hubert *et al.*, 1998)

Their best materials were obtained from a starting mixture containing an excess of B_2O_3 reacted at 1700^oC, between 4 and 5.5 GPa. After the products were washed in water, well- crystallized single-phase product dominated by icosahedrally twinned particles to 30 µm in diameter was easily recovered. Oxygen occupancies ascertained from Rietvelt refinements showed data consistent with the chemical compositions determined by Parallel electron energy- loss spectroscopy (PEELS). The highest oxygen occupancy, $B_6O_{0.96}$, was obtained for the micrometer- size icosahedral particles prepared. The refined

hexagonal cell parameters and oxygen occupancies for B_6O_{1-x} are given in Table 2.2 along with published data.

Table 2.2: *Cell parameters for some selected B_6O materials (Space group, $R\bar{3}m$, hex. axes)*

Compound	$\mathbf{a_h}$ (Å)	$\mathbf{c_h}$ (Å)	$\mathbf{c_h}$: $\mathbf{a_h}$	**V**(Å ^{3})	**O-occup. (XRD)**	**Prep. Method**	**Reference**
$B_6O_{0.72}$	5.361(1)	12.340(1)	2.301	307.44	0.72[a]	Amb. P.	Lundstrom and Bolmgren (1994)
$B_6O_{0.76}$	5.367(1)	12.328(2)	2.297	307.53	0.76 [a]	Amb. P.	M. Kobayashi *et al.*, (1993)
$B_6O_{0.77}$	5.3696(4)	12.3258(6)	2.295	307.77	0.77	Amb. P.	H. Hubert *et al.*, (1998)
$B_6O_{0.78}$	5.3824(4)	12.322(1)	2.289	309.15	0.787 [a]	Amb. P.	Lundstrom and Andreev (1996)
$B_6O_{0.839}$	5.3761(7)	12.326(3)	2.293	308.52	0.839 [a]	Amb. P.	Lundstrom and Andreev (1996)

$B_6O_{0.89}$	5.3872(1)	12.3152(3)	2.286	309.53	0.89	5.5 GPa 1800°C	H. Hubert *et al.,* (1998)
$B_6O_{0.95}$	5.3902(2)	12.3125(4)	2.284	309.78	0.95	5.5 GPa 1700°C	H. Hubert *et al.,* (1998)
B_6O_x	5.395	12.342	2.288	311.10	-	hot P.	H. F. Rizzo *et al.,* (1962)
B_6O_x	5.435	12.415	2.284	317.60	-	3.5 GPa 1200°C	X. Liu *et al.,* (1995)
B_6O_x	5.370(1)	12.328(3)	2.296	-	-	Amb. P	Shabalala (2007)
B_6O_x	5.390(1)	12.334(4)	2.288	-	-	Hot. P	Shabalala (2007)

[a] O occupancy reported at ambient pressure.

P.F McMillan et al., (1999) confirmed that increasing the synthesis pressure in the presence of an oxidizing agent will result in an increase in the oxygen chemical potential, and that this drives the composition of the B_6O phase closer to the nominal stiochiometry.

2.2.2 PROPERTIES OF BORON SUBOXIDE

The scope of investigations was broadened when researchers discovered that boron suboxide (B_6O) displayed a range of interesting physical and chemical properties such as great hardness, low mass density and high chemical inertness due to its short interatomic bond lengths and strongly covalent character.

Hideaki Itoh et al., (1998), studied the oxidation resistance properties of B_6O and found that B_6O compact exhibited an oxidation resistance in air up to 600^oC and a mild oxidation behavior in the temperature range of 700-1000^oC, resulting in the formation of a liquid film of B_2O_3. In addition, it was found that this B_6O compact had a superior oxidation resistance in air at high temperatures in comparison with B_4C compact, sintered at the same conditions. The porosities in both materials were not reported, but the B_6O compacts were reported to have densities higher than 95% theoretical. Fig 2.5 shows the results of thermal analysis that was performed using TG-DTA on both single phase compacts.

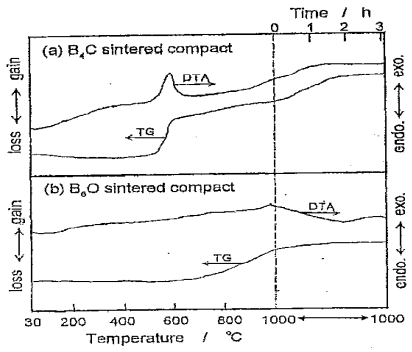

Fig2. 5: *TGA and DTA analyses of single phase compacts a) B_4C and B_6O prepared at 5GPa, 1700^oC and 20 minutes. Heating rate: 3^oC/min, atmosphere: air*

Fig 2.6 shows the B_2O_3 film thickness after the oxidation of B_6O sintered compact. It was found from the graph that the thickness of the oxidation film increased by a small amount until the treatment temperature reached 1100°C, however, when the treatment temperature reached 1200°C or more, the thickness of the oxidation film increased despite the fact that the B_2O_3, which played a role as a protective film, volatized rapidly. This indicates that when the treatment temperature is 1200°C or greater, the B_6O sintered compact is rapidly oxidized whether or not a protective film is present.

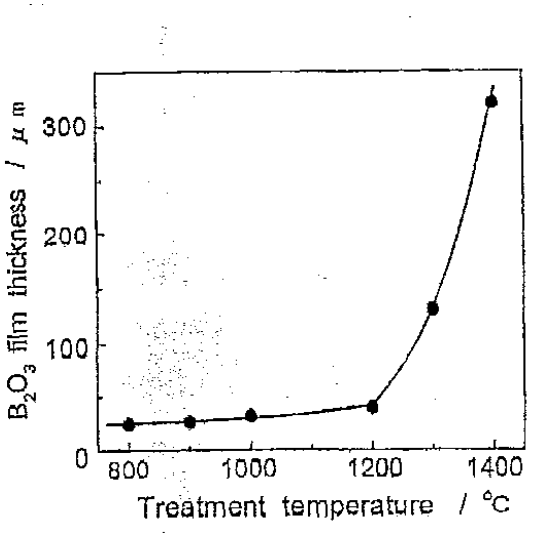

***Fig2.6**: B_2O_3 film thickness after oxidation in air for 4 hours as a function of treatment temperature.*

The thermochemical properties of boron suboxide (B_6O) were studied by V.S Makarov and Y.A Ugai (1986). They found the standard enthalpy of formation of B_6O which was determined by calorimetric dissolution of B_6O and strong nitric acid to be: $\Delta H_f^{\Theta}(B_6O_S, 298.15K) = (527 \pm 32) KJmol^{-1}$, but this study was limited to temperatures up to 800K. Recently, A. Andrews *et al.,* (2008) studied the thermodynamic properties of boron suboxide (B_6O) over the temperature range of 800K to 2300K. This study was

based on the assumption that B_6O has similar heat capacity to B_6Si since both compounds have a similar structure, composition, and chemical bonding. The heat capacity of B_6O at 2300K was estimated to be 204J/K mol from this study.

In the study done by T.C Shabalala *et al.,* (2007), the elastic constants of hot pressed B_6O and of composites materials made with Al content of 2.2 and 5.6 *wt%* were measured using ultrasonic pulse-echo technique, the result are given in Table 2.3. The data obtained in this work was slightly higher than the data found in other literature (D.R Petrak *et al.,* 1974, B.F Goosey 1974). Shabalala claimed that the difference was due to the amount of boron oxide (B_2O_3) and oxygen content of the synthesized powder. It was also found that the elastic constant values decrease with the addition of Al, which was due to the lower elastic modulus of the aluminium borate phase present in the composite.

The procedure in naming the hot pressed (sintered) B_6O materials is as follows, $HP19B_6O$ means B_6O samples hot pressed at 1900^oC. While, $HPB_6O2.2wt\%$ Al, $HPB_6O3.7wt\%$ Al and $HPB_6O5.7wt\%$ Al implies B_6O composites hot pressed (at 1900^oC) containing 2.2, 3.7 and 5.7 wt% Al in secondary phases, respectively.

Table 2.3: *Elastic properties of hot pressed B_6O and B_6O composites*

Material	**Elastic Modulus *E*** (GPa)	**Shear Modulus** (GPa)	**Bulk Modulus** (GPa)
HP19B_6O (T.C Shabalala *et al.,* 2007)	540	227	300
B_6O(Petrak *et al.,* 1974)	470	206	230
B_6O (B.F Goosey 1974)	483	-	-
HPB_6O2.2wt%Al (T.C Shabalala *et al.,* 2007)	514	221	255
HPB_6O3.7wt%Al (T.C Shabalala *et al.,* 2007)	467	199	240
HPB_6O5.6wt%Al (T.C Shabalala *et al.,* 2007)	419	179	214

The hardness of B_6O is due to the strong covalent bonding and short interatomic bond lengths between the B_{12} icosahedral units and within the B_{12} units, as well as from the optimization of the B_6O stoichiometry as a result of using high pressure techniques. Duanwei *et al.,* (2002) grew B_6O single crystals (at pressures of about 5.5 GPa) with grain sizes greater than 100 μm which enabled them to measure the intrinsic properties of B_6O. The Vickers hardness of B_6O single crystals was measured using a diamond indentation method, after the samples had been polished using diamond abrasive disks and slurries. Under a loading force of 0.98 N, an average hardness of 45GPa was obtained. The fracture toughness was found to be very promising at 4.5 $MPa.m^{1/2}$ which approaches that of single crystal diamond at 5 $MPa.m^{1/2}$.

Kayhan and Inal (1999) made sintered B_6O compacts under *vacuum* through hot pressing and found good hardness (37 GPa- 100g load) and fracture toughness (6.23 $MPa.m^{1/2}$) values but the samples had a high amount of porosity (7.5 or more), which resulted in materials with low strength values [50-80MPa]. Also, the radius of the notch used to measure the fracture toughness of the resulting material was 0.4mm, which makes the values obtained for that property very suspect.

Studies were made by Itoh *et al*. (2000) to improve the mechanical properties of B_6O materials by introducing other hard materials, like B_4C and c-BN, as a binder in the materials. Maximum microhardness $Hv_{0.1}$ of 46 GPa was obtained from B_6O-30vol% B_4C sintered composite under the sintering conditions of 4 GPa, 1700^oC and 20 minutes. The fracture toughness was approximately 1 $MPa.m^{1/2}$. The fracture toughness of the B_6O-x-cBN composites increased as the cBN content increased; the maximum fracture toughness (1.5-1.8 $MPa.m^{1/2}$) was observed for x=40-60 vol%. Slight crack deflection along the B_6O-cBN grain boundary contributed to the increase of that property.

2.3 B_6O- BASED SINTERED COMPOSITE

Different considerations have been given to the study of improving the mechanical properties of B_6O material in order to fully utilize the potentials of the material as grinding wheels, drill bits, abrasives and cutting tools. And a wide area of interest was initiated to investigate the type of materials that will emerge from high-pressure and high temperature treatments of B_6O powder with other superhard materials.

Hideaki Itoh (2004) synthesized single phase B_6O powder with grain sizes of 1.2-1.4μm at 1350°C for 300 min under normal pressure via a solid-liquid reaction between amorphous boron and boron oxide in a pure argon atmosphere. Fig 2.7 shows the preparation procedure of the composites. The synthesized B_6O powder was mixed with commercially available B_4C, cBN or diamond powder. Thus, the blended powder was heated in vacuum at 600°C for 60 min to remove the adsorbed moisture and oxygen, and treated under high-pressure and high-temperature conditions.

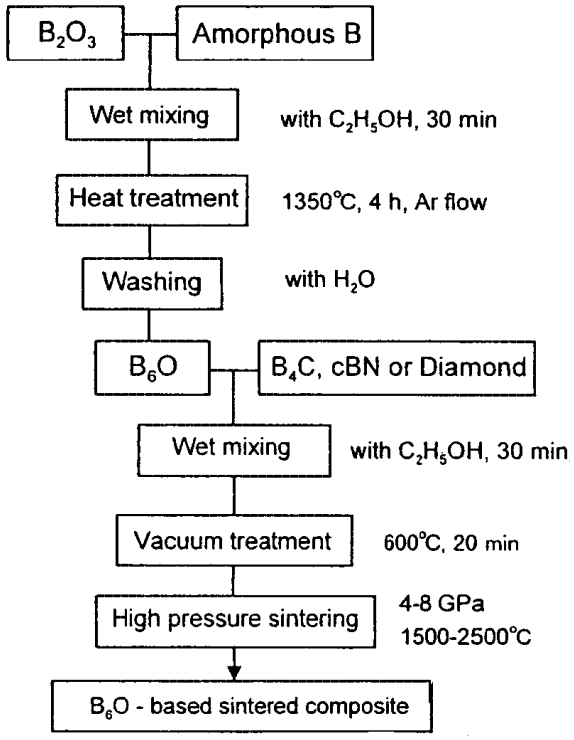

Fig 2 7: *Preparation procedure of B_6O- based sintered composites.*

2.3.1 B_6O-B_4C COMPOSITES

The X-ray diffraction patterns of B_6O-$\boldsymbol{x}B_4C$ specimens obtained at 4 GPa and 1700^oC for 20 min from the study made by Itoh *et al*. (2000) revealed strong diffraction peaks for single phase B_6O when there was no addition of B_4C, as shown in Fig.2.8. When 5 vol% or 40 vol% B_4C were added, the diffraction lines for B_4C were confirmed with their intensities increasing with increasing content of B_4C.

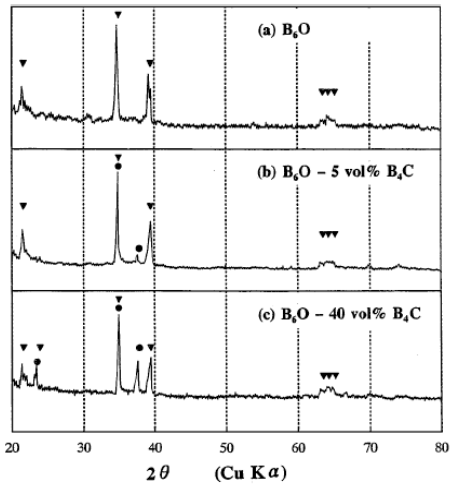

Fig2.8: *XRD patterns of the B_6O-$\boldsymbol{x}B_4C$ specimens for (a) x = 0 vol%, (b) x = 5 vol% and (c) x = 40 vol%. Sintering conditions: 4 GPa, 1700^oC and 20 minutes.* ▼*B_6O,* ● *B_4C.*

No variation of lattice constants for both B_6O and B_4C were observed, suggesting that neither formation of solid solution nor new compound formation occurs under the high pressure and high temperature conditions employed. The existence of mixed phase, B_6O and B_4C only was confirmed at higher pressures up to 6 GPa and higher temperatures up to 1800^oC. But, Hubert *et al.* (1997) and Garvie *et al.* (1997) synthesized composites of B_6O and B_4C by high pressure and high temperature treatment (7.5 GPa, 1700^oC, 30 min) of starting powder of B_2O_3, amorphous boron and graphite.

From the study, it was found that the effect of B_4C content was minor as far as microhardness is concerned. However, fracture toughness increases with increasing B_4C content. Fig 2.9 shows the effect of B_4C content on the microhardness and fracture toughness under the constant conditions of pressure 4 GPa, temperature 1600^oC and holding time 20 min.

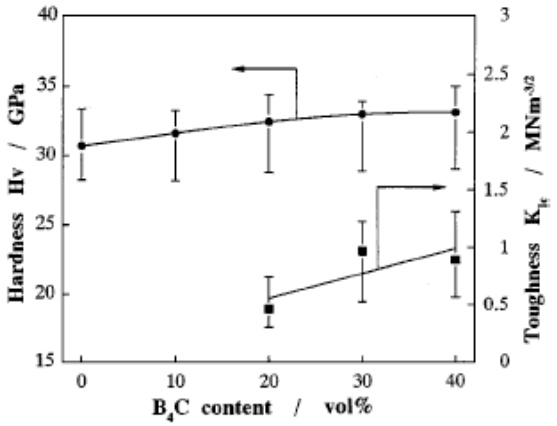

Fig2.9: *Vickers microhardness (●) and fracture toughness (■) of the sintered composites as function of B_4C content.*

Also, the effect of applied pressure on the microhardness and toughness was found to be minor, while sintering temperature was a critical factor for the properties. It was noted that the microhardness increases with temperature in the cases of high content of B_4C. A maximum microhardness of 46 GPa (200g-load) was attained at 1800^oC for the B_6O- 30 vol% B_4C composite in contrast to the hardness of the monolithic B_6O sintered compact of 34 GPa. Fig 2.10 shows the summarized diagram of microhardness vs. sintering temperature for various compositions of the sintered composites prepared in the pressure of 4 GPa and holding time of 20 min.

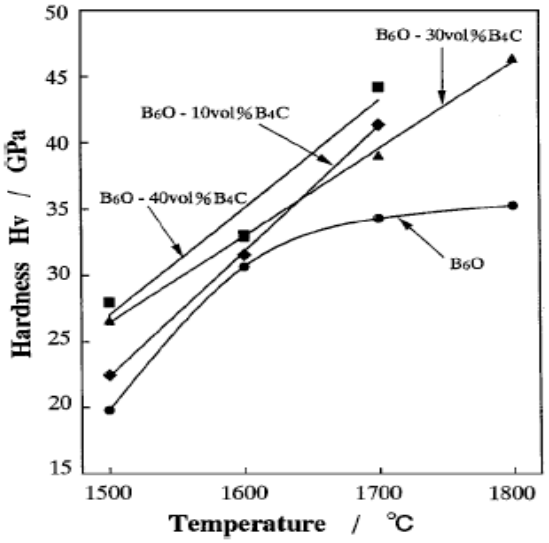

Fig2.10: *Microhardness (200g-load) as a function of sintering temperature for various compositions of the B_6O-B_4C sintered composites prepared at the constant pressure of 4GPa and holding time of 20 minutes.*

2.3.2 B_6O-cBN COMPOSITES

With the goal of obtaining better mechanical properties, Hideaki Itoh and Ryuuji Yamamoto (2000) used high pressure of 4-6 GPa and high temperature of 1500°-1800°C to sinter a mixture of B_6O (average grain size of 1.5μm) and commercially available c-BN powder (average grain size of 0.5, 3, or 6 μm) in an hexagonal boron nitride (h-BN) capsule using a girdle-type high-pressure apparatus. The sintered compact was further characterized and properties were measured.

The starting B_6O-cBN powder compositions were nominally 0, 10, 40, 60, and 100 vol% cBN. The average grain size of the cBN charge was 0.5 μm. Single –phase B_6O was identified as stoichiometric in the 0 vol% cBN specimen. Only the diffraction peaks of B_6O and *c*-BN were observed in the specimens with 10,40,60,80, and 90 vol% cBN. The

diffraction intensities increased with increasing cBN content, which indicates that no solid- state reaction or decomposition occurred in any compositions at 6 GPa and 1800^{o}C.

However, from the XRD pattern it was found that under higher pressure and higher temperature conditions (7.7GPa and 2300-2500^{o}C), sharp diffraction lines of an unknown new phase appeared instead of rhombohedral B_6O. Observation of the recovered specimens suggested a transformation of molten B_6O and crystallization to a higher temperature phase of boron suboxide under high pressure.

The influence of the amount of cBN added on the microhardness (H_v) and fracture toughness (K_{IC}) of the B_6O- cBN composites sintered at 6 GPa and 1800^{o}C is shown in Fig. 2.11. A maximum microhardness of 46 GPa was attained in the case of 40 vol% cBN addition. On the other hand, a fracture toughness of approximately 1.5 MNm$^{-3/2}$ was measured in the range of 40-60 vol%.

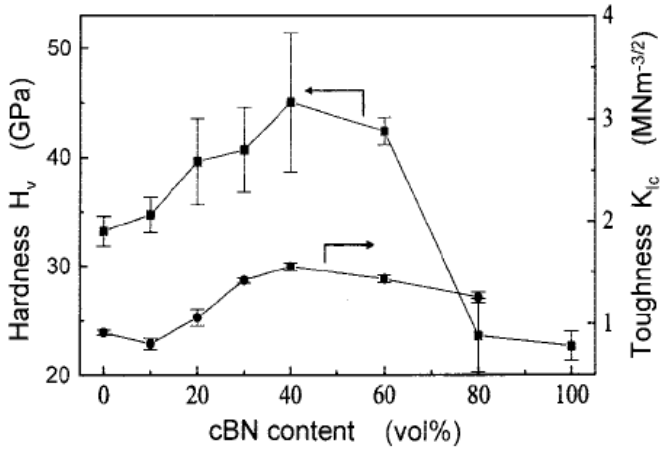

Fig2.11: *Influence of amount of cBN added on microhardness (H_V) and fracture toughness (K_{IC}) of the B_6O- cBN composites sintered at 6 GPa and 1800^{o}C.*

The toughness was also found to depend on the particle size of cBN, having a maximum of 1.8 $MNm^{-3/2}$ when 60 vol% cBN with a particle size of 3 μm was characterized. The toughness increase was attributed to the crack deflection along the grain boundary between B_6O and cBN.

2.3.3 B_6O-Diamond COMPOSITES

The combination of superior properties (Vickers hardness of between 70 to 100 GPa (Zhongwu *et al*., 2005), and fracture toughness of a single crystal of 5 $MPa.m^{1/2}$ (Duanwei *et al.,* 2002) in diamond, have triggered an interesting study of what type of material and properties will emerge from high-pressure and high- temperature sintering of mixed B_6O and diamond powders.

R. Sasai *et al.,* (2001) produced sintered composites in the B_6O-***x***diamond (x = 0- 80vol %) system, using high pressure and high temperature conditions (3-5 GPa, 1400°C-1800°C) from the mixture of in-laboratory synthesized B_6O and commercially available diamond powder with various grain sizes (<0.25, 0.5-3, 5-10 μm). In every specimen both B_6O and diamond were identified by XRD, indicating that neither solid solution nor new chemical compounds were formed under the conditions of temperature and pressure used. When the diamond particles used were larger than those of the B_6O, they were found to be evenly distributed over the B_6O matrix. In contrast, diamond particles behaved as matrix material for dispersing B_6O particles, when the diamond grain size is small.

Raman spectra of the B_6O- 40 vol% diamond composites sintered at 5 GPa, 1700^oC, and 20 min, showed a typical diamond peak at 1330 cm^{-1} in the case of using diamond powder with grain sizes larger than 0.5 µm, which indicates that the diamond structure would be maintained in the composite even under high pressure and temperature conditions. On the other hand, the Raman spectrum of the sintered composite prepared using finer grain sizes (<0.25 µm) showed two broad peaks, which correspond to the G- and D-bands of diamond-like carbon (DLC). Part of the fine- grained diamond located at the grain boundary between diamond and B_6O was transformed to DLC, since finer diamond grains have higher activity and surface energy than those larger than a few micrometers.

The treatment temperature has a great influence on the formation of strong interparticle bonding between B_6O and diamond, which increases the hardness of the sintered composites. A maximum microhardness of H_V = 60 GPa (200g-load) was measured in the B_6O- 60 vol% diamond composite with diamond grain sizes < 0.25 µm. The grain size of the added diamond particles greatly affected the microhardness and fracture toughness of B_6O- diamond sintered composites.

2.3.4 B_6O- Al_2O_3 COMPOSITES

Recently it was shown that the addition of Al or Al_2O_3 results in improved fracture toughness with only minor reduction in hardness (T.C. Shabalala *et al.,* (2007), Davis G. *et al.,* (2006), Shabalala T.C (2007)).

In the study carried out by Shabalala T.C (2007), he synthesized pure B_6O from boric acid and amorphous boron powder following the method reported in the literature, which was then coated with alumina of different amounts. The mean particle size of the coated powder was 3.5 µm. The synthesized powder was sintered, using a hot pressing furnace under argon atmosphere, at temperature of 1900^{o}C for 20 min, while the applied pressure was kept at 50 MPa. The main second phase, α-Al_2O_3, in the starting powder changed into $Al_{18}B_4O_{33}$ in the hot pressed material.

The SEM images for the hot pressed B_6O materials containing 2.2 *wt%* and 5.6 *wt%* Al respectively in the secondary phase are shown in Fig 2.12. The white phase on the micrographs is the aluminium borate phase while the black phase is B_6O. The sample was observed to be nearly dense, with the aluminium borate phases homogeneously distributed.

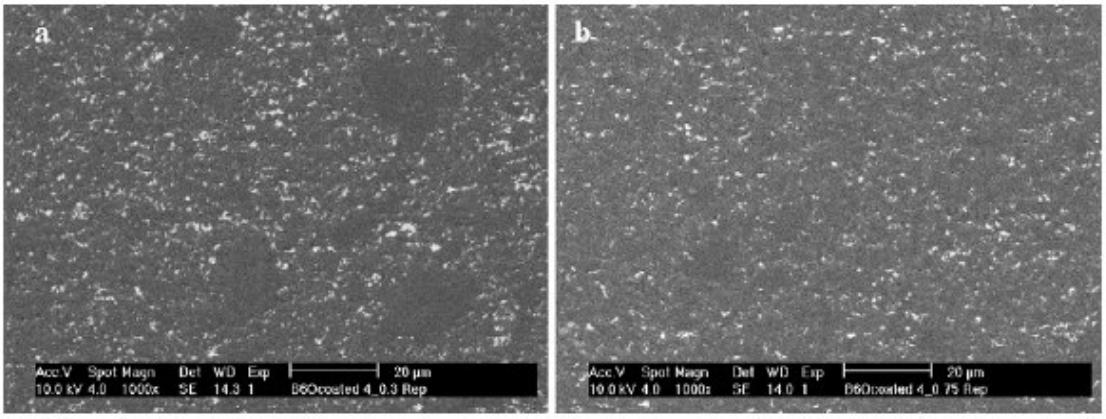

Fig2.12: *SEM images of hot pressed B_6O composite materials containing (a) 2.2 wt% Al and (b) 5.6 wt% Al. (Shabalala 2007)*

The analysis done using transmission electron microscopy (Fig 2.13) revealed that the grain growth occurring in these materials was minimal. However, some large grains were observed, at large Al-free regions in the SEM micrographs.

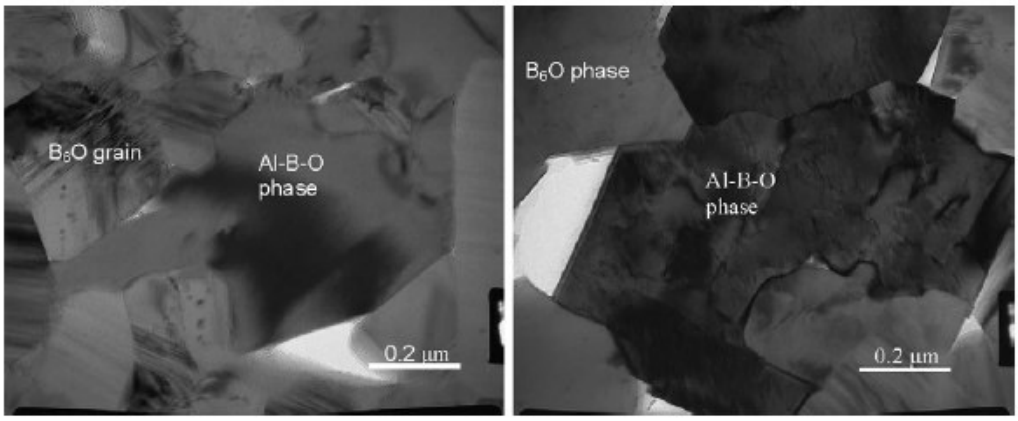

Fig2.13: *TEM images of hot pressed B_6O composite material (HPB_6O5.6 wt% Al) after sintering. (Shabalala 2007)*

The hardness and the fracture toughness of the materials obtained are given in Table 2.4. With increase in Al content the hardness (H_V) decreases from 29.3 to 27.8 GPa (5 kg-load) but the fracture toughness increases from 3.1 to 3.4 MPa.$m^{1/2}$. This means that the aluminium borate phases that were formed after sintering improve the fracture toughness of the material without degrading the hardness of the materials significantly, as compared to that of pure B_6O.

Table 2.4: *Mechanical properties of hot pressed B_6O materials (Shabalala 2007)*

Sample name	Density (g/cm^3)	Hv_5 (GPa)	K_{IC} (MPa m$^{1/2}$)	Phases (after sintering)
HP17B_6O	1.84	–	–	B_6O
HP18B_6O	2.12	–	–	B_6O
HP19B_6O	2.50	30.1 ± 1.2 (1 kg load)	Brittle	B_6O
HPB_6O2.2 wt% Al	2.52	29.3 ± 0.47	3.11 ± 0.12	B_6O, $Al_4B_2O_9$
HPB_6O3.7 wt% Al	2.45	28.2 ± 1.55	3.23 ± 0.15	B_6O, $Al_4B_2O_9$
HPB_6O5.6 wt% Al	2.51	27.8 ± 1.11	3.37 ± 0.13	B_6O, $Al_4B_2O_9$

HP17B_6O, HP18B_6O and HP19B_6O represent B_6O samples hot pressed at 1700, 1800 and 1900^oC, respectively. Furthermore, HPB_6O2.2wt%Al, HPB_6O3.7wt%Al and HPB_6O5.7wt% Al signify B_6O composites hot pressed at 1900^oC containing 2.2, 3.7 and 5.7 wt% Al in secondary phases, respectively.

Kayhan and Inal (1999) made sintered B_6O compacts under *vacuum* at 1800^oC through hot pressing for full densification and found good hardness (37 GPa- 100g load) and fracture toughness (6.23 MPa.$m^{1/2}$) values but the samples had a high amount of porosity (7.5 or more), which resulted in materials with low strength values [50-80MPa]. However, the mechanical properties of their materials were later improved by the infiltration of aluminium. Also, the radius of the notch used to measure the fracture toughness of the resulting material was 0.4mm, which makes the values obtained for that property very suspect.

2.4 POTENTIAL APPLICATIONS OF B_6O MATERIAL

The most promising useful property of the boron suboxide crystal is to take advantage of its abrasive qualities due to its high hardness. Boron suboxide (B_7O) with microhardness $Hv_{0.1}$ of 38.20 GPa has been reported to be highly refractory and suitable for use on surfaces subject to abrasion, e.g. grinding wheels, drill bits, machine tools, etc., and in structures employed in high temperature applications (Holcombe and Ottis, J.H, 1972). Kayhan and Inal (1999) successfully made aluminium infiltrated boron suboxide drag cutters and drill bits. Their boron suboxide (B_6O) material had a stability higher than

1800^{o}C (under vacuum), which dramatically exceeds that of polycrystalline diamond (PCD) cutters.

B_6O is thermally stable at high temperatures above 1000^{o}C. For this reason, it should have an advantage over the use of diamond. As an abrasive, it could handle the high heat generated by cutting through high-strength steel materials and it is possible it would not interact with the iron, as much as diamond or cBN because it does not contain C or N. Diamond in the presence of transition elements is not thermally stable at these high temperatures and will react with ferrous materials under these conditions. It is well accepted that the development of boride-based materials has been driven by the fact that they have a better oxidation resistance than diamond or cBN-based materials.

Hayashi *et al*. (1994), claimed to have produced a method of removing a material from a surface, by abrading a surface with an abrasive tool, an abrasive powder or slurry, comprising a boron suboxide (B_xO) composition, where during the abrading step the boron suboxide (B_xO) composition is maintained at low temperatures. The abrasive, which is from boron suboxide (B_xO) family of compounds, exhibits unexpected high quality abrasive properties, comparable with the highest quality particulate, natural and synthetic, diamond, which has hardness twice that of boron suboxide (B_xO). The powder is made from a dense, finely crystalline boron suboxide (B_xO) material with Knoop hardness KNH_{100} of about 28 to 38 GPa. Therefore, boron suboxide material has the potential to be used in the abrasives field.

Boron Suboxide, together with Boron carbide, has high potential for successful use in ballistic amour, nuclear power engineering, chemical industries, in thermoelectric energy

converters. The material can also be used in coatings for wear-resistant metallurgical equipment.

B_6O material, with hardness close to that of cBN, as well as similar chemical inertness and thermostability as cBN, has been produced. A big advantage is that B_6O can be synthesized at ambient pressure or relatively low pressure compared to diamond and cBN. Therefore, one can expect B_6O and its composites to have a great potential for new superhard materials with industrial applications. These potential applications of ultra-hard B_6O materials have not been realized because of the low fracture toughness and strength of the materials produced up to now. An exception to this statement is the material produced by T.C Shabalala *et al.,* (2007), which begin to approach in properties to those of PcBN cutting tools. This work intends to build on the findings of those authors.

2.5 TOUGHENING MECHANISM IN CERAMIC MATERIALS

Technological advances are continually placing greater demands on the performance characteristics of engineering materials. Traditionally, engineering ceramics have been considered for heat containment, wear resistance, static load bearing, and electro-optical applications owing to the generalized properties of ceramics which include hardness, corrosion resistance, stability at high temperatures, creep resistance, high elastic modulus, and electrical & thermal resistivity. Unfortunately, these properties come at the expense of toughness. While metals typically have toughness values of 15 to 150 $MPa.m^{1/2}$, ceramics usually have toughness values below 5 $MPa.m^{1/2}$ frequently below 2 $MPa.m^{1/2}$ (A.G Evans, 1988).

Significant research effort has been directed toward the development of tough ceramics, since such materials have the potential to open up a large range of specialized engineering applications. Toughness can be significantly improved with the production of ceramics with a very small grain size (< 50 μm). A general solution is to engineer the microstructure of ceramics in such a way to inhibit crack propagation (F.Lee *et al.,* 1993).

A number of toughening mechanisms such as crack deflection, crack branching, crack bridging, transformation toughening, frictional interlocking and microcracking have been suggested in literature, but there is an ongoing debate about the relative importance of each of these mechanisms (T. Hansson *et al*., 1993, Seung K.L and Chong H.K, 1994). Some authors believe that crack deflection is the main toughening mechanism (S.A Meguid, 1996). The more commonly active mechanisms have been classified in a general way by Wachtman (1996) and are given for the present discussion in Table 2.5.

***Table 2.5: A** general classification of some of the toughening mechanisms in ceramics. Taken and adapted from Wachtman (1996)*

Class of effect	**Mechanism**
Crack deflection	Generation of out of plane components by a tilting or twisting of a crack plane around grains and secondary –phase inclusions.
Crack bowing	Pinning of a crack front by secondary-phase pinning points, leading to an in plane bowing of the crack front
Crack branching	Subdivision of a crack into multiple propagation fronts.
Crack bridging	Inhibited crack opening and enhanced crack energy dissipation around ligamentary grains that span the crack wake.
Crack-tip shielding	A reduction of the crack-tip stress intensity, through direct stress modifications, or through crack-tip blunting by ductile deformation, phase transformation, or microcracking processes.
Transformation Toughening	Occurs as a result of a stress-induced phase transformation of particulate inclusions in a ceramic matrix. Residual stresses surround each particle which acts across the projected fracture plane, and have to be nullified for the crack to propagate through the transformed zone.

The general concept of impeding the growth of a crack by placing inhomogeneities (obstacles: second phase particles, whiskers and fibres) in the crack path thereby increasing the fracture toughness of ceramics has been studied (Clarke & Farber 1987). Although the presence of such obstacles would encourage the pinning of the crack, the crack path could deviate from the obstacle by either bowing around the obstacle (Fig. 14(a)) or by deflecting out of the crack plane (fig 14 (b) and (c)). Crack deflection takes place whenever the crack path adopts a least resistant path. This may occur as a result of the presence of residual stresses and different phase elastic moduli.

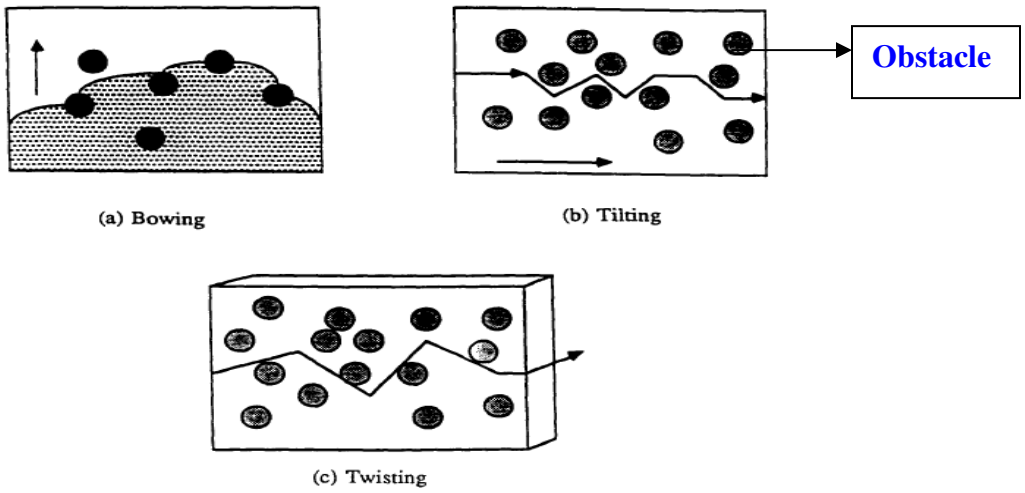

***Fig2.14**: Effect of obstacles upon crack-tip interaction. (S.A. Meguid 1996)*

Lange (1970) and Evans (1972) examined the effect of crack bowing on the fracture toughness of brittle materials and claimed that the extent of the toughening is strongly influenced by the stress state.

This mechanism serves as the motivation for introducing some obstacles as second phase into the B_6O matrix, to interact with the crack front and impede the growth of such crack, thereby improving the fracture toughness of the B_6O-based composite produce in this work.

CHAPTER THREE

3.0 EXPERIMENTAL DETAILS

This section gives detailed explanation of the characterization of the starting powder, the equipment used, procedure for making boron suboxide (B_6O), conditions for milling the powder into the sub-micron size range, mixing of the powder with additives, consolidation of the admixed powder and characterization of the sintered materials in terms of phases present, morphology of the phases, density, hardness and fracture toughness.

3.1 MATERIALS & CHARACTERIZATION

The starting materials used for the synthesis of boron suboxide (B_6O) consist of amorphous boron (average particle size of about 2 μm) and boric acid. The particle size distribution for the boron powder was analyzed using a Malvern Mastersizer 2000 (Microscientific), with water as a carrier fluid (Fig 3.1).

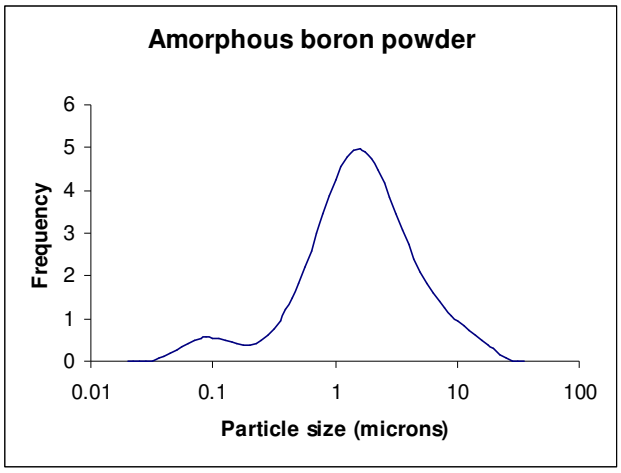

Fig3.1*: Particle size distribution of the amorphous boron powder (used in synthesizing B_6O powder).*

The morphology of the powders was also analyzed using Field Emission Scanning Electron Microscopy (FESEM). Fig 3.2 shows the particle arrangement and the agglomeration present in the amorphous boron powder, while Fig 3.3 shows the plate-like morphology of the boric acid powder.

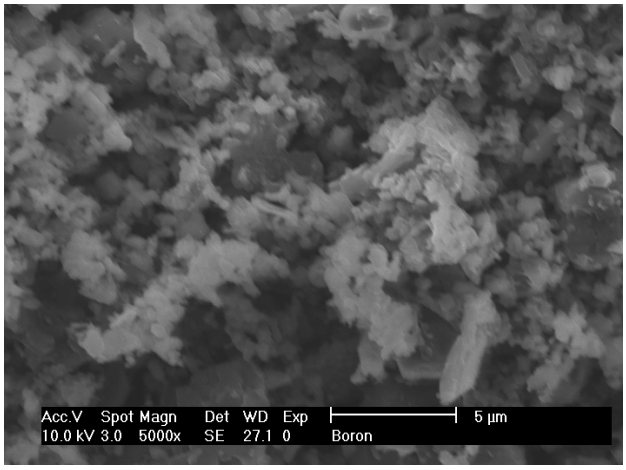

Fig3.2: *SEM image of amorphous boron powder*

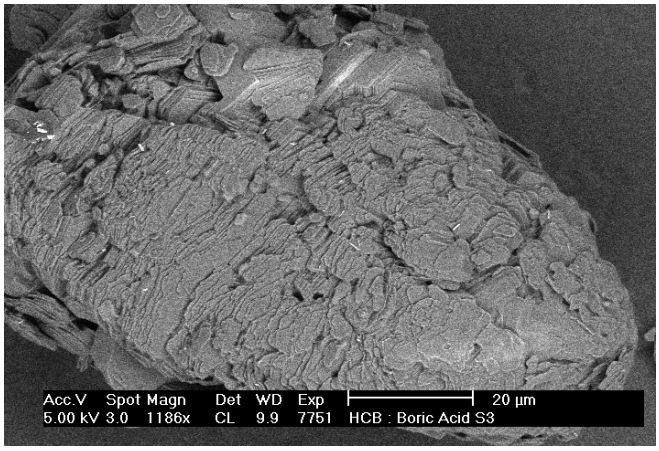

Fig3.3: *SEM image for boric acid powder*

Other powders used in this study were mixed with the boron suboxide (B_6O), to improve the overall mechanical properties of the sintered B_6O composites. Table 3.1 shows all the powders, as well as chemicals, gases, solvent and their suppliers used for this work.

Table 3.1: *Material used*

Material	Purity (%)	Colour	Supplier
Amorphous boron	96	Brown	H.C. Stark
Boric acid	99	White	Saarchem
Iron (Fe)	99	Reddish-brown	Industrial Analytical
Iron oxide (FeO)	99.5	Black	Industrial Analytical
Iron boride (FeB)	98	Grey	Industrial Analytical
Chromium (Cr)	99	Silver grey	Industrial Analytical
Chromium oxide (CrO_3)	98+	Dark red	Industrial Analytical
Cobalt (Co)	99.5	Grey	Industrial Analytical
Scandium oxide (Sc_2O_3)	99.99	White	Industrial Analytical
Lanthanum oxide (La_2O_3)	99.99	White	Industrial Analytical
Ytterbium oxide (Yb_2O_3)	99.99	White	Industrial Analytical
hBN	-	White	H.C. Stark
Poly-vinyl pyrrolidone (PVP)	-	White	Fluka
Argon, UHP	-	Colourless	Saarchem
Methanol	99	Colourless	Saarchem
Ethanol	99	Colourless	Saarchem
Acetone	99	Colourless	Saarchem
Distilled water		Colourless	-

3.2 EQUIPMENT USED

The following pieces of equipment were used during this work:

3.2.1 Turbula mixer

A turbula mixer was used to dry mix the starting powders during the synthesis of B_6O powder. Alumina balls with a diameter of 12 mm were used as milling media during this mixing. The number of alumina balls used depended on the amount of powder that was mixed while the mixing time/cycle was not less than 120 min for each mixing run made. To maximize homogeneity during mixing the turbula mixer was stopped after 30 to 40 minutes and the sample container (usually a plastic bottle sealed with a tape) was manually shaken, and after that the mixing run was allowed to continue.

3.2.2 Attrition ball mill

An attrition ball mill was used for size reduction of the synthesized B_6O powder from the micron grain to the sub-micron grain size. Fig 3.4 shows the attrition ball mill.

Fig3.4: *An attrition ball mill*

3.2.3 Planetary ball mill

A planetary mill, Fritsch Pulversette 6, was used during wet mixing of powders, using ethanol or methanol as a solvent. The mixing vessel used inside the planetary ball mill was made from alumina with a capacity of 250 ml. Steel balls of 2.5 mm in diameters were used as milling media. The mill was operated at a speed of 250 rpm for 2 hours. Fig 3.5 shows the planetary ball mill.

Fig3.5: *A planetary ball mill, PM100*

3.2.4 Tube furnace

A tube furnace (Elite TSH17/75/150), bought from Elite Thermal Systems Limited, with capabilities of running to a maximum temperature of 1600 ^{o}C was used for the synthesis of boron suboxide B_6O powder. The centre tube was aluminium oxide, with an inner diameter of 7.40 cm, outer diameter of 7.70 cm and a length of 120 cm. Rectangular alumina crucibles were used as the sample holder and placed at the centre (hot zone area) of the tube furnace. The furnace has a Eurotherm microprocessor that controlled the

temperature profile executed during experimentation, i.e. heating rate, dwelling times and cooling rate. The furnace temperature was measured by a standard Pt-Rh thermocouple, which was connected to the microprocessor. All the experiments carried out were done under argon atmosphere. The picture of the tube furnace is shown in fig 3.6.

Fig3.6: *The tube furnace*

3.2.5 Uniaxial Hot Press

A Uniaxial hot press (HP20 Thermal Technology), from Thermal Technology Industries, was used for sintering and densification of samples. It consists of a furnace which is heated by carbon element and circulated with water to cool the system. The maximum obtainable furnace temperature is 2100^{o}C and the maximum pushing force that can be applied to compacts during hot pressing is 100 KN. The force is applied through graphite punches uniaxially from the bottom graphite punch. A rotary vacuum pump is attached to the hot press and is capable of vacuum levels of 10 mtorr. Fig 3.7 below shows the

picture of this Uniaxial Hot Press. A programmed computer was used to monitor the sintering cycle (densification stages) during hot pressing.

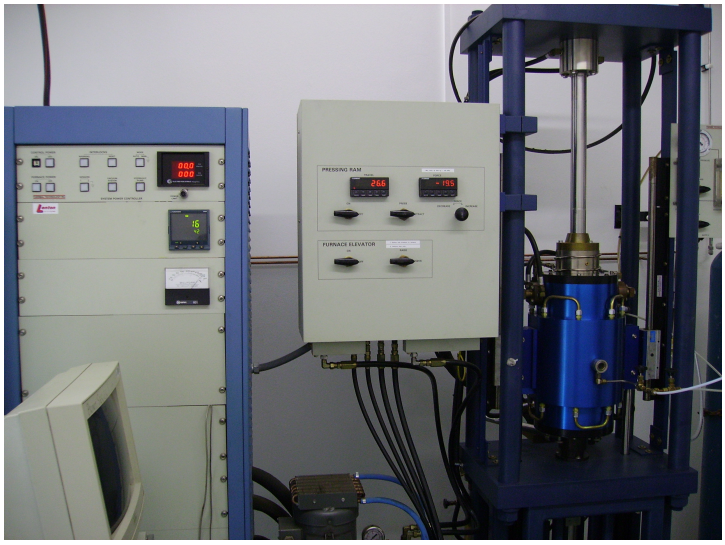

Fig3.7: *The Uniaxial Hot Press used for sintering*

The graphite components that were placed in the hot-zone of the furnace were coated before sintering with an h-BN suspension, which was stabilized using poly-vinyl pyrrolidone (PVP). The suspension was made by mixing 37g of h-BN and 100 ml of water, with poly-vinyl pyrrolidone (2g) used as a stabilizer. All the ingredients in the suspension are stirred together vigorously, in a 250 ml beaker, using a magnetic stirrer until the constituency of the entire suspension is uniform. The suspension was then applied by paint brush to the clean hot graphite components.

3.2.6 Capsule

Hexagonal-BN was chosen as a crucible material in this work due to its high temperature stability (decomposition temperature around 3000^{o}C), chemical inertness (stability in argon gas atmosphere up to 2200^{o}C), high thermal shock resistance and high thermal

conductivity. The sample cell was made from h-BN, while the piston was a graphite rod coated with layers of h-BN suspension. A 3mm h-BN cylindrical plate was placed between the graphite piston and the sample to avoid any carbon contamination. Fig 3.8 shows the drawing of the capsule used in this work.

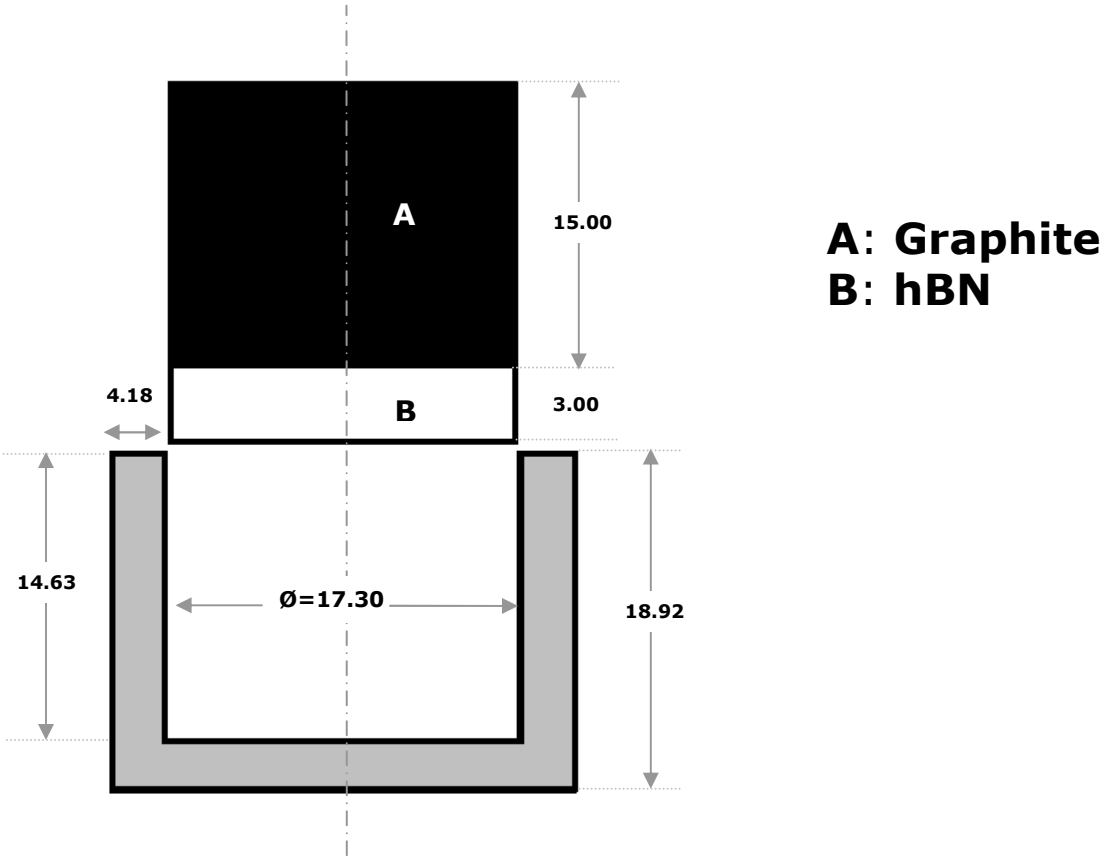

Fig3.8: *Drawing of Capsule used*

3.3 SYNTHESIZING BORON SUBOXIDE (B_6O) POWDER

The powder was synthesized from the reaction of amorphous boron and boric acid (instead of B_2O_3) powders. This was done by first mixing the two starting materials, approximately 50g per batch, using the turbula mixer for 2 hours. An excess amount (3

mol %) of boric acid was added to compensate for the evaporation of B_2O_3 that occur during synthesis. The mixture was then put into an alumina boat and heated inside the tube furnace. This heat treatment was done under an argon inert atmosphere. The temperature was kept at 300°C for 30 minutes to allow complete formation of boron oxide (B_2O_3). The reaction (synthesis) temperature was 1380°C and the reaction time was 6 hrs. The rate of heating and cooling was 5°C/min. A flow chart, showing how the B_6O powder was synthesized, is given in fig 3.9. The reaction taking place is given in equation 3.1 and 3.2 respectively. The resultant B_6O was washed in warm water and/or ethanol to remove any soluble impurities.

$$2H_3BO_3 \rightarrow B_2O_3 + 3H_2O \quad \ldots\ldots\ldots\ldots\ldots\ldots\ldots\ldots\ldots\ldots \quad 3.1$$

$$B_2O_3 + 16B \rightarrow 3B_6O \quad \ldots\ldots\ldots\ldots\ldots\ldots\ldots\ldots\ldots\ldots\ldots\ldots \quad 3.2$$

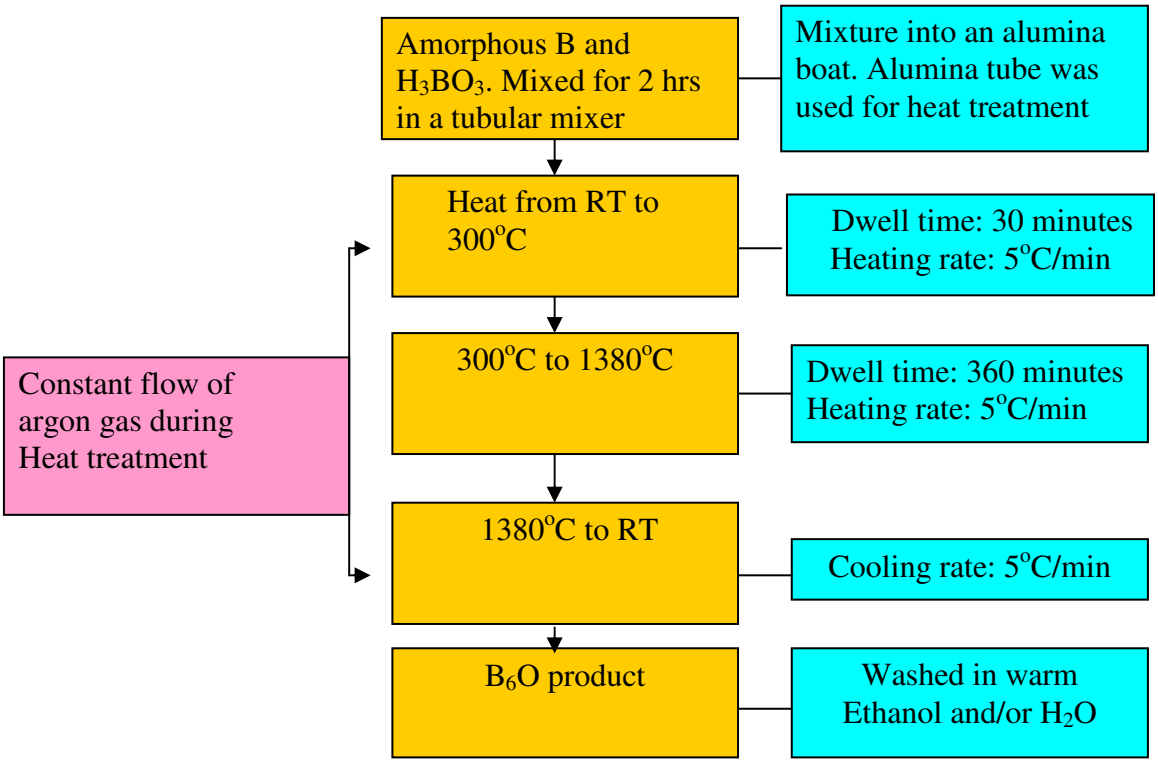

Fig3.9: *A flow chart showing the process of synthesizing B_6O powder*

3.4 MILLING OF BORON SUBOXIDE (B_6O) POWDER

B_6O powder were charged into the attrition ball mill to induce particle size reduction using steel balls of 2.5mm diameter, milling speed of 200rpm and isopropanol as the media, while the ratio of charge to steel ball was kept at 1: 10. After milling for 30 hours, the milled powder was withdrawn and washed with HCl to remove any iron contaminations introduced during the milling and in ethanol to remove B_2O_3. The milling conditions stated above were found to produce the optimum size reduction. Initially, the particle size distribution was measured at 5, 20, 30, 35 and 50 hours. It was observed that increasing milling time decreases the average particle size of B_6O and that it remained almost constant after 30 hours of milling. Further milling above this time, resulted in higher percentage of iron contaminant in the powder, without necessarily decreasing the particle size. Table 3.2 shows the parameters needed for optimum milling. The purpose of milling B_6O powder was to reduce its particle size, which in turn would be beneficial in terms of the mechanical properties after sintering.

Table 3.2: *Milling parameters employed for the attrition ball mill.*

Component	Parameter
Mixing pot	Steel
Milling balls	2.5 mm (Steel)
Milling speed	200 rpm
Milling time	30 hrs
Mass of B_6O	100 g
Mass of steel balls	1000 g
Solvent	Isospropanol

3.5 CHEMICAL ANALYSIS OF THE B_6O POWDER (ICP METHOD)

The milled B_6O powder was chemically analyzed using Inductively Coupled Plasma analysis (ICP) to determine the amount of iron and chromium contaminant present in the powder. A Spectrociros CCD ICP analyser equipped with an end on plasma and a coupled charged detector was used to do the analyses. The plasma was operated at 1200 W. 0.1g of the sample was digested in a solution containing HNO_3 (55%) and HF (40%) by microwave digestion in a Multiwave 3000 SOLV analytical sample preparatory microwave supplied by Anton Paar. Digestion was done at 1200 W for 65 minutes. The actual quantitative results will be discussed in detail in chapter 4.

3.6 MIXING B_6O POWDER WITH OTHER COMPOUNDS

Submicron B_6O powder was mixed with different compounds from Fe-Cr-Co-B-O system and rare-earth oxide (Sc_2O_3, La_2O_3 & Yb_2O_3) in methanol for 2 hours using the planetary ball mill. The mixing speed was kept at 200 rpm, while using 2.5mm steel ball as the media. The calculation of the weight % of each additive was carefully done in order to retain the same volume % in the B_6O powder; this is shown in the Appendix of this dissertation. After the mixing, the slurry was dried using the rotavap, and then characterized using X-ray powder diffraction to identify the phases present and then SEM to check the homogeneity of the admixed powder.

3.7 HOT PRESSING OF POWDERS

In this work, two different sintering profiles were used to achieve dense materials. The first was used to sinter pure B_6O, while the other was used for sintering B_6O composite.

A typical hot pressing procedure of pure B_6O sample was as follows: the hot press was evacuated to pressures less than 200 mtorr and then back filled with argon. Argon was then allowed to flow through the furnace during the furnace temperature cycle. The furnace was heated to 1700°C at 15°C/min and held at this temperature for 20 minutes, to apply the load. The furnace was further heated to 1900°C (sintering temperature) at 10°C/min and held at this temperature for 20 minutes. The furnace was then cooled to room temperature at 20°C/min. At temperatures lower than 500°C the load was removed from the sample. At room temperature the sample cell was removed from the graphite die/insert and the sample was then removed from the h-BN crucible for analysis. Fig 3.10 shows this sintering profile.

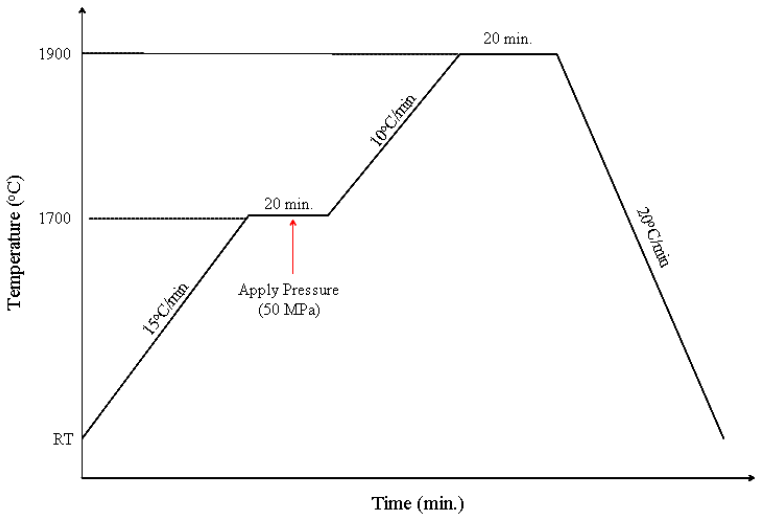

Fig3.10: *Optimum Sintering Temperature profile for pure B_6O*

This same profile was used for sintering B_6O composites, but high densification was not achieved due to the heterogeneity of the samples. Many other profiles were tried to achieve high density, until one was arrived at that gave a good sintered product. Table 3.3 shows some of the profiles tried in this work and the densities obtained for B_6O composites.

***Table 3.3**: Some heating profile and densities obtained.*

Heating Profile	**Pressure** (MPa)	**Density Obtained** *(g/cm^3)*
Room Temp.→ 1700°C *(15°C/min)* Held for 20 min to apply pressure 1700°C→ 1900°C *(10°C/min)* Held for 20min Cool to room temp. *(20°C/min)*	50	1.79
Room Temp.→ 1400°C *(20°C/min)* Held for 20 min to apply pressure 1400°C→ 1900°C *(20°C/min)* Held for 20min Cool to room temp. *(20°C/min)*	50	2.25
Room Temp.→ 1400°C *(20°C/min)* 1400°C→ 1600°C *(20°C/min)* (apply pressure) 1600°C→ 1850°C *(20°C/min)* Cool to room temp. *(20°C/min)*	50	2.31

✚ Room Temp.→ 1400°C *(20°C/min)* ✚ Held for 5 min to apply pressure ✚ 1400°C→ 1850°C *(20°C/min)* ✚ Cool to room temp. *(20°C/min)*	**50**	**2.54**

In this profile, the furnace was heated to 1400°C at 20°C/min and held at this temperature for 5 minutes, to apply the load. The furnace was further heated to 1850°C (sintering temperature) at 20°C/min and held at this temperature for 20 minutes. The furnace was then cooled to room temperature at 20°C/min. Fig 3.11 shows this sintering profile.

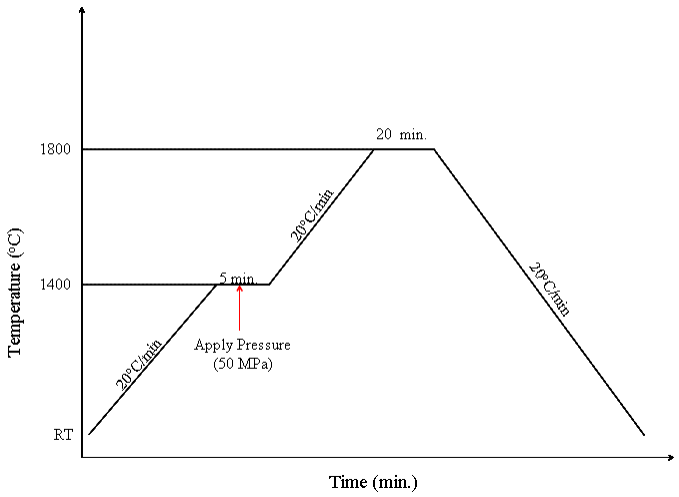

Fig3.11: *Optimum Sintering Temperature profile for B_6O composite*

3.8 ANALYTICAL PROCEDURE

After sintering the materials were ground on the surface to remove any h-BN material (from the sample cell) stuck on the samples and also to remove any decomposed layer. The materials were then cleaned before further analyses.

All materials were cross-sectioned to give two halves which were thus analyzed. The one half was polished at the cross section, mounted and then analyzed using optical microscope (OM), X-ray diffraction (XRD) and scanning electron microscope (SEM/EDS). Hardness and fracture toughness measurements were performed on this polished part. The other half was used for density determination.

3.8.1 DENSITY MEASUREMENTS

The density of the samples was determined using the Archimedes method. Firstly, the samples were immersed in distilled water (in a beaker) and then boiled for 3 hours, using a hot plate, in order to displace air from the pores in the sample. The thickness of the sintered samples was about 4 mm, therefore it was decided that 3 hours of boiling is enough, instead of 5 hours that is suggested in the ASTM method. A few experiments were also carried out confirming that boiling the samples for 5 hours gives similar results. After boiling the samples were cooled down to ambient temperature.

The density of the material was calculated by first determining the mass of the water impregnated sample, i.e. suspended mass (m_s). The sample is then removed from the water and dried lightly on the surface using a paper towel to remove excess water from

the surface, and the water saturated mass (m_w) is then determined. Finally, the dry mass (m_d) of the sample was measured after the sample had been dried in an oven, for about 20 minutes, and then cooled to ambient temperature. For accuracy each mass was determined five times in order to calculate a mean value which was then used to determine the density (ρ_s) and the porosity (P_o) of the samples. The equation used to determine the density of the sample is given in equation 3.2 and the porosity in equation 3.3

$$\rho_s = \frac{m_d \rho_{water}}{(m_s - m_w)} \qquad \ldots\ldots\ldots\ldots\ldots\ldots\ldots\ldots (3.2)$$

$$P_o = \left(\frac{m_w - m_d}{m_w - m_s} \right) \times 100 \qquad \ldots\ldots\ldots\ldots\ldots\ldots\ldots (3.3)$$

where,

m_s = suspended mass

m_w= water saturated mass $\qquad \rho_{water} = 1.000 gcm^{-3}$

m_d = dry mass

P_o= Open Porosity

3.8.2 POLISHING OF THE SAMPLES

A cylindrical sintered sample was cut into two pieces using a diamond saw. One of the pieces was hot mounted in resin, using Lucite powder. After mounting, the cross-section of the sample was lapped for 20 minutes on a standard lapping wheel using diamond grit (350 µm). Samples were then lapped further, with 120 µm diamond grit, for 20 minutes

in order to remove the scratches on the surface of the samples caused by the 350 µm diamond grit.

By experimentation an optimum (best) method of finally polishing boron suboxide and boron suboxide (B_6O) composites was developed. The samples were further lapped using a Metlap platen with 9 µm diamond slurry, for 30 minutes, and then with 6 µm diamond slurry for another 30 minutes, with a speed of 200 rpm and a load of 200kPa. After this, the samples were polished, using diamond slurry (6 µm), on a nylon cloth for 20 minutes at a speed of 250 rpm. The final polishing step done was using 1 µm diamond slurry on a cloth at a speed of about 300 rpm, until all the scratches have been removed. Scratches were a big problem in polishing B_6O because the material is hard and the problem of particle pull out was experienced.

3.8.3 X-RAY DIFFRACTION (XRD)

X-ray diffraction was performed on a PW1710 Philips powder diffractometer, using monochromatic Cu Kα radiation at 40 kV and 20 mA. The XRD analysis was done to check the phases present in the powders and sintered samples. Diffractograms were collected over a range of 2θ between 10-80^o, with a step size of 0.02.

Diffraction data for pure phases, obtained from the International Centre for Diffraction Data (ICDD) database using JCPDS cards, was used to identify what phases were present in the actual samples.

3.8.4 FIELD EMISSION SCANNING ELECTRON MICROSCOPY (FESEM)

A Phillips (XL30 SERIES) scanning electron microscope (SEM) equipped with a field emission gun operating between 5 and 30 kV was used to assess the microstructure of the polished samples. Elemental analysis was done using an energy dispersive spectrometer (EDS) analyser.

3.8.5 OPTICAL MICROSCOPY (OP)

Polished sintered B_6O materials were also viewed under a light microscope.

3.8.6 HARDNESS AND FRACTURE TOUGHNESS DETERMINATION

Vickers indentation hardness (Hv) measurements were done using 1kg load for sintered "pure" B_6O and 5 kg load for B_6O composites. The diagonal lengths of the indentations (d_1 and d_2 in Figure 3.12) were used to calculate the hardness of the material (according to equation 3.4). The length of the cracks generated by the indentation (c_1 and c_2), were measured (as shown in Figure 3.12) and used to calculate the indentation fracture toughness (K_{1C}) of the materials, using Anstis equation (3.5).

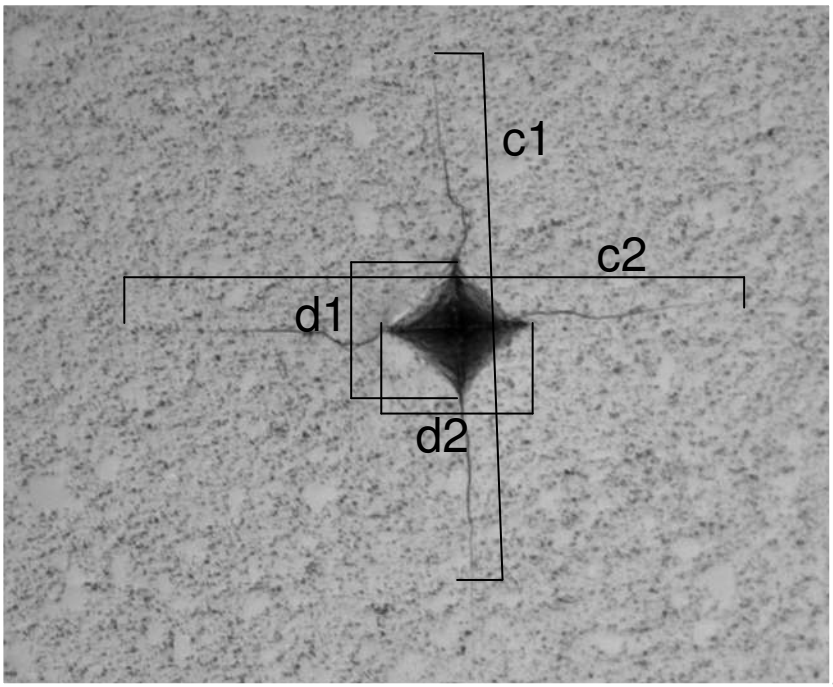

Figure 3.12: *Figure indicating how the diagonals of the Vickers indentations and the crack lengths are measured*

d_1 = vertical indentation length

d_2= horizontal indentation length

c_1=vertical length spanned by indentation cracks

c_2= horizontal length spanned by indentation cracks

d= average indentation length

c= average length spanned by indentation cracks

$$H_v = 1854.4 \times \frac{P}{d^2} \qquad \ldots\ldots\ldots\ldots\ldots\ldots\ldots\ldots \qquad (3.4)$$

where P is the applied load in Newton (N) and d is the arithmetic mean of the two diagonals in micrometers (μm).

$$K_{IC} = \xi\left(\frac{E}{Hv}\right)^{1/2}\left(\frac{P}{c^{3/2}}\right) \ldots\ldots\ldots\ldots\ldots\ldots\ldots\ldots \qquad (3.5)$$

where, ξ is the calibration constant (0.016), *E* is the Young Modulus of Elasticity (GPa) and *c* the radial crack length (in micrometer) (Anstis *et al.,* 1981).

CHAPTER FOUR

4.0 EXPERIMENTAL RESULTS

This section present the results obtained from the synthesis of boron suboxide, milling of the powder, mixing the powder with different additives, hot pressing of the admixed powder, characterization of materials using XRD and SEM/EDS to determine the phase (s) and the impurities present as well as the density, hardness and fracture toughness of the sintered material.

4.1 SUB-MICRON BORON SUBOXIDE (B_6O) POWDER

4.1.1 *Synthesis of boron suboxide (B_6O) powder*

Boron Suboxide (B_6O) powder was synthesized at Wits according to the method described in section 3.3. It was formed via solid-liquid reaction between B and B_2O_3 powders, with B_2O_3 (melting point of about 450^oC) formed from H_3BO_3. The synthesized B_6O powder was washed with warm water, and sometimes with warm ethanol, to dissolve any soluble impurities like amorphous boron oxide, B_2O_3, which formed (re-crystallized) as a result of using extra amount of boric acid during synthesis (as explained in section 3.3). The surface morphology of the powder was predominantly spherical and the colour of the powder was reddish brown.

Fig 4.1 shows the phase analysis done on the synthesized B_6O powder after washing in ethanol using XRD technique. The observed pattern in the end product was pure B_6O. The synthesized boron suboxide powder had the following lattice parameters, a=5.370 $\pm$ 0.001Å and c=12.328 $\pm$ 0.003 Å, determined using X-ray diffraction. This data

was compared with literature to estimate the oxygen content (occupancy) in the powder. Hence, the oxygen occupancy was estimated to be 0.77, which means that the synthesized boron suboxide has the stoichiometry; $B_6O_{0.77}$.

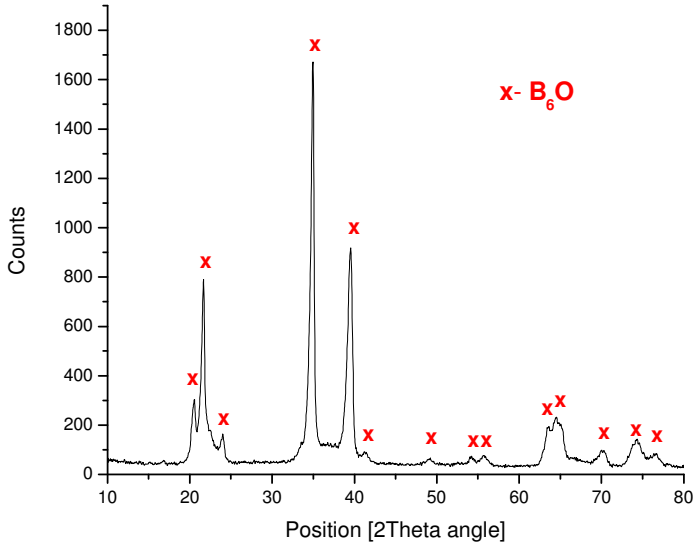

***Fig4.1**: XRD pattern for the synthesized B_6O powder*

The particle size distribution of B_6O powder (fig 4.2) which was determined using Malvern particle size analyzer had a similar particle size distribution as that of the starting amorphous boron, shown in fig 3.1. The similarities in the particle size distribution suggest that the particle size of the resultant B_6O powder depends on the size of the starting amorphous boron. Fig 4.3, showing SEM image of the synthesized B_6O powder, also confirms the similarities in the grain size between the two materials, but the particle morphology is different. It was noted that the synthesized B_6O powder needs milling after removal from the tube furnace because it tends to form agglomerates.

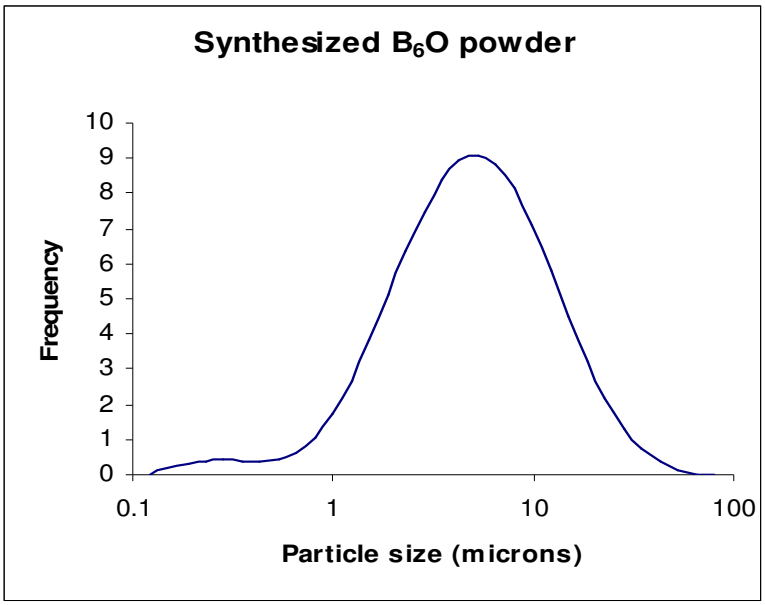

Fig4.2: *Particle size distribution of boron suboxide powder*

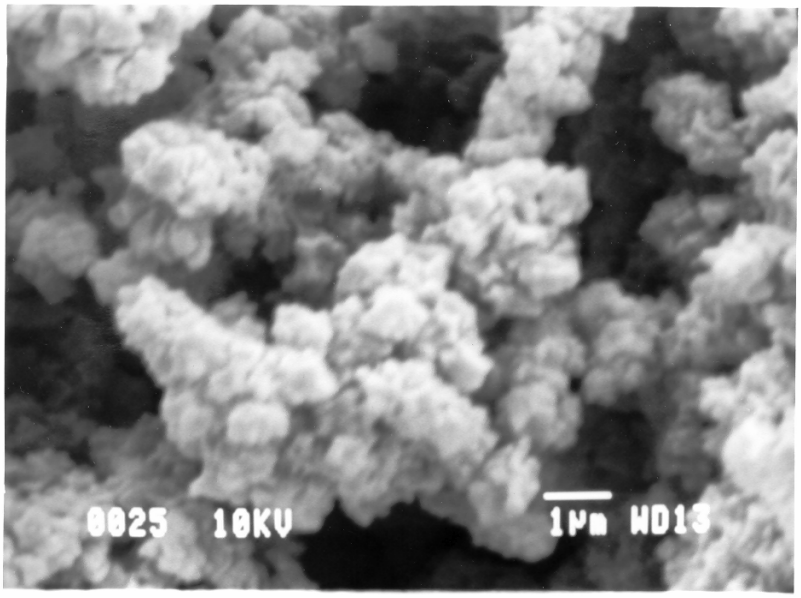

Fig4.3: *SEM image of boron suboxide (B_6O) powder*

4.1.2 *Milling of boron suboxide (B_6O) powder*

The B_6O powder produced at IKTS – Dresden from the procedure described in section 3.3 was milled in an attrition ball mill for 50 hours as described in section 3.4 to reduce the particle size, which in turn would be beneficial in terms of the mechanical properties after sintering. The particle size distribution was measured at 5, 20, 30, 35 and 50 hours.

Fig 4.4 shows how that the particle size distribution of the powder depends on the milling time. It was observed that increasing milling time decreases the average particle size of the powder and that it remained almost constant after 30 hours using 2.5mm steel balls. Further milling above this time increased the wear of the steel balls, without necessarily decreasing the particle size. From these investigations it was concluded that the optimum milling conditions are: 30 hours milling time at 200 rpm using 2.5 mm balls. These conditions resulted into d_{10}= 0.253μm, d_{50}= 0.529μm and d_{90}= 1.144 μm. Fig 4.5 shows the SEM micrograph of the sample milled for 30 hours. The scale bar on the micrograph gives an indication that each sphere of B_6O powder is in the sub – micron range. Therefore, sub- micron boron suboxide powder was successfully produced from the milling process described above.

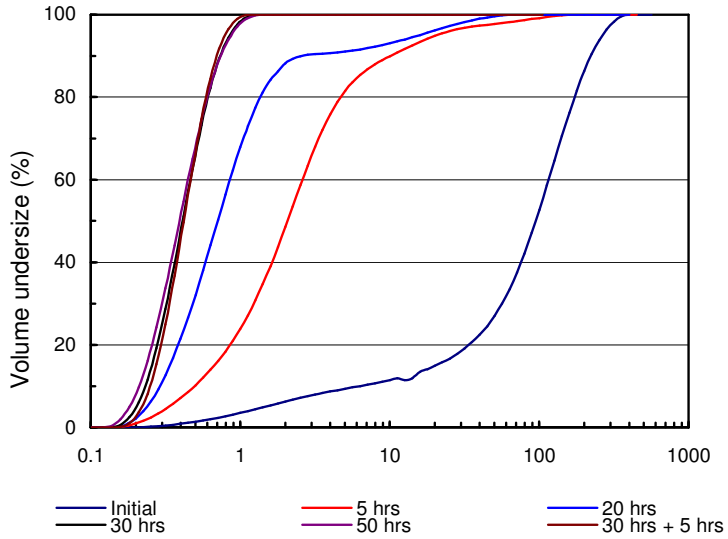

Fig4.4: *Particle size distribution of B_6O powder after milling for 5, 20, 30, 35 and 50 hours.*

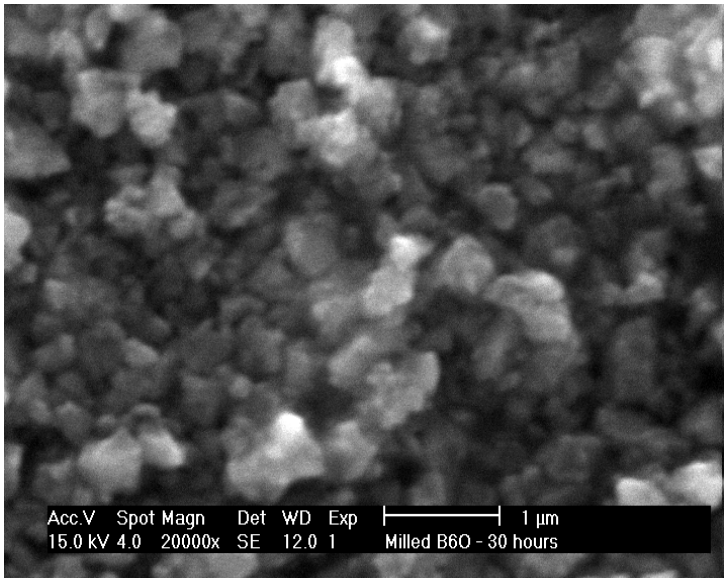

Fig4.5: *SEM image of boron sub oxide (B_6O) powder after milling for 30 hours*

4.2 CHEMICAL ANALYSIS OF THE BORON SUBOXIDE (B_6O) POWDER

The boron suboxide (B_6O) used in this work was milled in five different batches and the amount of iron (Fe) and chromium (Cr) impurities in the starting powder was determined using Inductively Coupled Plasma analysis (ICP). Table 4.1 shows the result obtained from the ICP analysis described in section 3.5. It can be seen that the total amount of impurities for each batch of powder is less than 0.15 *wt%.*

Table 4.1*: ICP measurements of the amount of iron & chromium impurities after washing*

Batch	Amount in *wt%*	
	Fe	***Cr***
1	0.085	0.008
2	0.040	0.012
3	0.089	0.023
4	0.045	0.033
5	0.057	0.039

4.3 PROPERTIES OF SINTERED PURE B_6O MATERIAL

B_6O powder was hot pressed in the uniaxial hot press at a temperature of 1900^oC and pressure of 50 MPa for 20 minutes according to the procedure described in section 3.7. By using Archimedes principle to measure the density of the sintered material, a nearly dense material having more than 95% of the theoretical density was produced.

Table 4.2 gives the summary of the properties obtained after cutting, grinding and polishing of the sintered material. During the hardness measurement, it was observed that

the material fractures while using a load of 5kg on the Vicker hardness tester, so a load of 1kg was employed on the machine. Due to the brittle nature of the sample, it was difficult to determine the fracture toughness of this pure sample.

Table 4.2*: Properties of hot pressed B_6O material*

Sample name	***Hot pressing conditions***	***Density (g/cm^3)***	***Open Porosity (%)***	***Vickers hardness (GPa)***
Pure B_6O	1900°C, 50 MPa, 20 minutes	2.46	3.7	30.2 ± 1.0 (*1 kg*)

Fig 4.6 shows the XRD pattern of the B_6O sample hot pressed at 1900°C. It can be noted that no phase difference was observed between the patterns of the synthesized B_6O powder and the hot pressed B_6O sample but there was reduction in the width of the peaks and the crystallinity had increased after hot pressing.

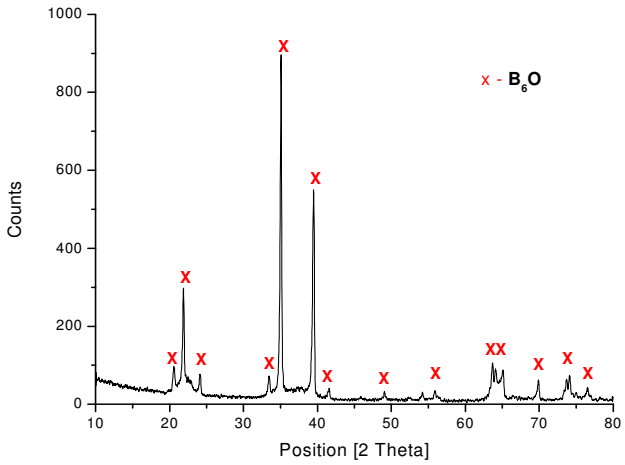

Fig4.6*: XRD pattern of B_6O sample hot pressed at 1900°C*

The sample was further characterized using SEM/ EDS and light optical microscope. There were small holes observed (see fig 4.7) which are assumed to represent porosity, but it must be mentioned that some of them came from material pull-out experienced during polishing. Further optical analysis showed that this hot pressed B_6O sample had porous edges, which were caused by slight decomposition at the sintering temperature. The overall EDS on the sample indicate the presences of B_6O, but on the white spot the presence of impurities (Fe & Cr) was detected in agreement with the ICP result. The grain size of the hot pressed compacts could not be determined from the SEM images. This is partly due to lack of good etchant for this material.

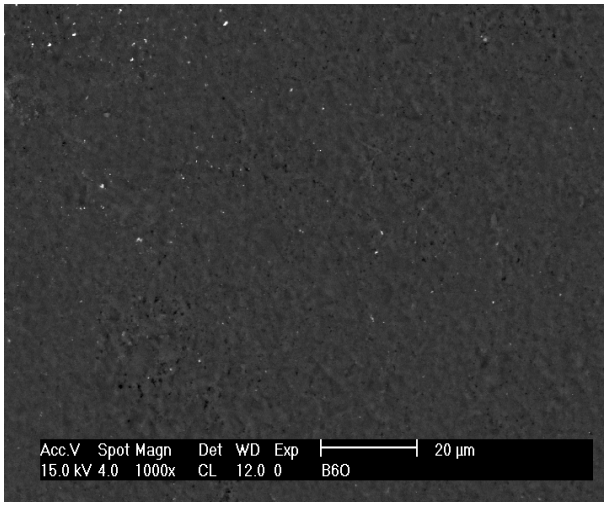

Fig4.7: *SEM image of a B_6O sample hot pressed at 1900^oC*

4.4 BORON SUBOXIDE (B_6O) MATERIALS WITH SINTERING ADDITIVES

With the primary aim of this research work being to produce B_6O- based materials with enhanced mechanical properties mainly in terms of fracture toughness, different elements and compounds having potential to achieve this objective were added to the B_6O powder. These additives were grouped into four parts: transition metals, transition metal oxides, transition metal borides & rare- earth oxides.

4.4.1 *Transition metal additives*

Three transition metals including iron (Fe), chromium (Cr) and cobalt (Co) were added to boron suboxide (B_6O) powder as sintering additives. The motivation for these experiments was to obtain B_6O materials with different grain boundary chemistry, which could assist in establishing a relationship between structure and mechanical properties.

Sub- micron B_6O powders were admixed separately with 1.17 *wt%* iron powder, 1.07 *wt%* chromium powder and 1.33 *wt%* cobalt powder *(these amounts corresponds to a constant value of 0.4 vol% of additives, which were pre-determined and shown in the Appendix A.2*) in ethanol using the planetary ball mill for 2 hours. Steel balls were used for the mixing, while the milling speed was kept at 200 rpm. The admixed powders were dried using a rotavap and then hot pressed.

The mixtures were first characterized using XRD and also the morphology was observed with SEM before using the heating profile described in section 3.7 to hot press the mixtures. After sintering, the densities of the composites were determined using

Archimedes principle and the samples were mounted, ground & polished for further characterization.

The XRD patterns of the admixed powders before sintering are shown in *Fig B.1 to Figure B.3* of *Appendix B*, to confirm the existence of the metallic phase in the mixture. The position of the main peak for the iron mixture was at $2\theta = 45^{o}$, for the chromium mixture at $2\theta = 44^{o}$ while that for the cobalt mixture was at $2\theta = 44^{o}$. The formation of boride secondary phase in the matrix after sintering (fig 4.8, 4.9 & 4.10) was observed by XRD. Comparing the admixed powders to the hot pressed composites, it was obvious that the Fe, Cr and Co have reacted completely and disappeared as pure metal phases in the final composite.

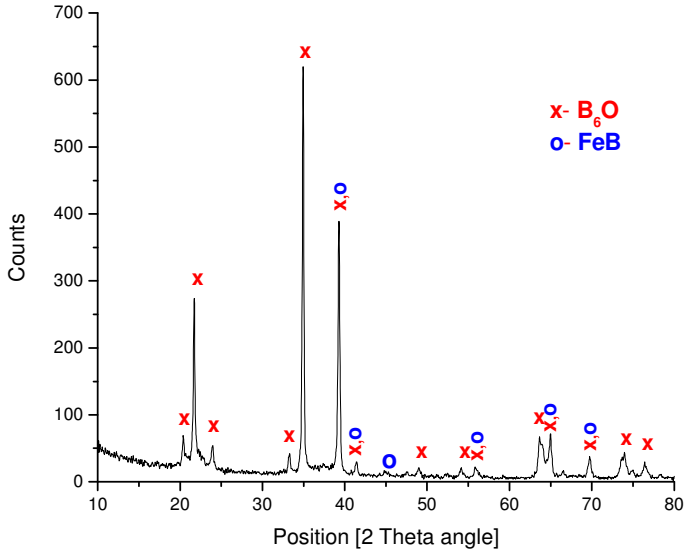

Fig4.8: *XRD pattern of sintered B_6O material with 1.17wt% Fe (00-050-1505, 01-076-0092).*

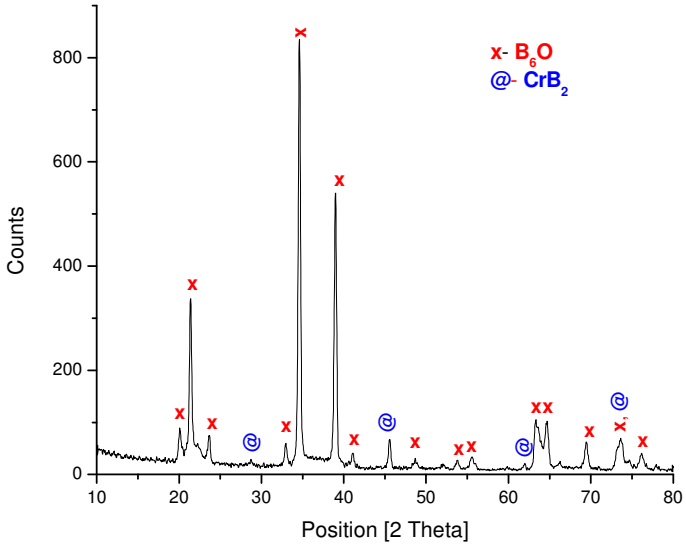

Fig4.9: *XRD pattern of sintered B_6O material with 1.07wt% Cr (00-050-1505, 00-034-0369).*

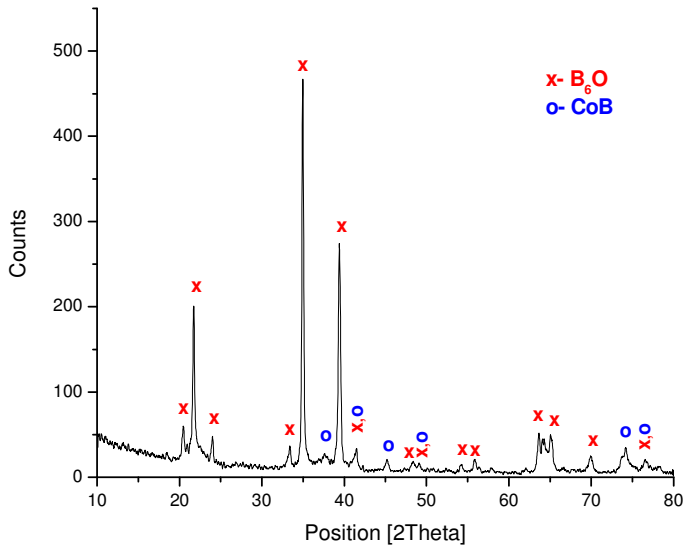

Fig4.10: *XRD pattern of sintered B_6O material with 1.33wt% Co (00-050-1505, 00-003-0959)*

The morphology of the admixed powders shown using scanning electron microscope in *Appendix C.1* gives an indication that the average particle size of the additives are less than 10μm. Cross- sections of the sintered materials were mounted, ground, polished and analyzed using SEM/ EDS and are shown in fig 4.11, 4.12 & 4.13 respectively.

It was observed that the B_6O+Fe and B_6O+Co composites had good homogeneous distribution of the boride secondary phase within the main matrix without grain growth. But for the B_6O+Cr composite segregations of Cr phases were observed in the microstructure. Energy dispersive X-ray (EDX) analyses show that these pockets of liquid phase have higher amount of chromium than other parts of the matrix. Although, the B_6O+Cr composite was fully dense (2.57g/cm^3), yet at higher magnification some dark spots which represents pull-out of the binder phase was observed. Since B_6O is a superhard material, it requires long polishing time to obtain a scratch free surface after grinding.

The segregation of boride second phase suggests variation in the properties of the materials at different points in the sample. EDS on each sample confirms that the grey phase represents B_6O, while the white represents the respective borides of the additives, in agreement with the phase composition obtained from the XRD analyzes.

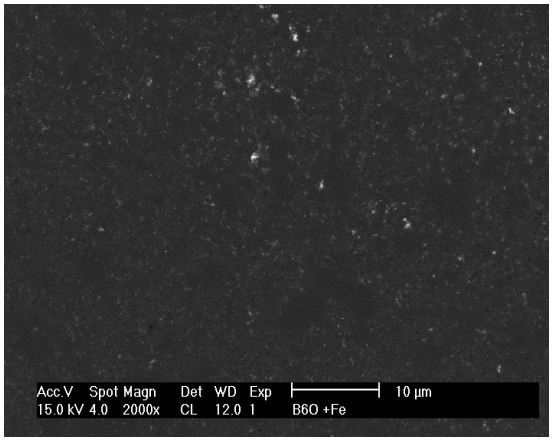

(a)

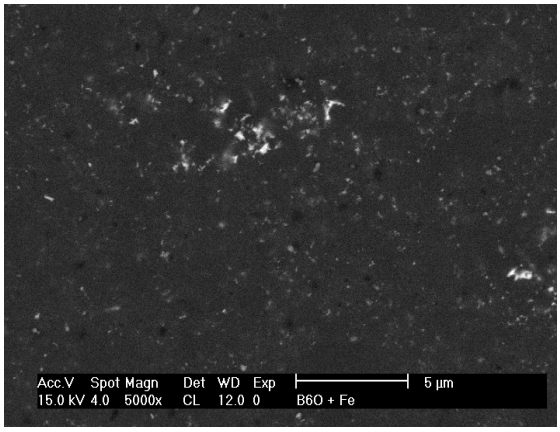

(b)

Fig4.11: *SEM image of the (B_6O + Fe) material sintered at 1850^{o}C for 20 min (a) x2000 (b) x5000.*

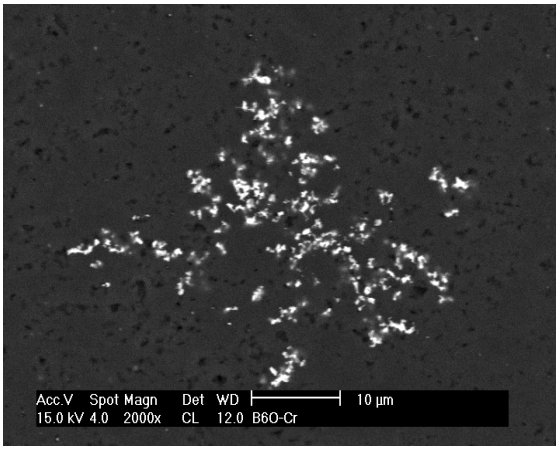

(a)

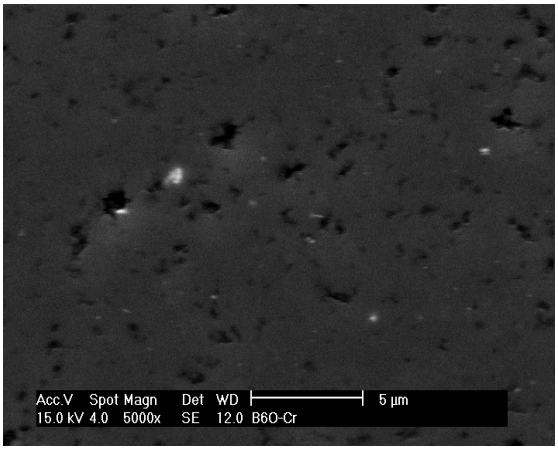

(b)

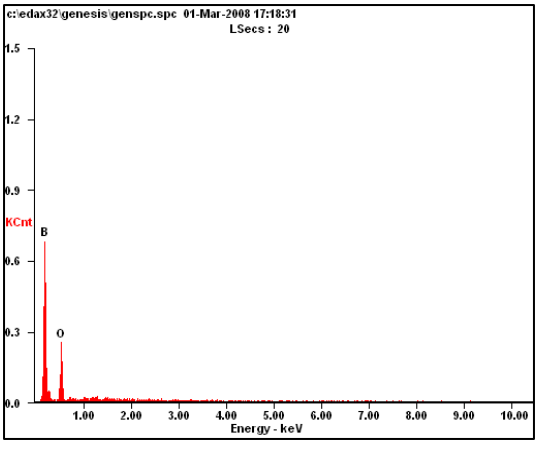

(c)

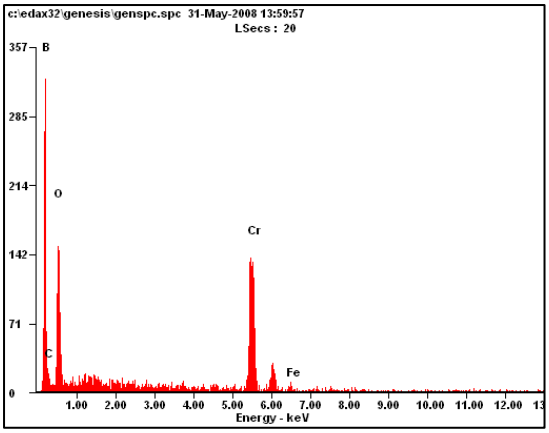

(d)

Fig4.12: *SEM image of the (B_6O + Cr) material sintered at 1850^{o}C for 20 min (a) x2000 (b) x5000 (c) EDS on grey phase (d) EDS on white phase.*

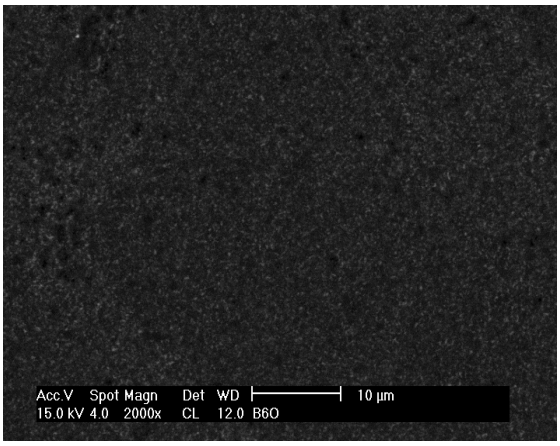

(a)

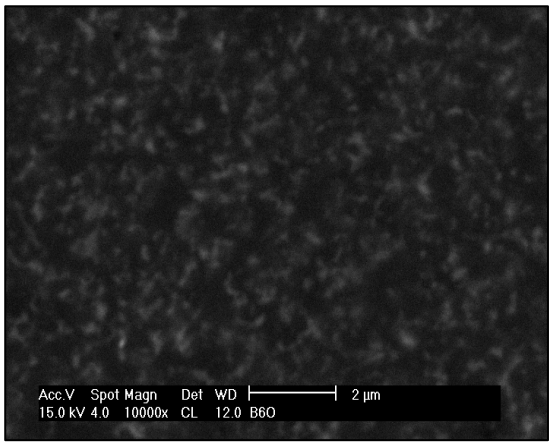

(b)

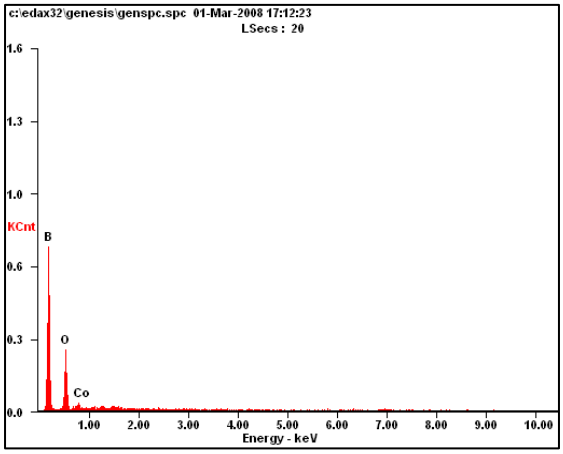

(c)

Fig4.13: *SEM image of the (B_6O + Co) material sintered at 1850^{o}C for 20 min (a) x2000 (b) x10000 (c) EDS on white phase*

The Vickers hardness was measured with a load of 5kg. An average was taken from 5 measurements. Table 4.3 gives the results obtained from analyzing the material. It could be seen that the open porosities obtained for the materials were lower than that of the hot pressed B_6O sample. This indicates the influence of the additives on densification. Also, for small weight % of the binder added the fracture toughness of the materials increased significantly compare to 'pure' B_6O which was found to be brittle.

Table 4.3: *Properties of the B_6O materials with transition metal additives sintered at 1850^oC for 20 minutes.*

Sample name	***Hot pressing conditions***	***Density (g/cm^3)***	***Open Porosity (%)***	***Vickers hardness (GPa)***	***Fracture Toughness ($MPa.m.^{0.5}$)***
Pure B_6O	1900^oC, 50 MPa, 20 min.	2.46	3.7	30.2 ± 1.0 (*1 kg*)	brittle
B_6O+1.17*wt%* Fe	1850^oC, 50 MPa, 20 min.	2.53	1.1	27.4 ± 1.5 *(5Kg)*	3.2 ± 0.8
B_6O+1.07*wt%* Cr	1850^oC, 50 MPa, 20 min.	2.57	0.7	29.4±2.9 *(5Kg)*	5.5 ± 0.4
B_6O+1.33*wt%* Co	1850^oC, 50 MPa, 20 min.	2.53	1.2	33.9±2.2 *(5Kg)*	5.3 ± 0.8

4.4.2 *Transition metal oxide additives*

Having produced and obtained a good combination of properties for B_6O materials containing transition metal additives when compared with the properties of pure B_6O, transition metal oxides were then introduced to the B_6O powder with the intention of improving densification, oxygen stoichiometry and further exploring structure to property relationships in the resulting materials.

In the planetary mill, 1.5*wt%* each of iron oxide *(FeO)* and chromium oxide (CrO_3) were mixed separately with boron suboxide powder in methanol for 2 hours and dried for sintering work. These amounts of additives were calculated in order to ensure that a constant value of *0.4 vol%* of transition metal was introduced into the mixture *(see Appendix A.2)*.

X-ray diffraction (XRD) patterns of the mixed powders are given in Appendix B (fig B4 & B5). It shows a major peak of iron oxide (FeO) at position $2\theta = 17^o$ & 61^o and that of chromium oxide (CrO_3) at position $2\theta = 44.3^o$. But after sintering of the powders at 1850^oC for 20 minutes in the hot press, peaks of iron boride (FeB) and chromium boride (CrB_2) were observed (fig 4.14 & 4.15). This implies that the boron suboxide (B_6O) has been oxidized by the transition metal oxide additives to form boride phase.

$$16FeO + 5B_6O \rightarrow 7B_2O_3 + 16FeB \quad \ldots\ldots\ldots\ldots\ldots\ldots\ldots \quad 4.1$$

$$8CrO_3 + 6B_6O \rightarrow 10B_2O_3 + 8CrB_2 \quad \ldots\ldots\ldots\ldots\ldots\ldots\ldots \quad 4.2$$

The advantage of this oxidation reaction is that there is possibility of improving the oxygen content and the crystallinity of boron suboxide.

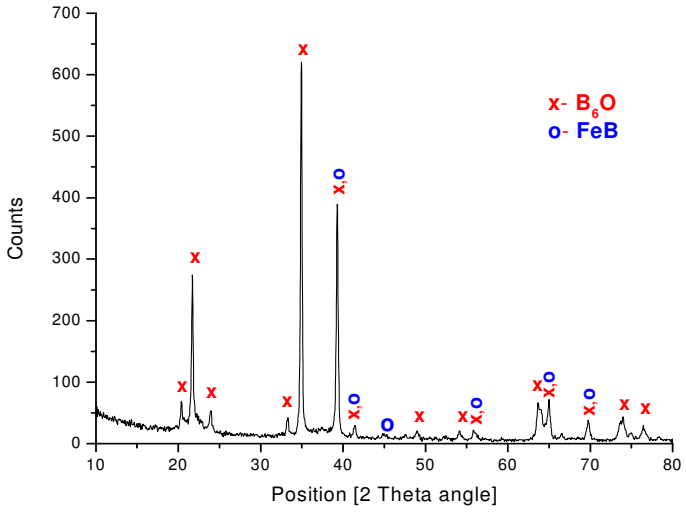

Fig4.14: *XRD pattern of sintered B_6O material with 1.5wt% FeO (00-050-1505, 01-076-0092).*

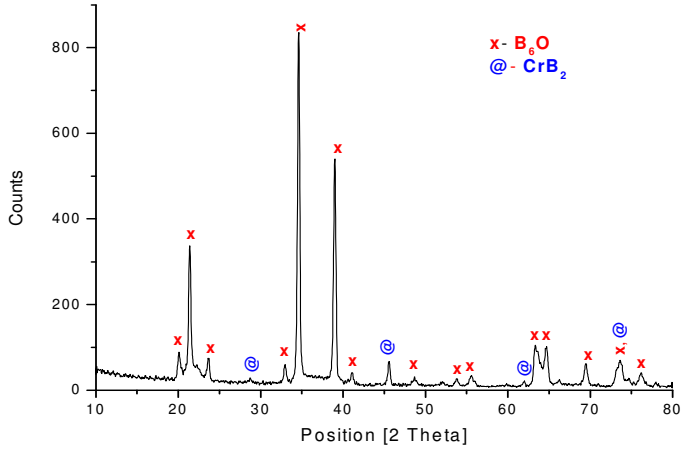

Fig4.15: *XRD pattern of sintered B_6O material with 1.5wt% CrO_3 (00-050-1505, 00-034-0369).*

Fig 4.16 & 4.17 show the SEM photographs of the polished sintered materials, which were prepared at 1850^{o}C for 20 minutes. It can be observed from the micrographs that a homogeneous distribution of the binder phase was obtained in both materials. EDS on the

white phase on the images shows the present of the boride second phase in the matrix. Pores which could be inherent in the matrix due to the decomposition reactions at the sintering temperature were seen as dark spots in the samples. At higher magnifications, one could observe some grain growth in the hot pressed compacts which may be connected to the dwelling time (20 minutes) at the sintering temperature for the B_6O+CrO_3 material. Therefore, hardness measurement done on this B_6O-rich area will yield a high value compared to other parts in the composite.

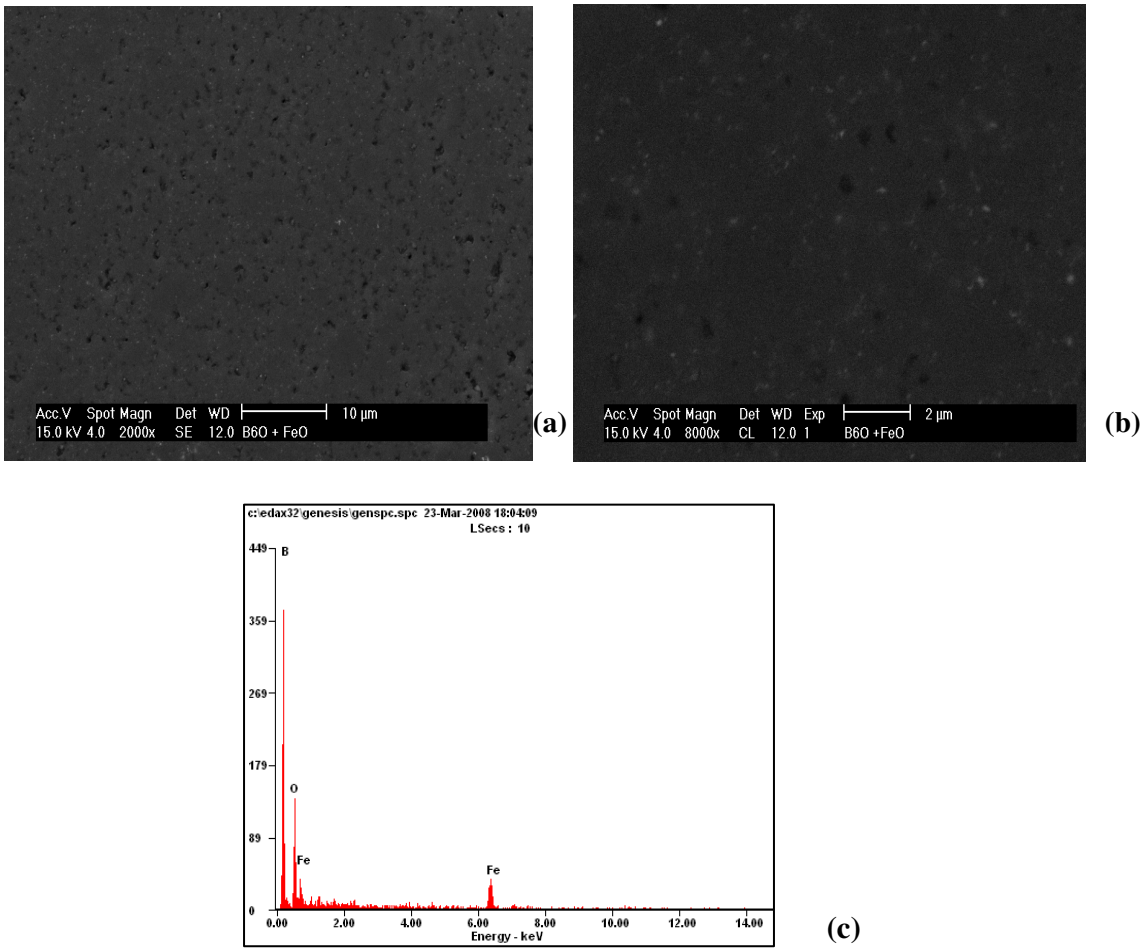

Fig*4.16:* *SEM image of the (B_6O + FeO) material sintered at 1850^{o}C for 20 min (a) x2000 (b) x8000 (c) EDS on grey phase (d) EDS on white phase.*

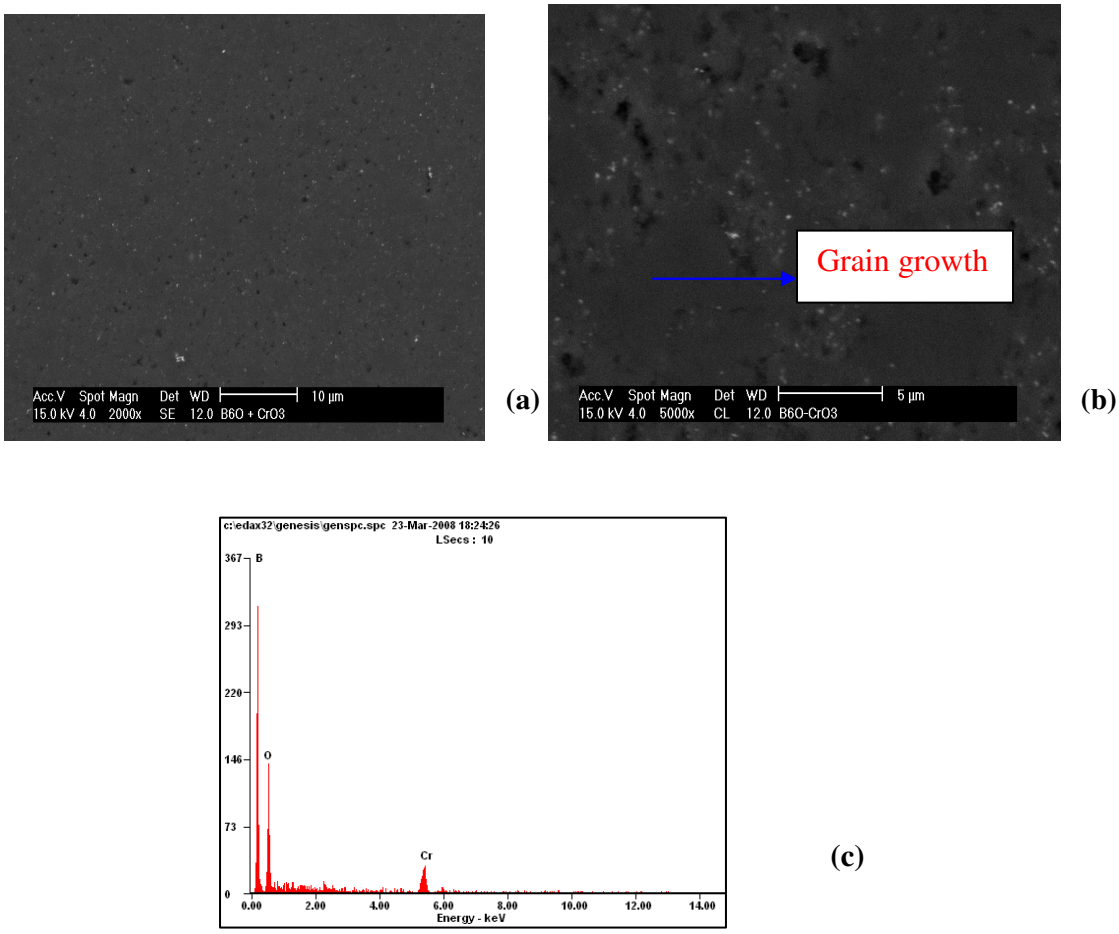

Fig4.17: *SEM image of the (B_6O + CrO_3) material sintered at 1850°C for 20 min (a) x2000 (b) x5000 (c) EDS on white phase*

Table 4.4 gives a summary of the properties obtained for each sample. It can be noted that the open porosity present in the composite is less compared with that of the pure B_6O, implying that the additives improve the densification of the boron suboxide composite. Hardness and fracture toughness measurement were performed on the samples by means of a Vickers indentation method. The loading force on the microhardness tester was set at 5kg-force. Higher hardness and fracture toughness were obtained for the B_6O+CrO_3 composite which gives an indication that chromium

containing B_6O materials might yield better combination of properties and a potential material with good potential for industrial application.

Table 4.4*: Properties of the transition metal oxide materials sintered at 1850^oC for 20 minutes*

Sample name	***Hot pressing conditions***	***Density (g/cm^3)***	***Open Porosity (%)***	***Vickers hardness (GPa)***	***Fracture Toughness (MPa.m.$^{0.5}$)***
Pure B_6O	1900^{o}C, 50 MPa, 20 min.	2.46	3.7	30.2 ± 1.0 (*1 kg*)	Brittle
B_6O+1.50*wt%* FeO	1850^{o}C, 50 MPa, 20 min.	2.51	0.9	28.4 ± 1.4 *(5Kg)*	3.1 ± 0.2
B_6O+2.06*wt%* CrO_3	1850^{o}C, 50 MPa, 20 min.	2.53	1.2	30.4±2.6 *(5Kg)*	4.8 ± 0.3

4.4.2 *Transition metal boride additives*

In this work, iron boride (FeB) was used as a representative transition metal boride added to boron suboxide (B_6O) powder. After mixing 1.40*wt%* iron boride with boron suboxide powder the mixture was hot pressed at 1850^{o}C under a pressure of 50 MPa for 20 minutes. From the XRD patterns obtained it was discovered that the iron boride (FeB) crystalline grain boundary phase was retained beside B_6O for both the mixed powder and the sintered compact. No variation of lattice constants for both B_6O and FeB were observed, suggesting that neither formation of solid solution nor new compound is

formed under the sintering conditions employed. XRD pattern of the hot pressed composite is shown in fig 4.18.

The measured density and mechanical properties of the composite are given in table 4.5. Density higher than 96% of the theoretical density was achieved. The high density achieved is connected with the hot pressing temperature used which resulted in high amount of liquid phase present to accelerate mass transport via liquid phase sintering. Additionally, the open porosity remaining in this composite has 89% reduction when compared with that of the hot pressed B_6O. This indicates the efficiency of liquid phase assisted sintering.

The Vickers hardness (Hv_1) value of 30.8 GPa measured for this composite is similar to that of the hot pressed B_6O (30.2 GPa) under the same load of 1kg, with a high fracture toughness of 7.6 $MPam^{0.5}$. The addition of 1.4*wt%* of FeB to boron suboxide powder has resulted into a significant improvement of the fracture toughness considering the brittleness of B_6O material.

Table4.5*: Properties of the composite (B_6O + FeB) sintered at 1850^oC for 20 min*

Sample name	***Hot pressing Conditions***	***Density (g/cm^3)***	***Open Porosity (%)***	***Vickers hardness (GPa)***	***Fracture Toughness ($MPa.m.^{0.5}$)***
Pure B_6O	1900^{o}C, 50 MPa, 20 min.	2.46	3.7	**30.2 ± 1.0 (*1 kg*)**	brittle
B_6O+1.40*wt%* FeB	1850^{o}C, 50 MPa, 20 min.	2.56	0.4	**30.8±2.6 (*1 kg*)** 27.2±2.2 *(5Kg)*	7.6 ± 1.1

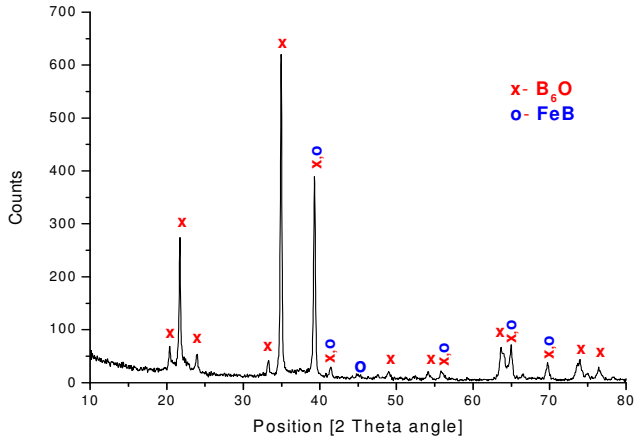

Fig4.18: *XRD pattern of sintered B_6O material with 1.40wt% FeB*

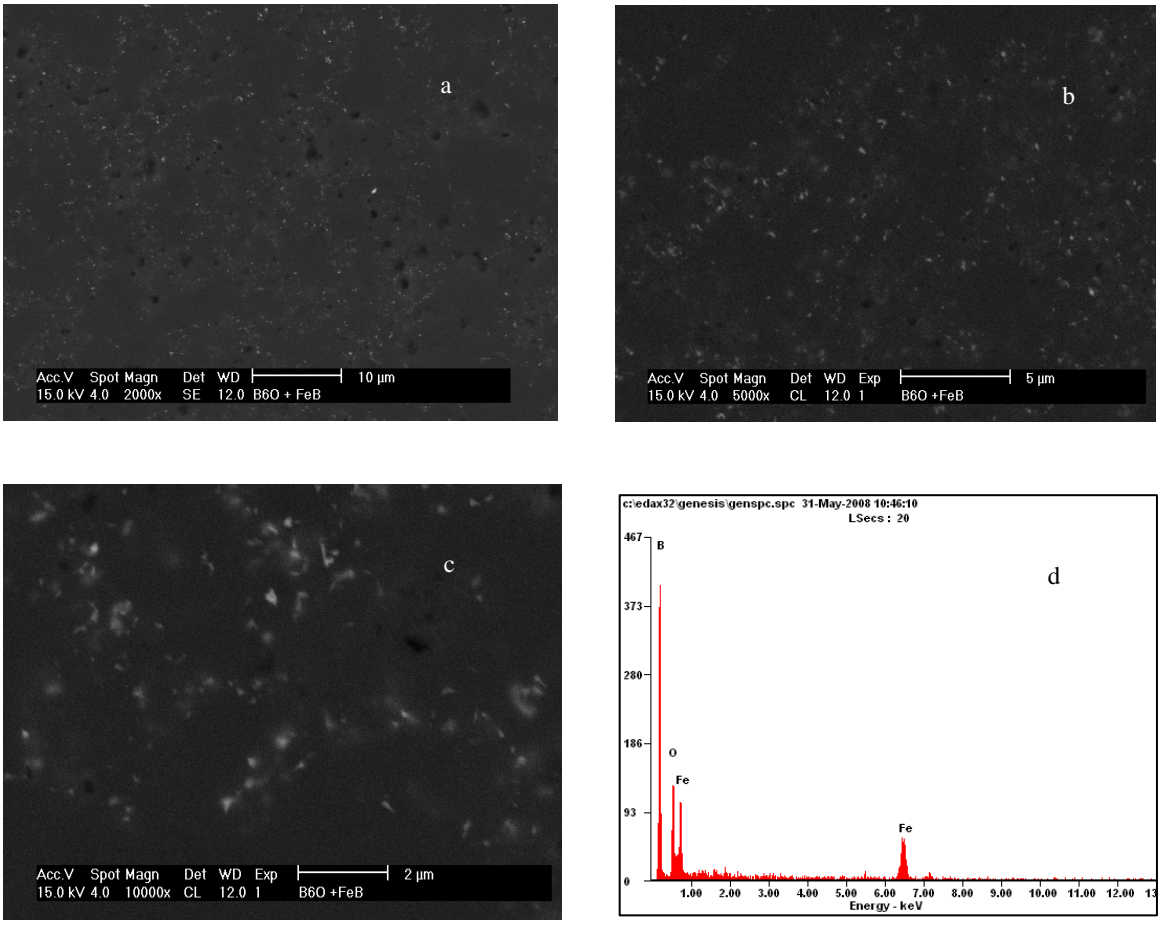

Fig4.19: *SEM image of the (B_6O + FeB) material sintered at 1850^{o}C for 20 min (a) x2000 (b) x5000 (c) x10000 (d) EDS on white phase.*

The SEM image in fig 4.19 shows that the material had a nearly homogeneous distribution of the binder phase and EDX analyses revealed that the sintered material has two phases (B_6O & FeB) with some pores retained in the sample which might be due to decomposition at the sintering temperature or pull-out of the softer secondary phase during grinding of the sample. The FeB is seen to form clusters around the grains of B_6O, therefore the hardness values obtained at this area having FeB clusters was low while the fracture toughness was high. At higher magnification, one could observe little or no grain growth in the hot pressed compact.

By comparison, it was observed that the B_6O materials with iron derivatives show a better distribution of the boride secondary phase than those materials with chromium derivatives. On the other hand, a good combination of hardness-to-fracture toughness properties were achieved for the B_6O materials with chromium derivatives. Although the reason for these differences could not be established in this work, it is presumed that further optimization of the additive content and composition are needed to better understand the microstructure formation, mechanical properties and toughening mechanisms existing in these materials, thereby enhancing the probability of producing materials with better properties useful for industrial applications.

4.4.4 B_6O materials with r*are-earth metal oxide additives*

The development of thermodynamic data for B_6O at high temperatures has made possible the prediction of the stability of the phases present in B_6O in the presence of different other materials. On this basis, it was predicted that rare earth oxides will be at equilibrium with B_6O considering the Gibbs free energy of the reaction and can form an oxide secondary phase. This phase forms a liquid during the sintering process, through interaction with some remaining B_2O_3 (A. Andrews *et al.,* 2008).

B_6O composite materials containing 1.5*wt%* Sc_2O_3, 2.5*wt%* La_2O_3 and 1.5*wt%* Yb_2O_3 respectively were additionally produced at a hot pressing temperature of 1850^oC for 20 minutes. The admixed powders were analyzed using XRD to identify the phases present before sintering *(pattern shown in Appendix B)*. Figure 4.20, 4.21 & 4.22 shows the phase composition of the sintered material. For B_6O+Sc_2O_3 composite, only peaks for B_6O were found, which implies that the grain boundary phase was amorphous and could not be detected by XRD technique. On the other hand, in the B_6O+La_2O_3 and B_6O+Yb_2O_3 composites, contrary to the thermodynamic prediction, boride phase (LaB_6 & YbB_6) were formed; suggesting that oxidation of B_6O occurred at the sintering temperature, which could bring about an improvement in the oxygen stoichiometry of the boron suboxide phase. The other explanation is that a strong reduction occurred during the sintering process as shown in equation 4.3.

$$B_6O + 0.5La_2O_3 + C \rightarrow LaB_6 + 2.5CO \quad \ldots\ldots\ldots\ldots\ldots\ldots \quad 4.3$$

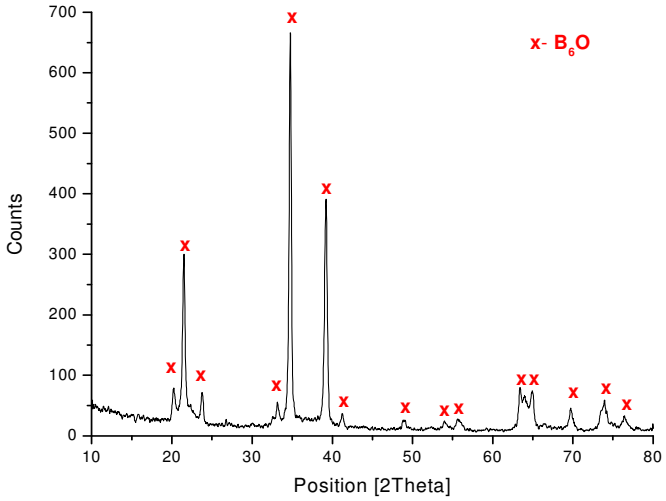

Fig4.20: *XRD pattern of sintered B_6O material with 1.5wt% Sc_2O_3*

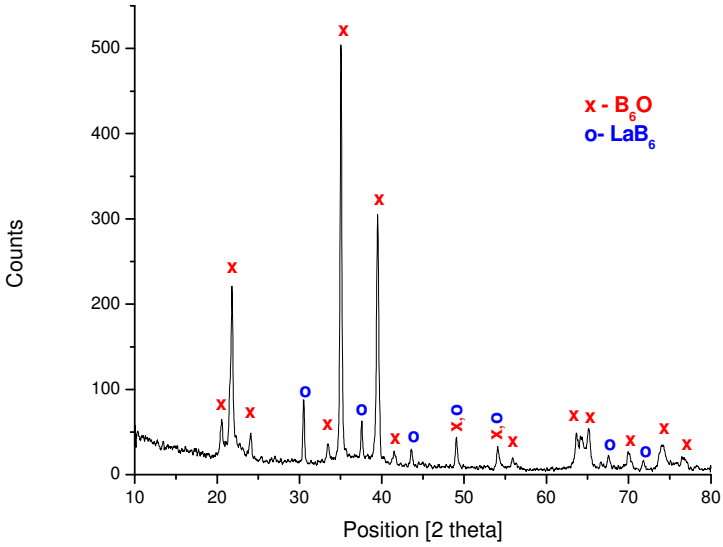

Fig4.21: *XRD pattern of B_6O sintered B_6O material with 2.5wt% La_2O_3 (00-050-1505, 01-034-0427).*

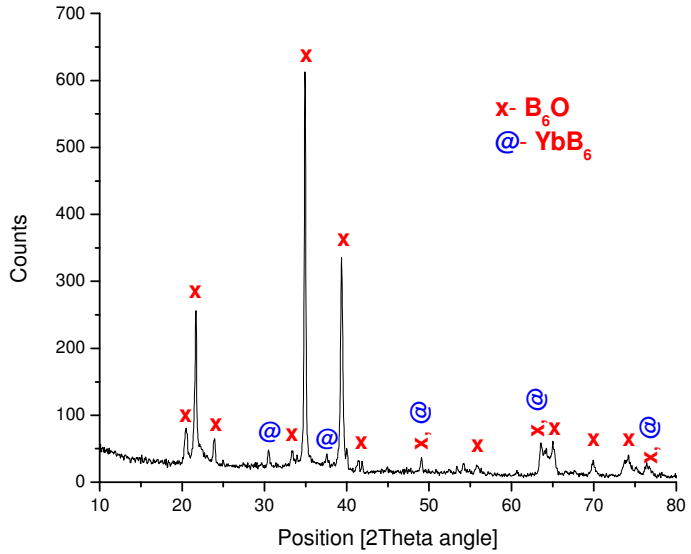

Fig4.22: *XRD pattern of sintered B_6O material with 1.5wt% Yb_2O_3 (00-050-1505, 01-025-1343).*

Fig 4.23, 4.24 & 4.25 shows the backscatter images of the hot pressed composite materials. It could be seen from the micrographs for the B_6O+Sc_2O_3 composite, that there was segregation of liquid phase in the microstructure which might be due to the presence of liquid B_2O_3 or bad wetting behaviour of Sc_2O_3. Energy dispersive X-ray (EDX) analysis shows that the grey phase represents B_6O, while the pockets of white phase constitute an amorphous Sc-B-Mg-Al-O compound. The Mg detected originates from the boron powder used to produce B_6O, while Al might come from the mixing of the powder in an alumina vessel. It was also noted that there was segregation of the secondary phase in the B_6O+ La_2O_3 composite, with evidence of porosity in the micrograph at higher magnification. The segregation also gives an indication of the bad wetting behaviour of La_2O_3 on B_6O. The B_6O+ Yb_2O_3 composite has much finer B_6O grains (no grain growth observed) with an even distribution of the secondary phase although agglomerates of this

binder phase were also present. The microstructure also shows that this hot pressed material was nearly dense without any evidence of porosity.

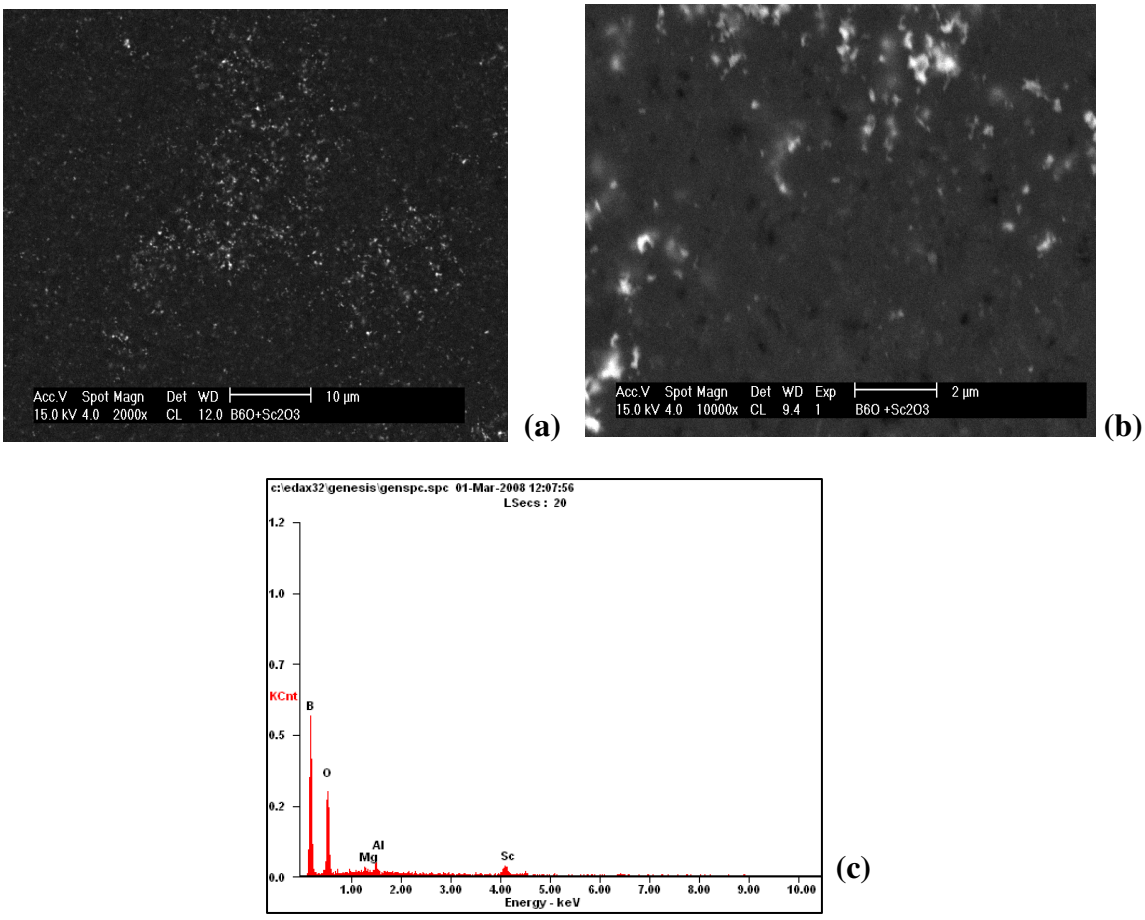

Fig4.23: *SEM image of the (B_6O + Sc_2O_3) material sintered at 1850^{o}C (a) x2000 (b) x10000 (c) EDS on white phase.*

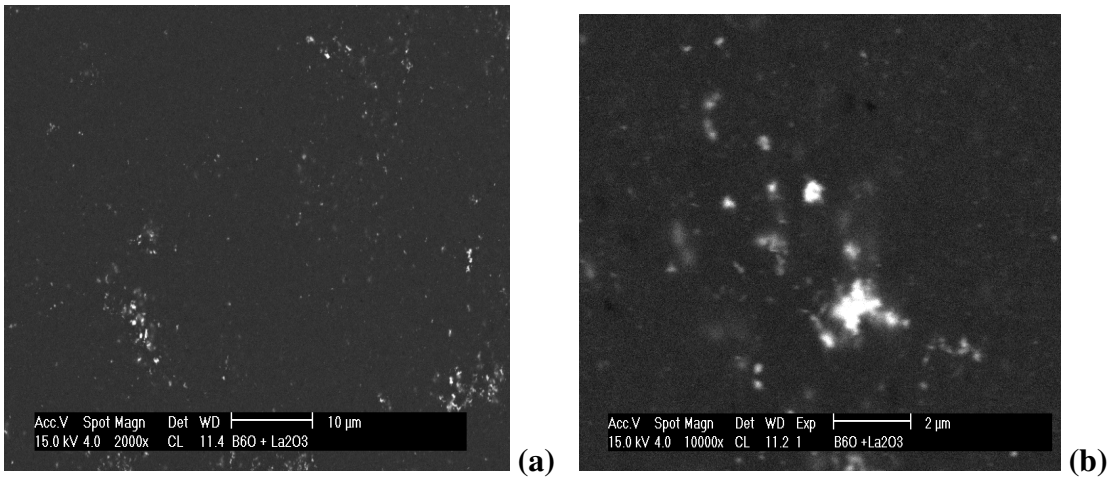

(a) **(b)**

Fig4.24: *SEM image of the (B_6O + La_2O_3) material sintered at 1850°C for 20 min*

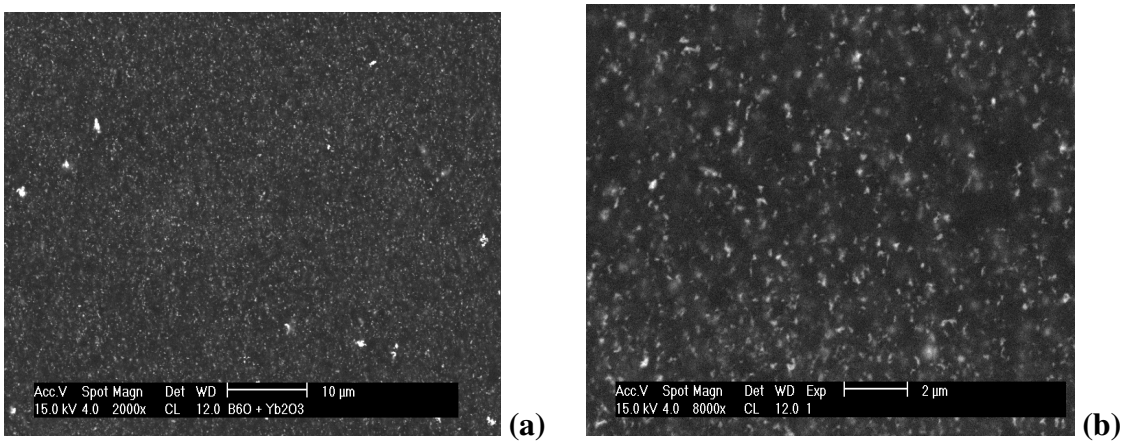

(a) **(b)**

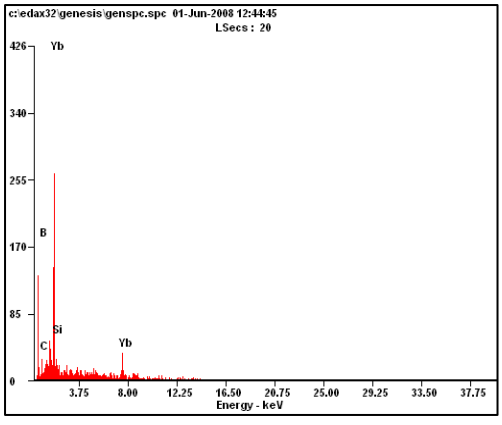

(c)

Fig4.25: *SEM image of the (B_6O +Yb_2O_3) material sintered at 1850°C for 20 min*

Table 4.6 summarizes the mechanical properties of the sintered material at 1850°C for 20 minutes. The density of the composites was better than that of the pure B_6O, which confirms the influence of the additives in assisting the densification process. Densities higher than 97% of their theoretical densities were achieved. The Vickers hardnesses measured under a load of 5kg for all the hot pressed materials were similar. Also, the fracture toughness values were also similar except for the B_6O+ Yb_2O_3 composite where lower fracture toughness was obtained. This might be connected to the low amount of open porosity which could have assisted in arresting crack propagation.

Table 4.6*: Properties of rare-earth oxide composites sintered at 1850°C for 20 min*

Sample name	***Hot pressing conditions***	***Density (g/cm^3)***	***Open Porosity (%)***	***Vickers hardness (GPa)***	***Fracture Toughness (MPa.m.$^{0.5}$)***
Pure B_6O	1900°C, 50 MPa, 20 min.	2.46	3.7	30.2 ± 1.0 (*1 kg*)	brittle
B_6O+1.50*wt%* Sc_2O_3	1850°C, 50 MPa, 20 min.	2.48	1.6	31.6±0.9 *(5Kg)*	5.6±0.2
B_6O+2.50*wt%* La_2O_3	1850°C, 80 MPa, 20 min.	2.47	2.1	31.0±1.8 *(5Kg)*	5.6 ±0.8
B_6O+1.50*wt%* Yb_2O_3	1850°C, 80 MPa, 20 min.	2.51	0.9	30.5±1.7 *(5Kg)*	3.9±0.8

CHAPTER FIVE

5.0 DISCUSSION

This section gives detailed explanation of the results obtained in this work, in terms of the relationship between the microstructure, densification, hardness and fracture toughness of the various composites produced.

5.1 DENSIFICATION AND MICROSTRUCTURE OF MATERIALS

Although the synthesis of boron suboxide (B_6O) at or near ambient pressure comes with the advantage of reduced cost of production and avoids the risk of working with gases at high pressure, it is related to the formation of a non-stoichiometric B_6O compound, generally oxygen deficient (B_6O_x, $x < 0.9$). For brevity, a nominal formula B_6O has been used in this research work.

Theoretical densities of the hot pressed materials were calculated based on the rule of mixtures (*Formula in Appendix A3*). Errors in these calculations are inevitable since the density of B_6O changes with oxygen and B_2O_3 content. Fig 5.1 shows the dependence of the theoretical density on the oxygen content (**x)** in B_6O. The theoretical values in the figure were adapted from International Centre for Diffraction Data (ICSD) card. It can be seen from the graph that the theoretical density increases with increasing oxygen content (**x**). The presence of B_2O_3 also lowers the theoretical density of B_6O (*Shabalala, T. C. 2007).* In this work, the theoretical density of B_6O has been assumed to be 2.55 g/cm^3, which corresponding to oxygen content of 0.9. Therefore the determined value would be close to an upper limit of the density. This oxygen content can only be achieved

at high pressure sintering condition. It was also assumed that all the additives in the powder completely transformed to their respective secondary phase after sintering. Another assumption made in the calculation of theoretical densities was the weight percent of B_2O_3 (1 *wt. %*) which is present in the starting powder. A summary of the densities and theoretical densities obtained for the various hot pressed materials is given in table A3 (Appendix A).

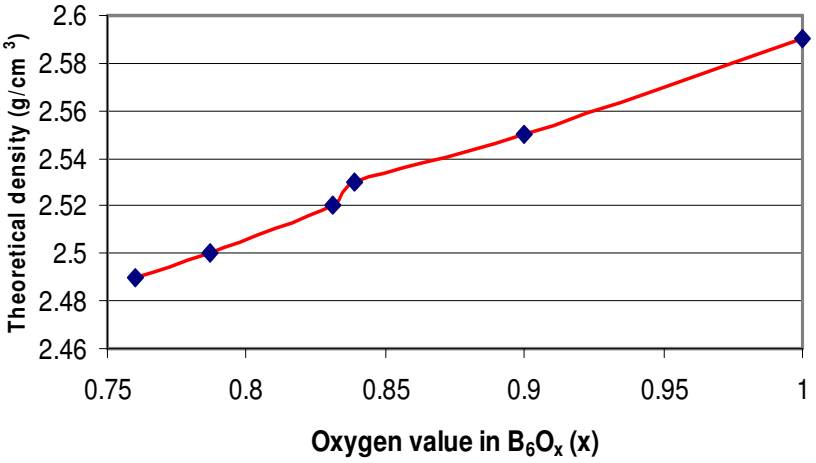

Fig5.2: *Dependence of the theoretical density on x in B_6Ox. Theoretical densities have been taken from ICSD data cards 81-2192, 87-2286, 87-2287, 87-2288 & 50-1505.*

B_6O is known to be difficult to densify, especially through self-sintering, even if aided by hot pressing or ultra-high pressures. Previous hot pressing studies [Bairamashvili *et al.,* (1979), Kayhan I.O. and Inal O.T (1999), Brodhag C and. Thevenot F (1986) and Shabalala, T. C. (2007)] concerning the densification of boron suboxide (B_6O) powders, made from mixing amorphous boron with boron oxide or with zinc oxide, have produced

B_6O materials with densities in the range of 85-97% theoretical density. These materials were hot pressed either under vacuum or argon conditions at temperatures in the range of 1600°C- 1900°C. Fig 5.2 shows a comparison between the densities of hot-pressed B_6O materials made in this study and other studies. In this study, the density of pure B_6O obtained was 2.46 g/cm^3, which was 96.5% of the theoretical density and agrees with the value obtained by Kayhan I.O.and Inal O.T (1999). The difference between the value obtained in this work and others could be connected with the high amount of porosity in the sintered material as a result of B_2O_3 present in the starting powder. It must be stated that the presence of 1*wt*% B_2O_3 in the B_6O powder will cause a reduction of 0.4% in the overall density of the B_6O material.

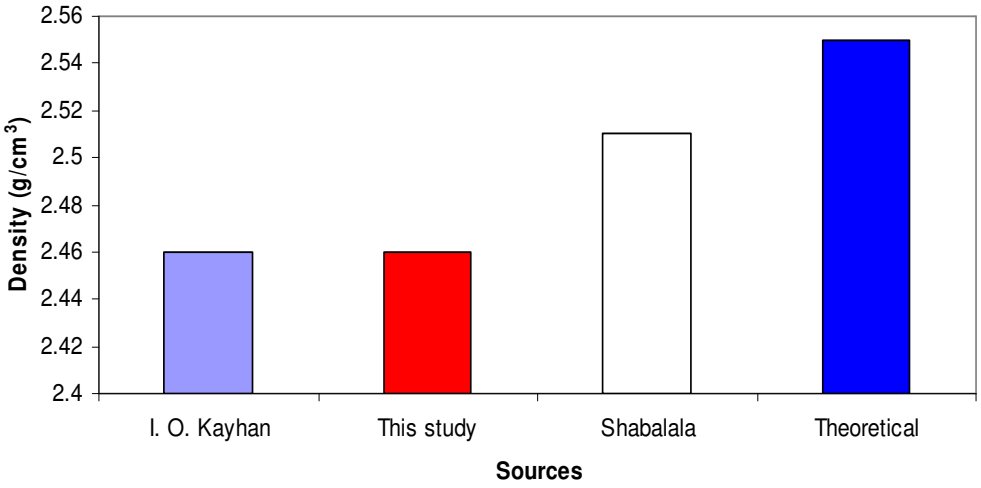

Fig5.3: *Comparison of the density of hot-pressed B_6O obtained from different studies*

The Optical image (see fig 5.3) of this hot pressed B_6O sample shows some small holes representing open porosity (3.7%). It is possible that the small amount of B_2O_3, which may have volatilized at high temperatures, partly acts as the source of small pores in the microstructure, resulting in surface layers with higher porosity than in the centre of the

samples (as *shown in the Appendix C.6 & C.7*) . Part of the pores observed in the image may also be caused by the removal of the remaining B_2O_3 during polishing or due to bad polishing (The figure shows clearly the scratches from the bad polishing). The density of the hot pressed B_6O samples does not reach 100% theoretical. The theoretical density of B_2O_3 is 2.46 g/cm^3, which is less than that of B_6O at 2.55 g/cm^3; therefore a small amount of B_2O_3 in the samples will lower the overall theoretical density of a hot pressed B_6O sample.

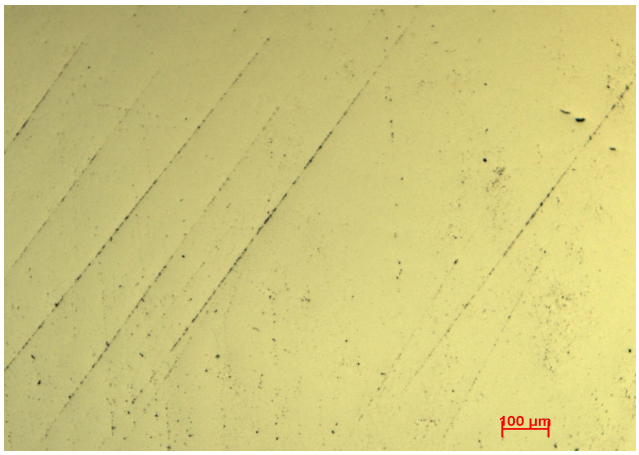

Fig5.4 : Optical image of B_6O sample hot pressed at 1900^{o}C

An ultra-high pressure high temperature study, concerning the sintering of B_6O at pressures in the range of 3-5 GPa, done by Itoh *et al*. (1998), also did not produce fully dense materials. The density of the materials was reported to be above 95% theoretical. Therefore, the use of ultra-high pressures does not guarantee a completely dense material. Petrak *et al*. (1974) claimed to have produced B_6O materials with densities greater than 99% of theoretical via reactive hot pressing. A fully dense B_6O material made by hot pressing, with density of 2.60 g/cm^3, was reported by Goosey (1974), although this density is higher than the theoretical density.

The synthesized B_6O mixed with different additives (drawn from transition metals and rare-earth compounds) were hot pressed at 1850°C for 20 minutes, resulted in higher densification of the materials, compared to the pure B_6O sintered at 1900°C. XRD patterns of the sintered materials show the formation of a boride secondary phase, and an amorphous phase for the Sc_2O_3 additive. The theoretical density of the composites was calculated (see Appendix A.3) to ascertain the percentage densification obtained by the hot pressing process. It was assumed that all the additives in the powder completely transformed to their respective secondary phase after sintering. Table 5.1 compares the density of each material measured with respect to the theoretical density calculated. .

Table 5. 1*: Densification properties of B_6O materials.*

Material	**Vol% of Additives**	**Density measured**	**Theoretical density**	**Open Porosity (%)**	**% of Theoretical density**
B_6O	-	2.46	2.53	3.7	96.5
B_6O+ 1.17wt% Fe	0.4	2.53	2.57	1.1	98.4
B_6O+ 1.07wt% Cr	0.4	2.57	2.57	0.7	100
B_6O+ 1.33wt% Co	0.4	2.53	2.58	1.2	98.1
B_6O+ 1.50wt% FeO	0.7	2.51	2.57	0.9	97.7
B_6O+ 2.06wt% CrO_3	2.0	2.53	2.57	1.2	98.4
B_6O+ 1.40wt% FeB	0.5	2.56	2.57	0.4	99.6
B_6O+ 1.50wt% Sc_2O_3	1.0	2.48	2.56	1.6	96.9
B_6O+ 2.50wt% La_2O_3	1.0	2.47	2.58	2.1	95.7
B_6O+ 1.50wt% Yb_2O_3	0.4	2.51	2.58	0.9	97.3

There are two possible explanations for the improvement in the densities obtained for the materials; one is that the additives form a liquid phase in which B_6O partially dissolves,

and which assists with the densification of the materials at the sintering temperature and which recrystallizes during cooling to form a boride phase at the grain boundaries as shown in the XRD patterns, or on the other hand, the formation of B_2O_3 as a result of the oxidation reaction occurring in most cases between the B_6O and the sintering additives, suggest that diffusion would be aided, thereby improving the densification behaviour. Hence, a precise control of the oxygen content would be necessary for the reproducible densification of the materials.

Fig 5.4 shows the graph of the percentage densification measured for B_6O and iron containing materials hot pressed at 1850^{o}C. To understand and properly explain the densification process of these materials, one needs to consider the phase diagram of Fe-B system which is shown in fig 5.5. The composition under consideration has been indicated with an arrow in fig 5.5. According to the phase diagram, at 1850^{o}C there is a liquid phase formed, which accelerate mass transport and therefore improve densification. Hence, densities more than 97% of theoretical densities were achieved. By comparison, the iron containing materials had higher densification than the pure hot B_6O. However, high amount of B_2O_3 in the system can also have a negative effect on the densification because it has high vapour pressure and result in some decomposition of the materials.

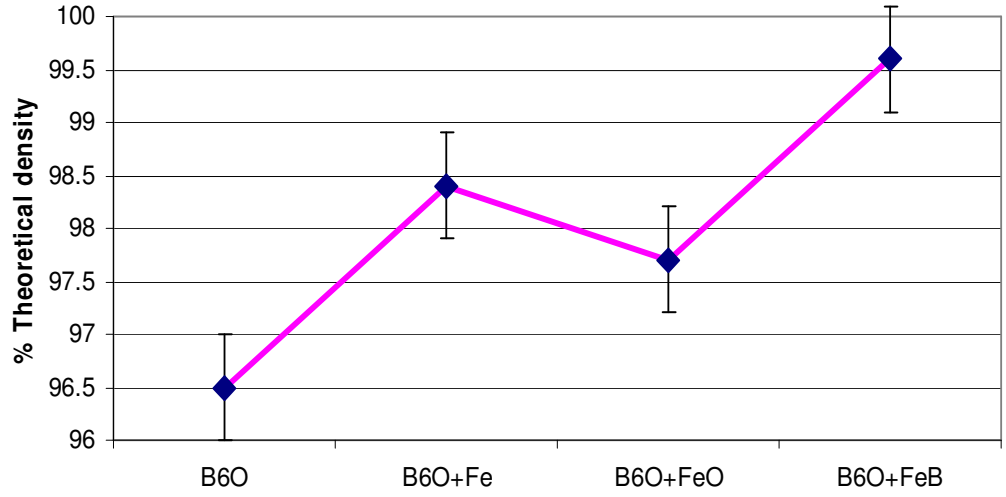

Fig5.5: *% Theoretical density of B_6O and iron containing materials hot pressed at 1850°C.*

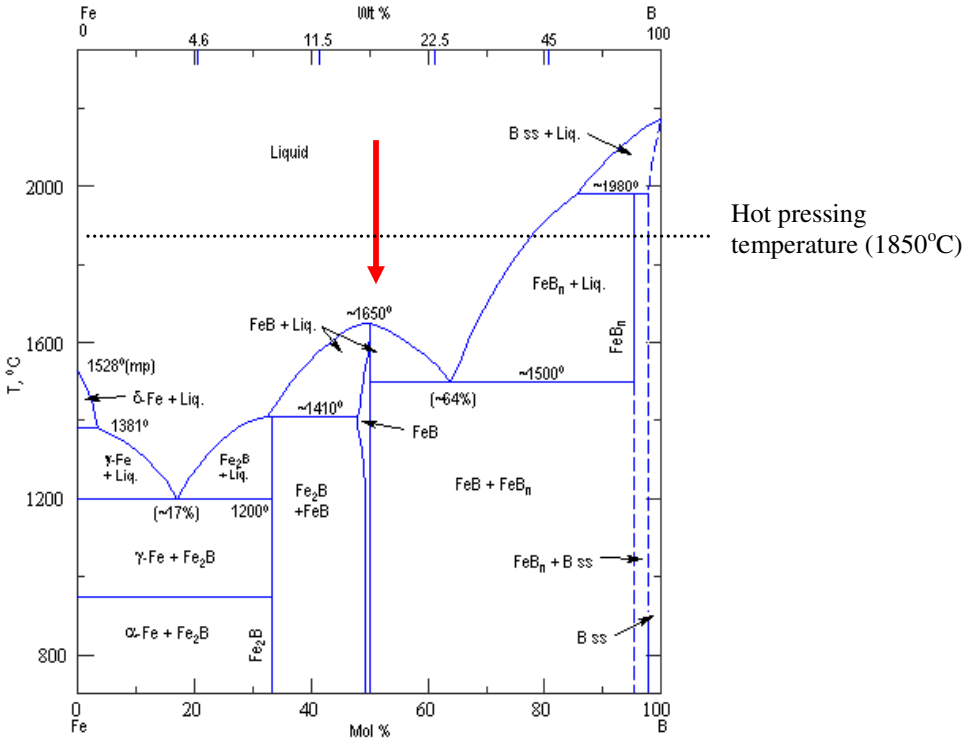

Fig5.6*: Phase diagram of Fe-B system.* (Massalski *et al.,* 1986). *The arrow represents the composite under consideration*

From the graph in fig 5.4, it is obvious that B_6O+FeO composite had the least densification, while a densification of 99.6% was obtained for the B_6O+FeB material. Although SEM images of these materials shown in chapter 4 indicate homogeneous distribution of iron boride secondary phase within the matrix, yet the densification achieved differs in each material. The difference in the densification achieved is connected to the amount of B_2O_3 produced by the interaction of these additives with B_6O. With the assumption of 1 wt% of B_2O_3 in the starting powder, it was deduced (see equation 5.1 & 5.2) that more B_2O_3 was produced in the B_6O+Fe & B_6O+FeO composites, while a constant value was present in the B_6O+FeB composite, where there was no further formation of B_2O_3 through the interaction of B_6O and FeB.

$$16Fe + 3B_6O \rightarrow B_2O_3 + 16FeB \quad \ldots\ldots\ldots\ldots\ldots\ldots\ldots\ldots \quad 5.1$$

$$16FeO + 5B_6O \rightarrow 7B_2O_3 + 16FeB \quad \ldots\ldots\ldots\ldots\ldots\ldots\ldots \quad 5.2$$

Considering the above reactions, it is expected that the same mol% of additive (Fe or FeO) will produce the same volume of second phase after hot pressing (FeB), but for one (1) part by volume of B_2O_3 produced for the B_6O+Fe composite, seven (7) parts by volume will be produced in the B_6O+FeO composite. With the addition of 1.17 *wt%* Fe to the B_6O powder, 0.07 *wt%* B_2O_3 was produced, while 1.50 *wt%* FeO added resulted into the formation of 0.7 *wt%* B_2O_3 after sintering at temperature of 1850^oC for 20 minutes. This gives an indication of the higher amount of B_2O_3 in the B_6O+FeO material. The theoretical density of B_2O_3 is 2.46 g/cm^3, which is less than that of B_6O at 2.55 g/cm^3; therefore a small amount of B_2O_3 in the samples may lower the overall theoretical density

of a hot pressed B_6O sample. Furthermore, some of the B_2O_3 will evaporate at the sintering temperature.

The influence of chromium and CrO_3 content in the starting composition on densification was also studied (fig 5.6). The phase diagram of the Cr-B system is shown in fig 5.7. The type of chromium boride (CrB_2) form was identified with the XRD pattern shown in fig 4.10, which gives an indication of the composition under consideration (see arrow in fig 5.7). According to the phase diagram, at 1850^{o}C there will not be any liquid present in the material at sintering temperature. Nevertheless, there is some level of solubility of B_6O in the system resulting into the formation of transient liquid or it could be that the composition is not pure CrB_2 and therefore a liquid is formed which lowers the melting point in this system, creating enough liquid for densification to occur via liquid phase sintering.

Densities more than 98% of theoretical densities were achieved. A higher densification was observed for the B_6O+Cr composite compared to the B_6O+CrO_3 composite. This is also connected with the high amount of B_2O_3 produced from the interaction between B_6O and CrO_3. It is expected to produce 10 times the amount of B_2O_3 produced in the B_6O+Cr composite (equation 5.3 & 5.4).

$$8Cr + 3B_6O \rightarrow B_2O_3 + 8CrB_2 \quad \text{..... 5.3}$$

$$8CrO_3 + 6B_6O \rightarrow 10B_2O_3 + 8CrB_2 \quad \text{..... 5.4}$$

The addition of 1.07 *wt%* Cr to the B_6O powder increased the amount of B_2O_3 in the final sintered material by 0.13 *wt%*. However, the addition of 1.50 *wt%* CrO_3 in the B_6O powder resulted into the formation of 1.9 *wt%* B_2O_3 after sintering at temperature of 1850°C for 20 minutes. As earlier stated, the presence of 1*wt%* B_2O_3 in the B_6O powder will cause a reduction of 0.4% in the overall density of the B_6O material. This gives an indication of the effect of the higher amount of B_2O_3 on densification in the B_6O+CrO_3 material.

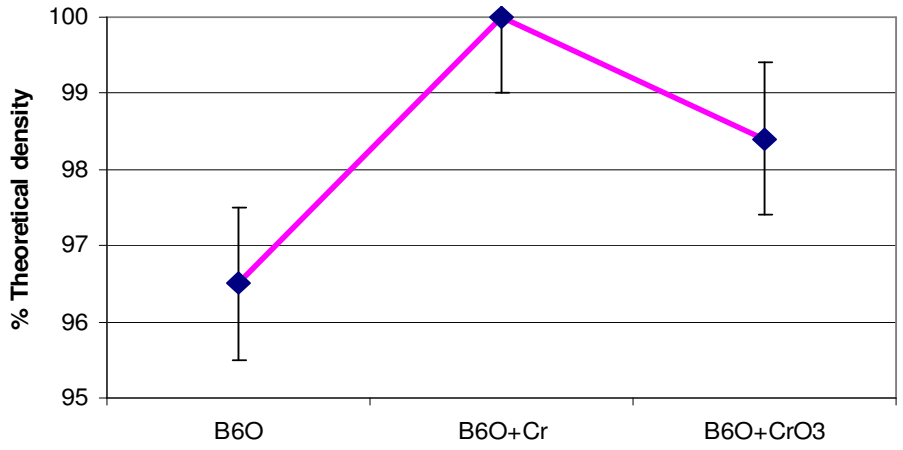

***Fig5.7: %** Densities of B_6O and chromium containing materials hot pressed at 1850°C, expressed on a percentage of corresponding theoretical density.*

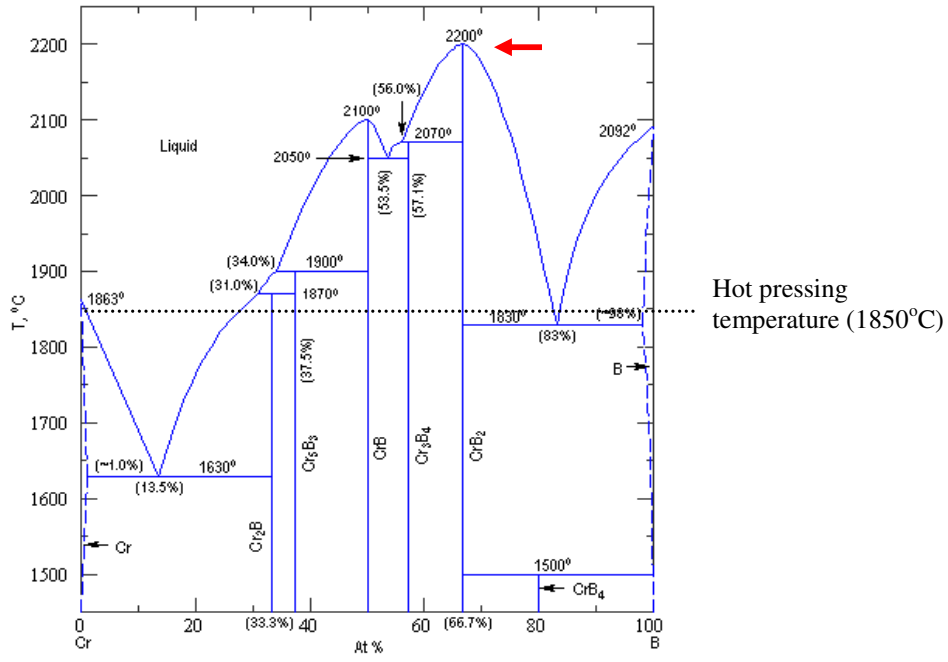

***Fig5.8**: Phase diagram of Cr-B system.* (Massalski *et. al.,* 1986). *The arrow represents the composition under consideration*.

SEM micrographs of the Cr-containing composites, shown in fig 5.8 revealed a non-homogeneous distribution of the boride second phase within the matrix. Although the B_6O+Cr composite was fully dense (2.57g/cm^3), yet at higher magnification some dark spots which represent pull-out of the binder phase were observed; these are formed as a result of incomplete polishing of the material. Since B_6O is a superhard material, it requires a long polishing time to obtain scratch free surface after grinding. Although the formation of liquid phase is strongly dependant on the B_2O_3 content, a high amount of liquid phase in the B_6O+CrO_3 composite at hot pressing temperature resulted in grain growth of the material.

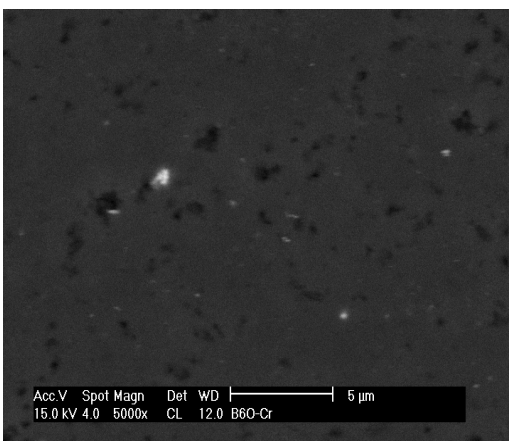

(a)

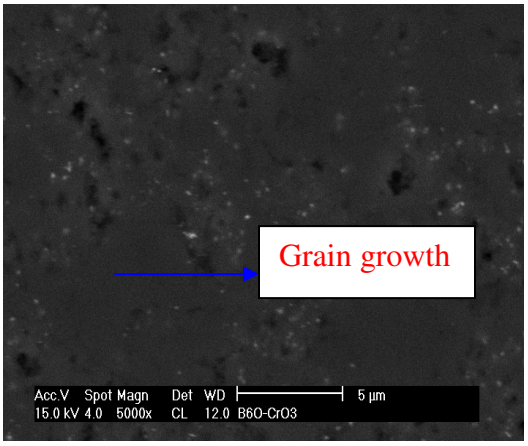

(b)

Fig5.9: *SEM image of materials sintered at 1850°C for 20 min (a) B_6O + Cr (b) B_6O + CrO_3*

B_6O material containing 1.33*wt%* cobalt was densified to nearly theoretical density by hot pressing at 1850°C under a pressure of 50 MPa for 20 minutes. The melting of cobalt-boron in the starting powder takes place below 1500°C (Fig. 5.9) which is far below the sintering temperature, suggesting that there is enough liquid phase present to accelerate mass transport thus improving densification. Hence, a nearly fully densified material was achieved. Densities more than 98% of theoretical were measured. The availability of high amount of liquid at lower temperatures resulted in exaggerated grain growth in the material, as shown in fig. 5.10.

The oxidation reaction between the B_6O and Co resulted into the formation of liquid phase, which recrystallises during cooling and forms cobalt boride (CoB) at the grain boundaries as described in equation 5.5. The type of cobalt boride formed will depend on the amount of boron dissolved in cobalt. The CoB secondary phase was homogeneously

distributed within the matrix, resulting into a good combination of hardness-fracture toughness properties (i.e., 33.9±2.2 GPa & 5.3 ± 0.8 MPa.m.$^{0.5}$).

$$16Co + 3B_6O \rightarrow B_2O_3 + 16CoB \text{ .... } 5.5$$

The combination of properties obtained for this material suggest that if this material is suitably prepared and optimized, it could be potentially used in cutting tool and other wear part applications in industry.

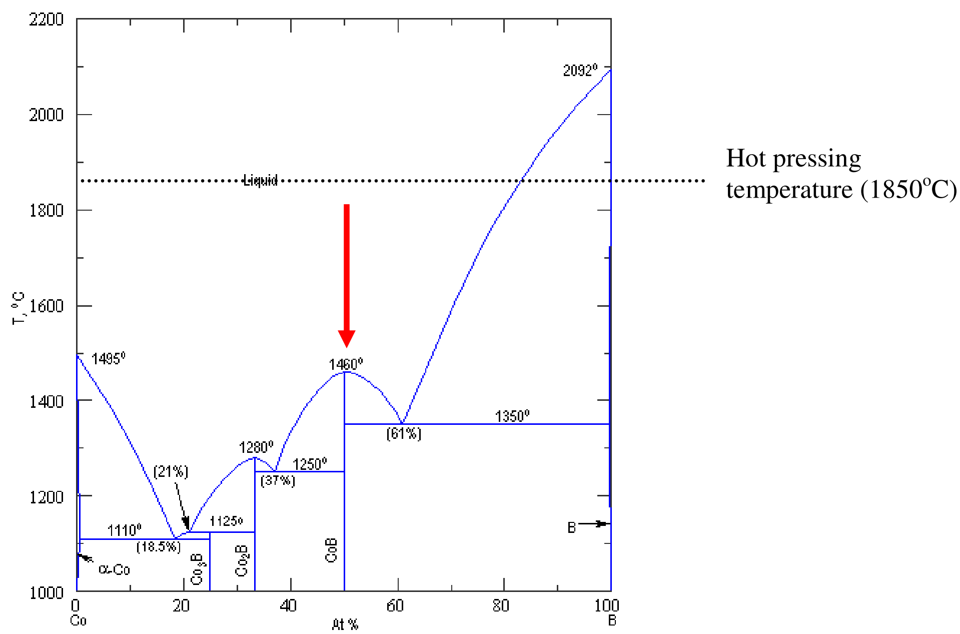

Fig5.10*: Phase diagram of Co-B system.* (Massalski *et. al.,* 1986). *The arrow represents the composite under consideration.*

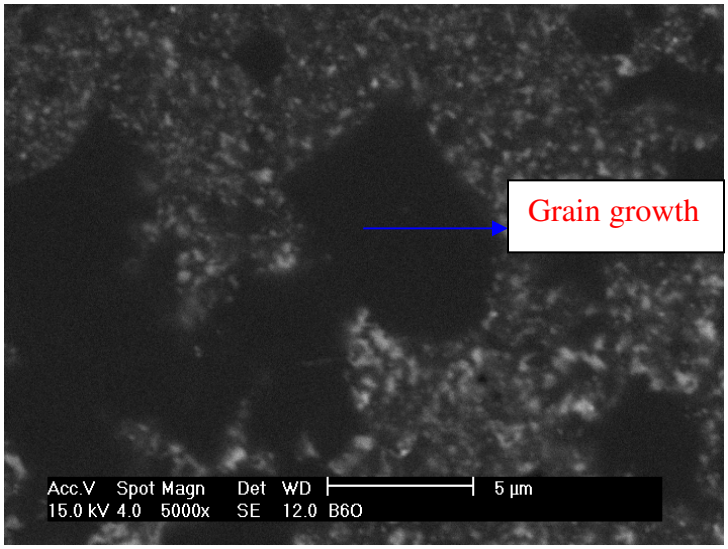

Fig5.11: *SEM image of the B_6O + Co material sintered at 1850^oC for 20 min*

Fig 5.11 shows a plot of percentage densification against B_6O of the rare-earth metal oxide containing materials. The trend of the densities obtained and the observed microstructures are an indication that these composites are to some extend densified via liquid phase sintering. A sharp increase in densification was observed from B_6O+La_2O_3 material to B_6O+Yb_2O_3 material. This trend is in agreement with the SEM images of these materials shown in fig 5.12. It could be observed from the microstructure that the higher the homogeneity of the distribution of the binder phase of the hot pressed material the higher the degree of densification.

In B_6O+La_2O_3 material, there was complete segregation (pockets) of liquid phase in the microstructure which might be due to bad wetting behaviour of La_2O_3 on B_6O. This liquid tends to decompose at sintering temperature leaving pores within the material, which has a negative influence on the densification at such temperature. Also the B_6O+Sc_2O_3 material had segregation of the secondary phase within the matrix, but less liquid compared to the B_6O+La_2O_3 composite. On the other hand the B_6O+ Yb_2O_3 composite had much finer B_6O grains (no grain growth observed) with an even distribution of the secondary phase. The microstructure also shows that this hot pressed material was nearly dense without any evidence of porosity.

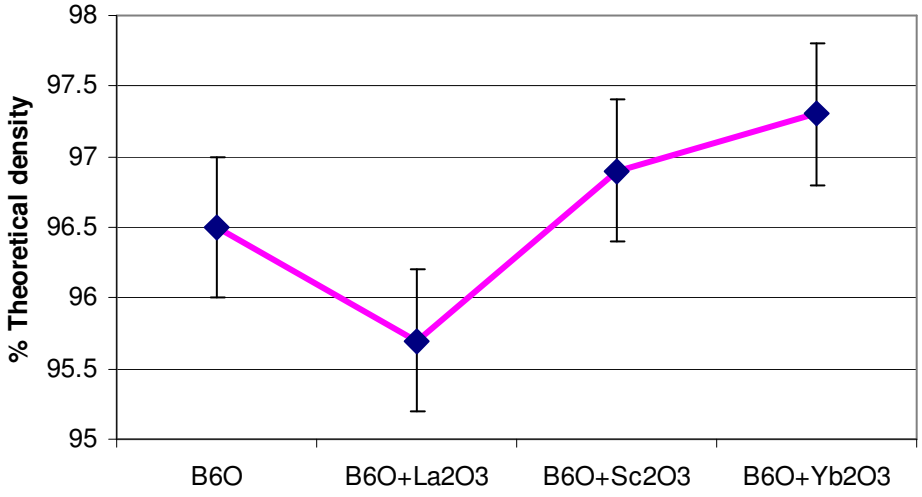

***Fig5.12:** % Theoretical density of B_6O and rare-earth metal oxide containing materials.*

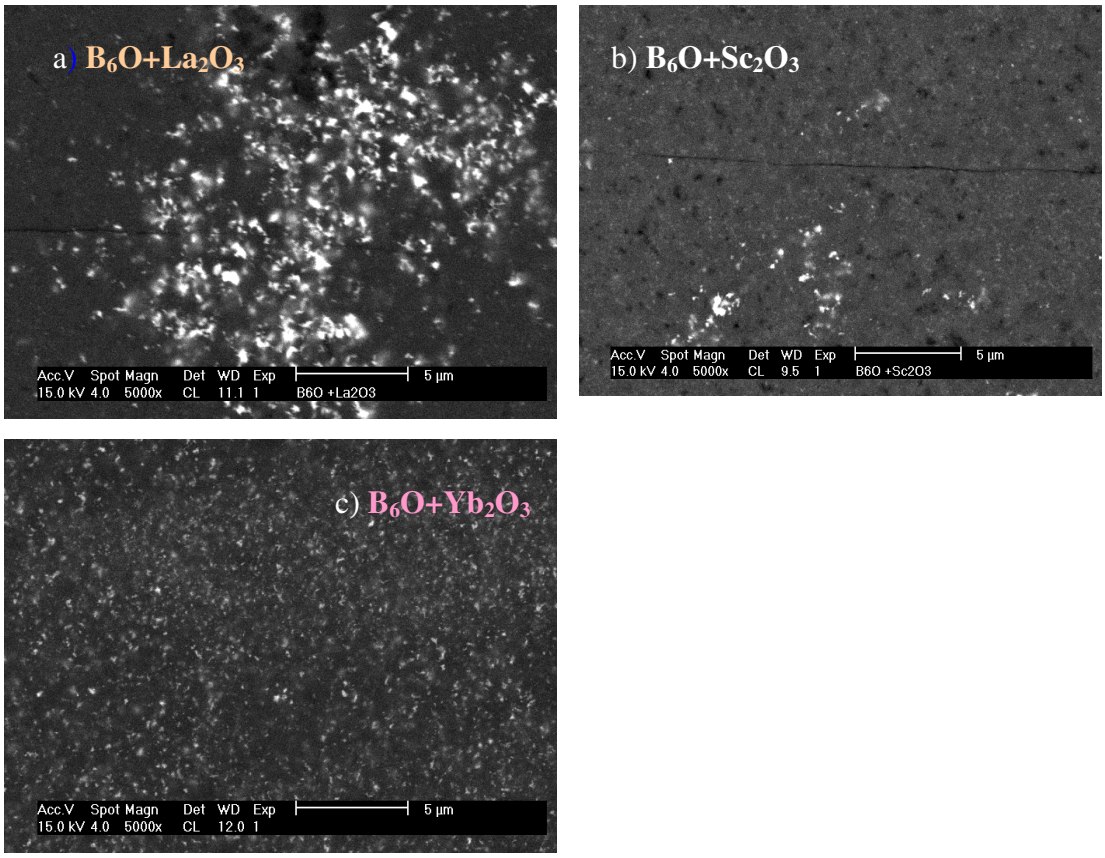

Fig5.13: *SEM images of B_6O and rare- earth metal oxide containing materials.*)

5.2 MICROSTRUCTURE AND HARDNESS OF COMPOSITES

In this work, B_6O powder was hot pressed at temperature of 1900^{o}C and pressure of 50 MPa for 20 minutes. The Vickers hardness measurement on the hot pressed B_6O compact yielded a value of 30.2 ± 1.0 GPa using a load of 1kg. A Vickers microhardness of 45 GPa (100g load) was obtained for B_6O single crystal ($100\,\mu$m) that was grown at pressures of 5.5 GPa (Duanwei *et al.,* 2002).

Figure 5.13 compares the hardness of the hot pressed "pure" B_6O sample to other sintered B_6O materials, made by other authors (Petrak et al, 1974, Itoh et al, 1998, Shabalala 2007 and Holcombe 1972). Although the Vickers hardness (30.2 GPa) of the B_6O sample measured in this study seems to the lower compared with 30.4 GPa (100g load) obtained via hot pressing by Petrak *et al* (1974), 31-33GPa (200g load) achieved by Itoh *et al. (1998)* at high pressures, 34.8 GPa by Shabalala (2007) as well as 38 GPa (100g load) by Holcombe (1972), a load of 1kg was used to indent the sample, which is 10 times bigger than those of Petrak and Holcombe. It was also noted that the stoichiometry of the boron suboxide material (B_6O_x) made in this study might be different from those reported in other studies. This further confirms the supposition that the stoichiometry of the produced B_6O compact may affect the hardness of the material depending on oxygen content. Also, a variation of the sintering conditions in terms of temperature, pressure, time and atmosphere could affect the amount of porosity present which has a negative effect on hardness.

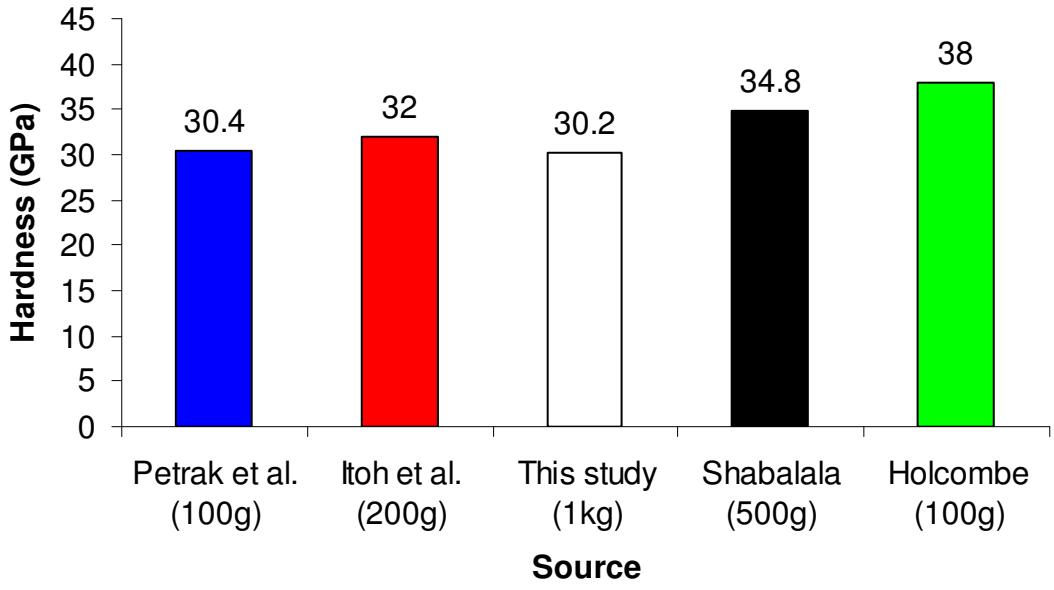

Fig5.14: *Comparison of the Vickers hardness of hot-pressed pure B_6O sample obtained from different studies.*

Figure 5.14 shows a comparison between the Vickers hardness of hot pressed B_6O-iron containing materials produced by sintering mixtures of boron suboxide with Fe, FeO and FeB at 1850^{o}C for 20 minute. It is important to note that these measurements were made using a load of 5kg. A typical indent obtained during a Vickers hardness measurement, using a load of 5kg is shown in figure 5.15 for a sample with 1.17 *wt% Fe* addition to the B_6O. Although the absolute values of hardness measured differ, a similarity in hardness values were observed if one considers the error bars. The difference in hardness values between these materials is less than 1.5 GPa, with B_6O+FeO material having the highest value. The reason for the increase in hardness in this material could not be determined.

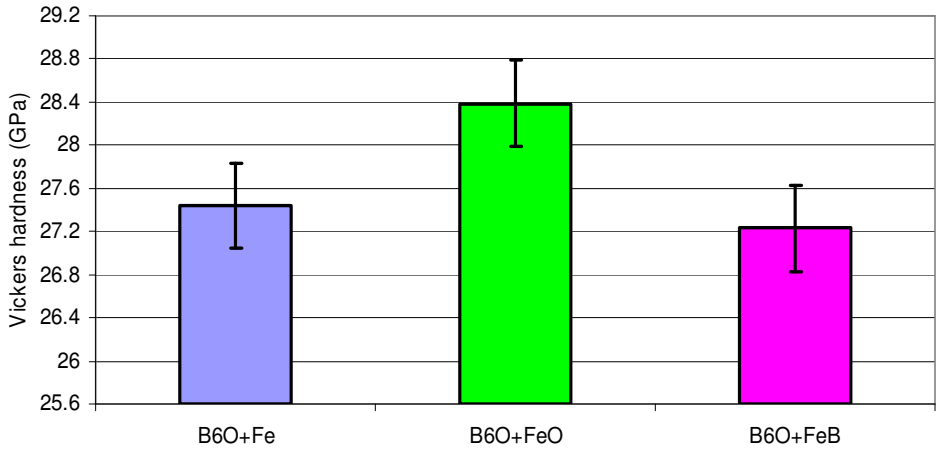

Fig5.15: *Comparison of the Vickers hardness of B_6O- iron containing composites.*

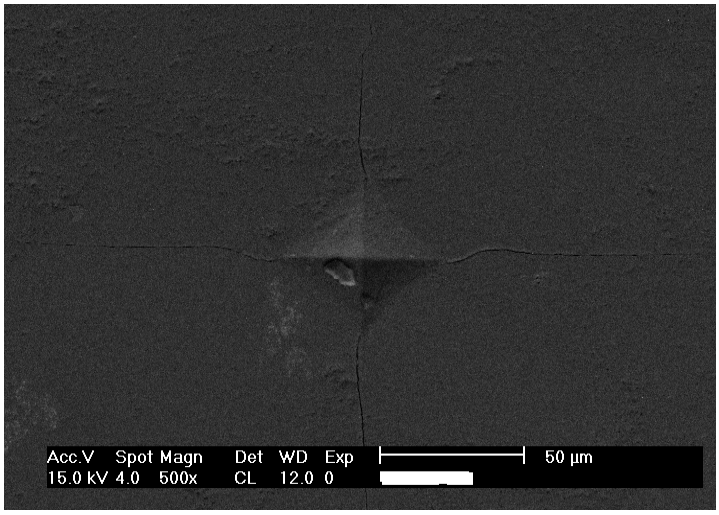

Fig5.16: *SEM image of a B_6O + Fe composite sintered at 1850^oC, showing an indent made using 5kg load.*

Figure 5.16 shows a comparison between the Vickers hardness of hot pressed B_6O-chromium containing composites produced by sintering at 1850^oC for 20 minutes. The difference in hardness between the B_6O+ Cr and B_6O+ CrO_3 is 1 GPa. This difference is

connected with the homogeneity of the second boride phase in the matrix (SEM images in chapter 4). B_6O+ Cr composite had a complete segregation of the binder phase due to bad wetting of the B_6O by the sintering additive, and some residual pores due to decomposition of B_2O_3 at sintering temperature, while the B_6O+CrO_3 material had an homogeneous distribution of the binder phase within the matrix (see fig. 5.8). The possible explanation to the reduction in the hardness in B_6O+ Cr material is that indentations could have been made on segregated boride-rich phase in the matrix with lower intrinsic hardness compared to B_6O.

On the other hand, B_6O+ CrO_3 composite had a homogeneous distribution of the binder phase with some growth of the B_6O grain. Although porosity of about 1.20% was retained in the hot pressed material, the even distribution of indentations around the matrix and also at points which are B_6O-rich resulted into an overall high hardness value.

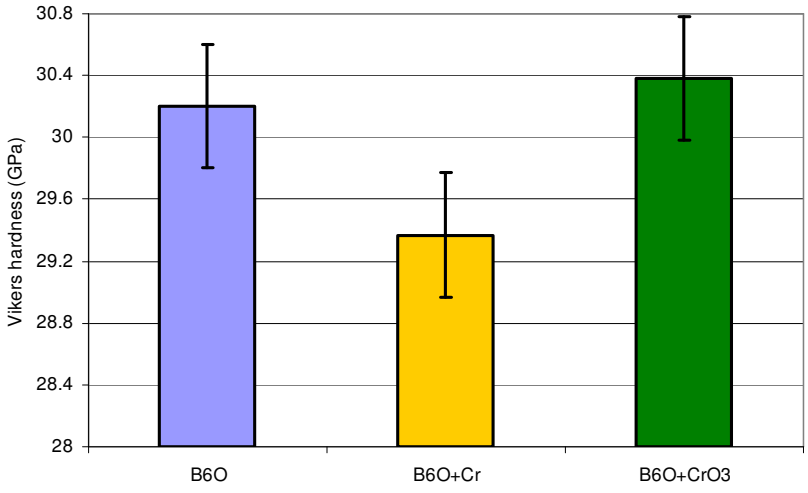

Fig5.17: *Comparison of the Vickers hardness of B_6O and B_6O-chromium containing composites.*

The hardness values obtained for the B_6O composite containing rare- earth metal oxide (Sc_2O_3, La_2O_3 & Yb_2O_3) were similar. Nevertheless, the macro-hardness value of B_6O+ Sc_2O_3 composite was slightly higher than those of B_6O+ La_2O_3 and B_6O+ Yb_2O_3 composites. The variation in the hardness values obtained gives an indication of the intrinsic hardness values of the secondary phases formed after hot pressing. Although, full densification was not achieved for these composites, the average hardness value might be higher than those of other group of sintering additives if the same volume percent of additives were used. It suggests that improvement of the densification of this group might result into better hardness values.

Fig 5.17 compares some of the hardness values reported for B_6O composites produced by other researchers with those of rare-earth metal oxide in this work. The doped materials have been given in brackets. It must be mentioned that the hardness values obtained for the materials produced in this work are very good considering the fact that it was measured using a load of 5kg, compared to 200g-load used by Itoh *et al*.(2000 & 2001) and Sasai *et al*. (2001) and 500g-load used by Shabalala (2007). The high microhardness obtained by Itoh *et al*. (2000 & 2001) and Sasai *et al*. (2001) was because of the relatively hard secondary phases in the composites. Both found that neither solid solutions nor new compounds were formed under the sintering conditions and that the sintered composites consist of the mixed phases of B_6O and B_4C, cBN, and diamond respectively. B_4C, cBN and diamond are all ultrahard materials compared to boride phase formed in composites produced in this work as well as the aluminium borate formed in the work of Kayhan and Inal (1999) and Shabalala (2007). Even though very high

hardness values were recorded for composites produced by Itoh *et al*. (2000 & 2001) and Sasai *et al*. (2001), their corresponding toughness values were very low. Also, the B_6O composites they produced were done using high pressure techniques.

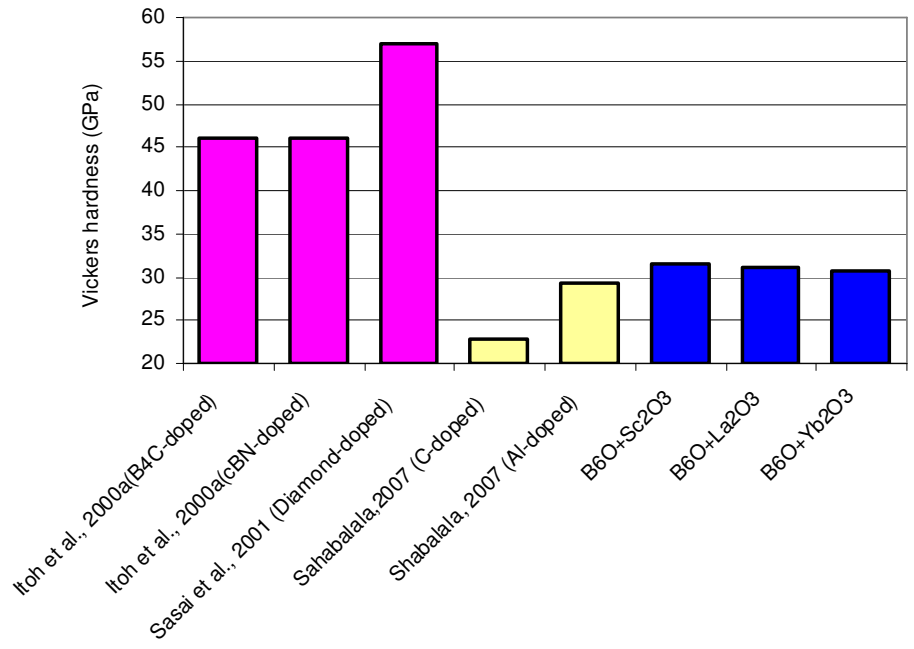

Fig5.18: *Comparison of Vickers hardness values of B_6O-rare earth metal oxide containing composites obtained in this work and those obtained by other researchers.*

5.3 MICROSTRUCTURE AND FRACTURE TOUGHNESS OF COMPOSITES

A fracture toughness of 4.5 MPam$^{1/2}$ was measured on single crystal B_6O made at ultra-high pressures of 3-5GPa (Duanwei *et al.,* 2002). Based on this result it may be assumed that fracture occurs through grain boundaries in sintered B_6O compacts. The fracture toughness of the sintered pure B_6O sample could not be measured due to the chipping of the B_6O crystals during indentation. It was concluded that the sample had low fracture toughness and it is brittle. It is not clear how fracture occurs in this sample but there were some evidences of both intergranular and transgranular fracture.

In this study, the addition of transition metal compounds and rare-earth metal oxides produced materials with improved fracture toughness compared with the results from other study. Fracture toughness values reported in this work were measured using 5kg load.

Figure 5.18 compares the fracture toughness of hot pressed B_6O-iron containing materials produced by sintering at 1850^{o}C for 20 minute. A similar fracture toughness of **3.2** MPa.m$^{1/2}$ and **3.1** MPa.m$^{1/2}$ were obtained for B_6O+Fe & B_6O+FeO materials respectively, while a maximum of **7.6** MPa.m$^{1/2}$ was achieved for B_6O+FeB material, which also had the least hardness value and could be reproducible by proper control of the procedure. This was a significant improvement in the fracture toughness considering the fact that the hot pressed B_6O sample was very brittle. Therefore, the introduction of the boride secondary phases caused the improvement in the fracture toughness of the materials.

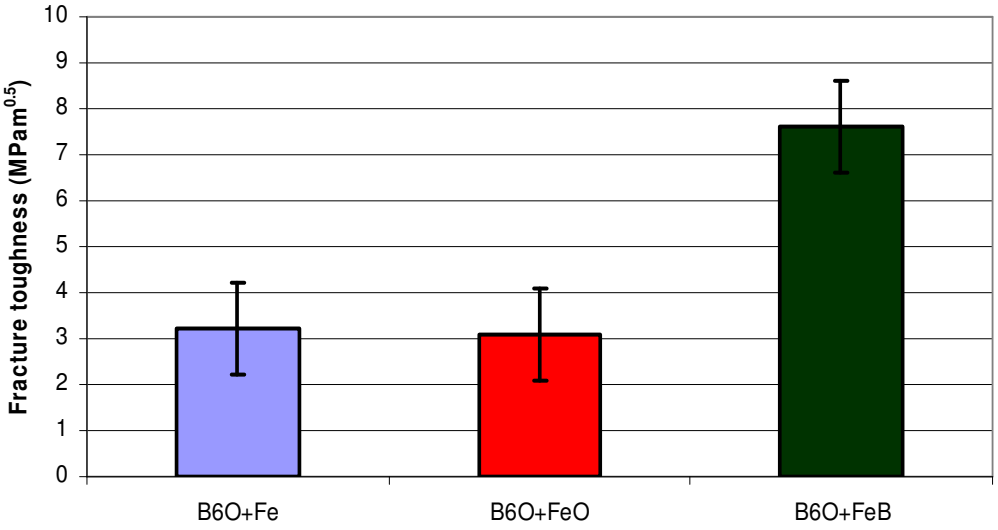

Fig5.19: *Comparison of the Fracture toughness of B_6O- iron containing composites.*

Fig 5.19 shows SEM images of the crack propagation on the polished surfaces of B_6O-iron containing sintered materials. A straight-line crack which cut across the grains of B_6O was observed mainly in all the materials indicating a transgranular fracturing mode. In addition, crack deflection was observed in the B_6O+FeB material, which was as a result of stresses that exist in the material. This leads to staggered crack paths which subsequently lead to greater energy loss per unit length of a straight line running perpendicular to the applied stress. Thus, the energy required to propagate a crack over a given range will be significantly higher than that of pure B_6O and therefore the material is said to be tougher.

Furthermore, B_6O and FeB phases exhibit substantially different coefficients of thermal expansion, CTE, [$\alpha_{B6O} = 5.5\times10^{-6}$ / $^{o}C^{-1}$ (Bairamashvili *et al.,*1979, Shabalala 2007) and

α_{FeB} = 23 $\times 10^{-6}$ / $^{o}C^{-1}$ (Celebi et al., 2005, Campos *et al*., 2006)]. This difference in thermal expansion coefficients can cause thermal residual stresses, which occur during cooling of the material after sintering. The residual stress (σ) between B_6O and FeB was estimated, using equation (5.6) [Liversage (2005), Jianxin (2000)], to be 6430 MPa, assuming the change in temperature is about 1000 ^{o}C.

$$\sigma = \left(\frac{(\Delta\alpha.\Delta T)}{[(1+\nu_m)/2E_m + (1-2\nu_s)/E_s]} \right) \quad \ldots\ldots\ldots\ldots\ldots\ldots\ldots (5.6)$$

$\Delta\alpha \equiv$ Difference in thermal expansion coefficient between B_6O and the secondary phase, FeB.

$\Delta T \equiv$ Change in temperature at which sufficient softening occurs to alleviate the stresses (~1000 ^{o}C)

$\nu_{m,s} \equiv$ Poison ratios of B_6O (0.197) and FeB [=0.28 (Kulka & Pertek 2008)]

$E_{m,s} \equiv$ Elastic moduli of B_6O (540 GPa) and FeB [=284GPa (Avril *et al*., 2006)]

Fracture toughness enhancement via this mechanism is very common in ceramic materials. The effect of residual stresses on fracture toughness that result from the mismatch between the thermal expansion coefficients of the two components in ceramic materials, was also reported by Wahi and Ilschner (1980) and Bingqiang (2007) in Al_2O_3-TiC composites, with Al_2O_3 as the matrix. Other studies are SiC-TiC ceramic composites (Liversage 2005), SiC_x/TiB_2 composites (Jianxin 2000) and SiC-AlN particulate composites (Pan *et al*., 1998).

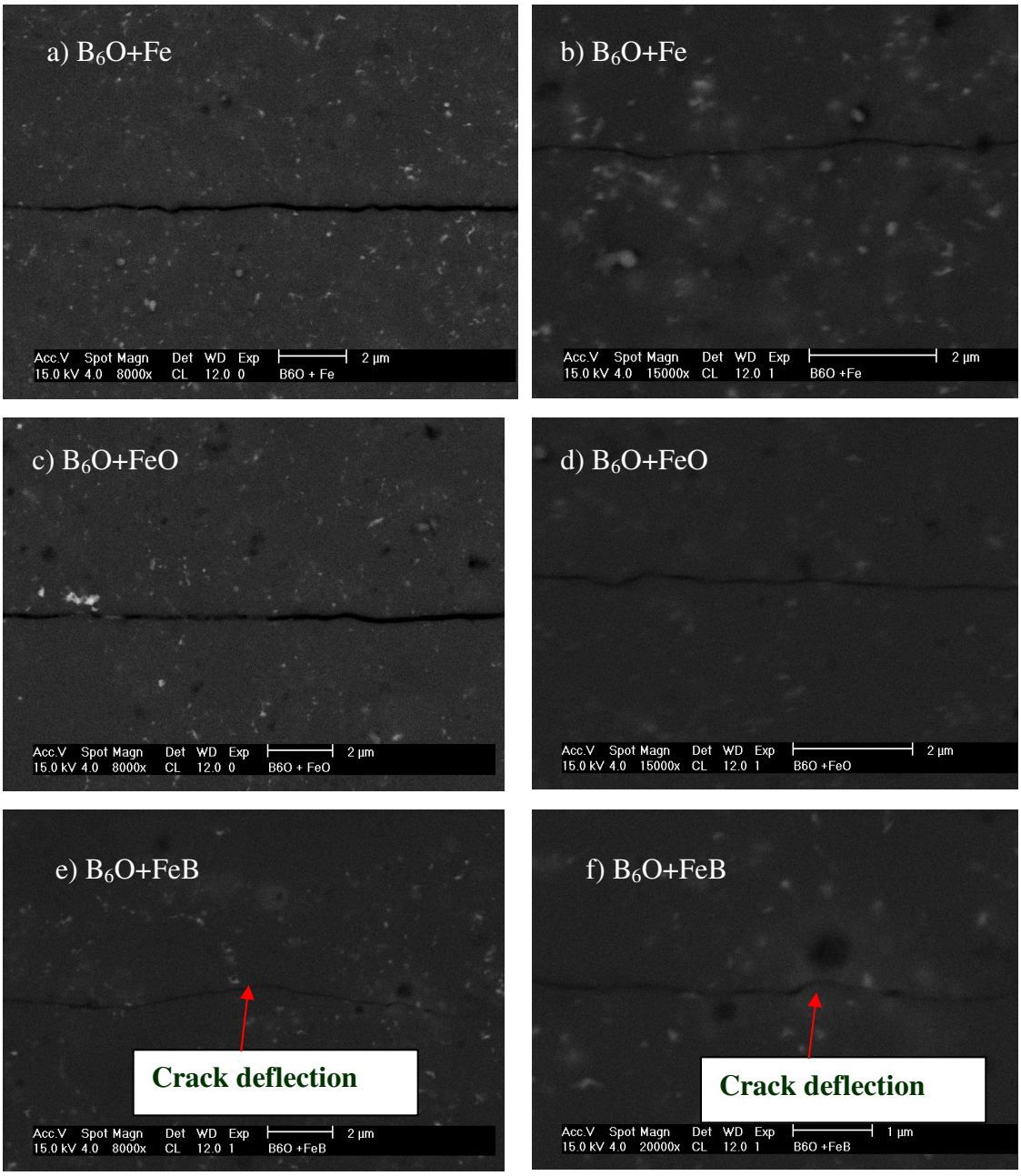

Fig5.20: *SEM micrographs of the polished surfaces (with propagating cracks) of B_6O sintered composites ((a) & (b) Fe, (c) & (d) FeO (e) & (f) FeB additives).*

Figure 5.20 compares the fracture toughness of hot pressed B_6O-chromium containing composites produced by sintering at 1850°C for 20 minutes. A high fracture toughness of **5.5** MPa.m$^{1/2}$ and **4.8** MPa.m$^{1/2}$ was obtained for B_6O+Cr and B_6O+CrO_3 composites respectively. The high fracture toughness measured in these composites was enhanced by a combination of fracture mechanisms. Fig 5.21 shows SEM images of the crack paths of polished Cr-doped and CrO_3-doped B_6O materials. A combination of crack bridging and deflection caused by bimetallic stresses gave rise to high fracture toughness in the B_6O+Cr material.

The coefficient of thermal expansion for the chromium boride (CrB_2) secondary phase was calculated based on the rule of mixture (equation 5.7 & 5.8) to be 7.8 $\times 10^{-6}$ / °C^{-1}. With the assumption that the Poison ratio for CrB_2 ranges between 0.2-0.3 and the change in temperature is about 1000 °C, the thermal stresses between the B_6O/CrB_2 interfaces was calculated using equation 5.6 to be in the range of 571-751 MPa.

$$\alpha_{CrB_2} = \frac{\alpha_{Cr} k_{Cr} f_{Cr} + \alpha_B k_B f_B}{k_{Cr} f_{Cr} + k_B f_B} \quad \ldots\ldots\ldots\ldots\ldots\ldots 5.7$$

$\alpha_{cr,B}$ =Thermal expansion coefficient of chromium and boron ($6.5\times10^{-6} C^{-1}$ and $8.3\times10^{-6} C^{-1}$ respectively (www.netzsch-thermal-analysis.com))

$$k_{Cr,B} = \frac{E_{Cr,B}}{2(1-v_{Cr,B})} \quad \ldots\ldots\ldots\ldots\ldots\ldots\ldots\ldots 5.8$$

$E_{Cr,B}$ = Elastic moduli of chromium and boron (279GPa and 441GPa respectively (www.webelements.com))

$v_{Cr,B}$ = Poisson's ratio of chromium and boron (0.21 and 0.18 respectively)

E_{CrB_2} = Elastic modulus of chromium boride (CrB_2) = 211.04 GPa (www.memsnet.org)

The difference between the thermal expansion coefficients of the B_6O matrix and the chromium boride secondary phase induces a tangential compressive stress near the particle/matrix interface and diverts the crack around the particle. The presence of twin boundaries in B_6O crystals, which is a characteristic of boron compounds, can make major cracks deflect and branch, and also make the development of main cracks consume more energy as shown in the micrograph. Consequently, this material showed high toughness.

From the microstructure, it was observed that pores in the B_6O+CrO_3 material helped to reduce the energy of the propagating crack, thereby causing an improving the fracture toughness of the composite.

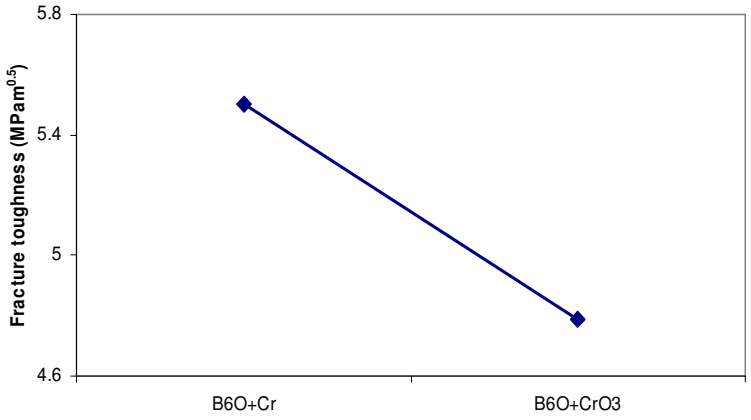

Fig5.21: *Comparison of the Fracture toughness B_6O-chromium containing composites*

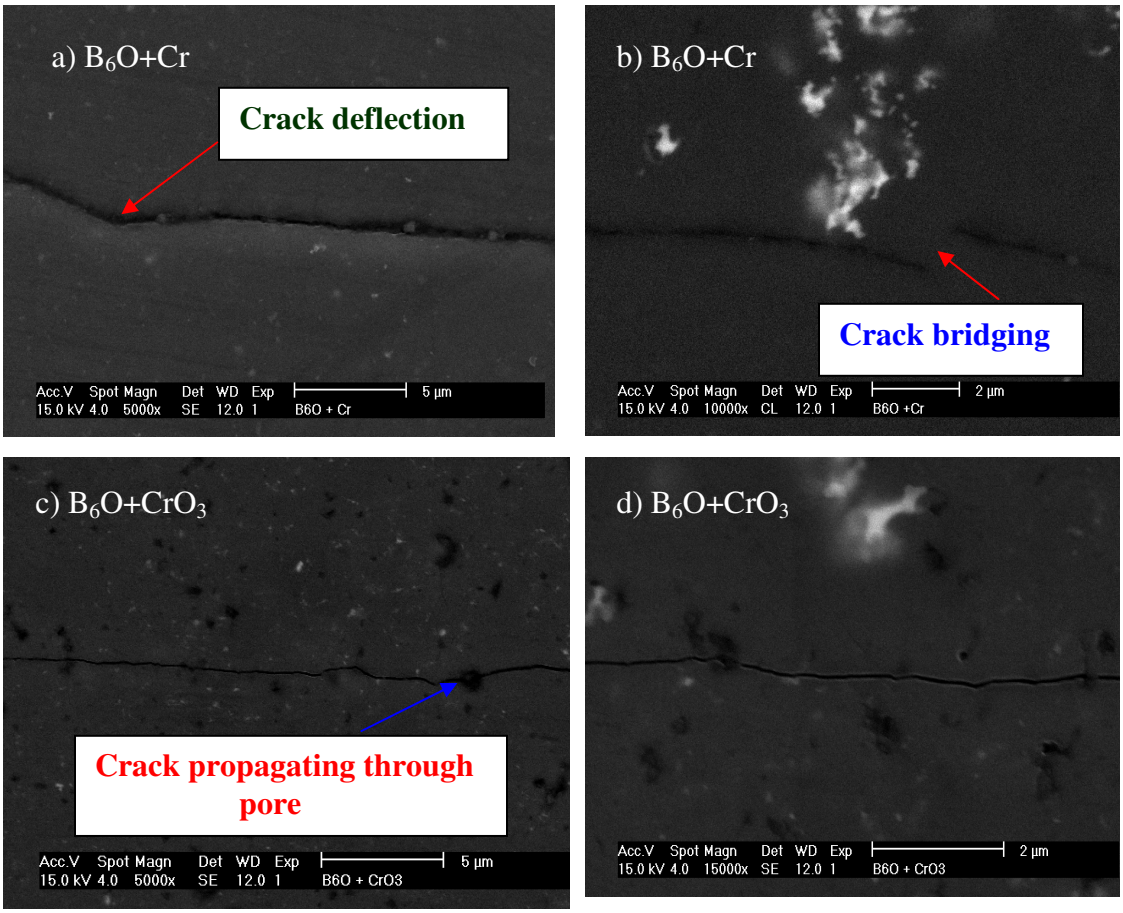

Fig5.22: *SEM micrographs of the polished surfaces (with propagating cracks) of B_6O sintered composites ((a) & (b) Cr, (c) & (d) CrO_3 additives).*

Good combinations of fracture toughness and hardness were obtained for B_6O composites doped with rare-earth oxides. Fig 5.22 compares the fracture toughness of hot pressed B_6O- rare-earth metal oxide containing composites produced by sintering at 1850^oC for 20 minutes. A similar fracture toughness value of **5.6** MPa.m$^{1/2}$ was obtained for B_6O+Sc_2O_3 and B_6O+La_2O_3 composites, while the toughness decreased to **3.9** MPa.m$^{1/2}$ for the B_6O+Yb_2O_3 composite.

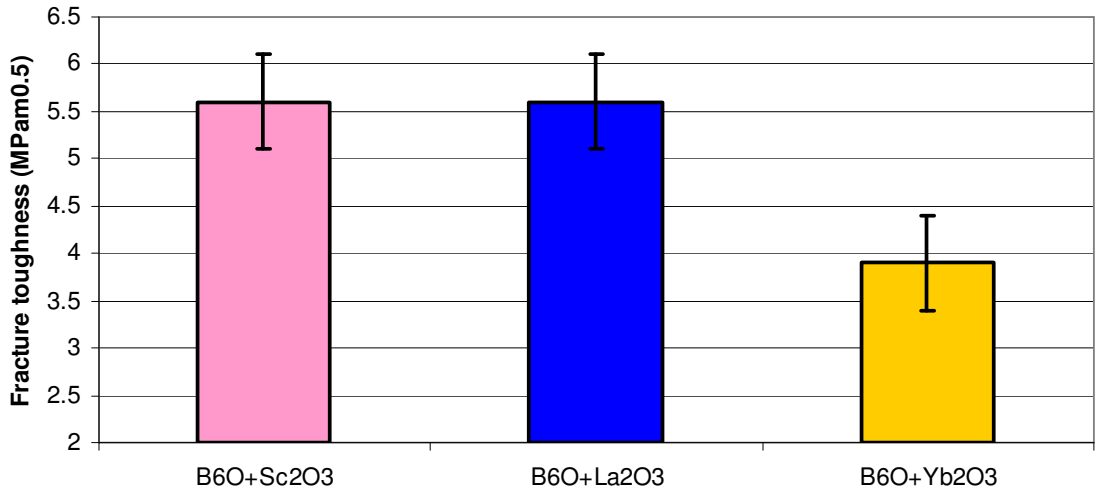

Fig5.23: *Comparison of the Fracture toughness of B_6O-rare earth metal oxide containing composites.*

SEM images of the crack paths of polished Sc_2O_3-doped, La_2O_3-doped and Yb_2O_3-doped B_6O composites are shown in fig 5.23. There was some form of toughening mechanism produced by the second phase in the B_6O composites. A large-scale bridging of the crack was observed in the Sc_2O_3-containing composite; while deflection of propagating crack was observed in the La_2O_3-containing composite. Both these crack-path modification mechanisms would give rise to an increase in fracture toughness. A straight-line crack which cut across the B_6O+Yb_2O_3 composite only requires minimum amount of energy to progress, which agrees with the lower fracture toughness measured for this material.

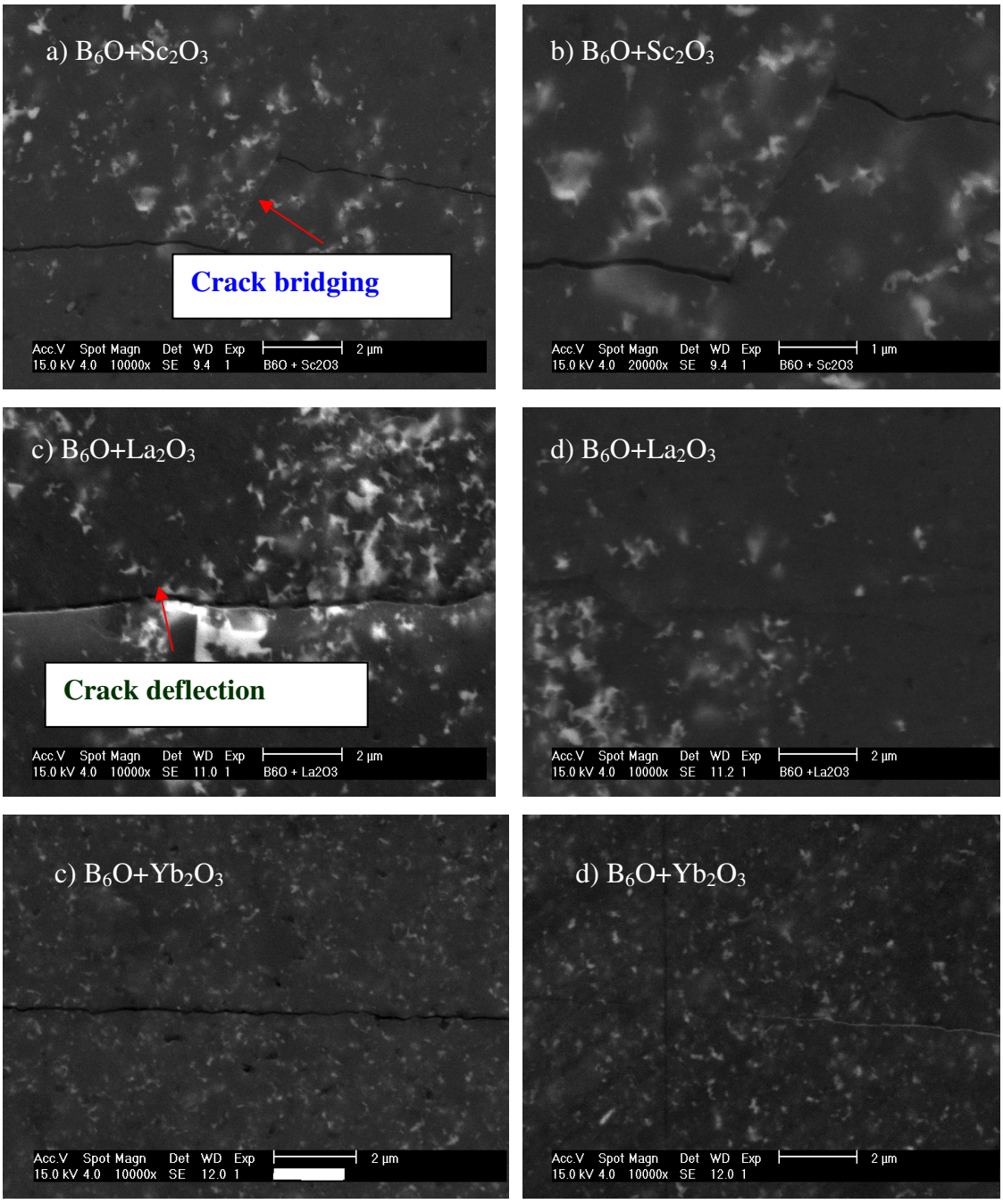

Fig5.24: *SEM micrographs of the polished surfaces (with propagating cracks) of B_6O sintered composites ((a) & (b) Sc_2O_3, (c) & (d) La_2O_3 (e) & (f) Yb_2O_3 additives).*

CHAPTER SIX

6.0 CONCLUSION

The boron suboxide powder was synthesized using the reaction of amorphous boron and boric acid powders at temperatures of 1380^{o}C for 6 hours, under argon atmosphere, using a tube furnace. It was established that B_6O powder could be produced without the application of pressure and that the particle size of the synthesized B_6O powder depends on the particle size of the starting amorphous boron powder. The synthesized powder was pure as evidenced by the resulting XRD trace, as well as from SEM/EDS analysis.

The synthesized boron suboxide powder had the lattice parameters of a=5.370 $\pm$ 0.001Å and c=12.328 $\pm$ 0.003 Å, as determined using X-ray diffraction. This data was compared with literature to estimate the oxygen content (lattice occupancy) in the powder. In this manner, the oxygen occupancy was estimated to be 0.77, which means that the synthesized boron suboxide has the stoichiometry $B_6O_{0.77}$. It has been shown in the past and widely accepted that boron suboxide (B_6O) powders made at ambient pressures are non-stoichiometric. Therefore, the X-ray data as well as the particle size and colour of the synthesized B_6O powder, studied in this work are in agreement with previous work in the literature (Duanwei *et al.,* 2002, Hubert *et al*., 1998, Kobayashi *et al*., 1993, Rizzo *et al*., 1962, Lundstrom and Bolmgren 1994, Lundstrom and Andreev 1996).

The synthesized B_6O powder was sintered using a hot pressing technique, at high temperature of 1900^{o}C and pressure of 50 MPa for 20 minutes under argon atmosphere. The density of pure sintered B_6O obtained was 2.46 g/cm^3, which was 96.5% of the

theoretical density and agrees with the value obtained by Kayhan I.O and Inal O.T (1999). The Vickers hardness measurement on this sintered compact yielded 30.2 ± 1.0 GPa using a load of 1kg. Although the Vickers hardness (30.2 GPa) of the B_6O sample measured seems to be lower compared to a hardness of 30.4 GPa (100g load) obtained for hot pressed sample by Petrak *et al* (1974), 31-33GPa (200g load) achieved by Itoh *et al. (1998)* at high pressures, 34.8 GPa (500g) by Shabalala (2007) as well as 38 GPa (100g load) by Holcombe (1972), it must be stated that a higher load of 1kg was used to indent the sample in this study.

The above findings, regarding the sintered "pure" B_6O samples, showed that a B_6O material, with respectable hardness, is attainable using a hot pressing technique, under argon atmosphere. It was shown that the hardness of this material is comparable to the hardness, for similar materials, achieved by other authors, and it even surpasses that of similar B_6O materials, obtained at ultra-high pressures. Clearly, ultra-high pressures are not a necessity for producing a hard sintered B_6O material. Furthermore, the hardness was measured using 1000g, which is 10 times higher than that used by most authors. However, the fracture toughness of the B_6O material was still low, with evidence of both inter- and intra-granular fracture.

The fracture toughness of the B_6O compact could not be measured as the sample fractured on increasing the load; therefore it was concluded that the material is too brittle for practical applications. Fracture surfaces indicating both inter- and intra-granular fracture were observed in the SEM microstructures. The fracture toughness of the

sintered "pure" B_6O compacts, made by hot pressing under argon atmosphere, has not been previously reported in the literature. In the work of Kayhan *et al.* (1999), high fracture toughness values, for hot B_6O compacts, made under *vacuum* at 1800^oC, were reported. However, the mode of fracture is not clearly indicated, and the materials had relatively high amount of porosity, resulting in low strength values. Furthermore, the radius of the notch used to measure the fracture toughness was 0.4mm, which makes these values of fracture toughness highly suspect. In the work of Itoh *et al* (1998), done at ultra-high pressures, the fracture toughness of sintered B_6O compacts is only reported to be low.

With the primary aim of this research work being to produce B_6O- based materials with enhanced mechanical properties mainly in terms of fracture toughness, different elements and compounds having potential to achieve this objective were admixed and hot pressed with the pure B_6O powder. These additives were grouped into four categories: transition metals, transition metal oxides, transition metal borides & rare- earth metal oxides. The mixing was done in the planetary mill for 2 hours and the quantity of additive used was such that the volume percent of the transition metal additives in the mixture remains constant. After sintering of the admixed powders at 1850^oC for 20 minutes, the density of each hot pressed B_6O material exceeds 95% of theoretical, indicating that good densification of boron suboxide could be achieved at lower temperature by the use of adequate additives.

By comparison, the best combination of hardness-fracture toughness properties was obtained from the B_6O- rare earth metal oxide materials, followed by the B_6O-transition

metal oxide materials. With a maximum fracture toughness of 7.58 MPam$^{0.5}$ obtained for the B_6O+FeB composite, it must be concluded that there was a significant improvement in the fracture toughness of these composite materials due to the introduction of the boride secondary phase at the grain boundary interface. The fracture toughness enhancement was attributed to the introduction of a second, minority phase. Further investigations are necessary to understand the relation between the achieved mechanical properties and the observed microstructures in these samples and also to vary the volume content of this secondary phase in the sintered material.

Some of the B_6O materials produced in this research study possess good mechanical properties, i.e. hardness-toughness combinations, especially the B_6O+Co, B_6O+Sc_2O_3 and B_6O+La_2O_3 composites. This suggests that suitably prepared B_6O materials could be potentially used in cutting tool, wear part and ballistic armour applications. Fig 6.1 and fig 6.2 shows the mechanical properties of hard materials (Ozbayraktar S and Riedel R (2000) and Lee W.E and W. M. Rainforth W.M (1994)) in comparison with the properties of some of the materials produced in this work. For comparison, these three composites were selected. The hardness values of B_6O+Co, B_6O+Sc_2O_3 and B_6O+La_2O_3 composites were 33.91 GPa, 31.59 GPa and 31.02 GPa respectively, comparable to some of the BN materials, e.g. DBC50 and Amborite. The fracture toughness of these composites was also greater than those of B_4C (Hv =35GPa, K_{IC}= 2.9-3.7 *MPa.m.$^{0.5}$, www.b4c.com.tw),* Al_2O_3/TiC composite and DBC50. Although, diamond and cBN possess better properties, the dominant methods for their industrial synthesis requires

high pressures and temperatures, which renders their manufacturing expensive and limit the sizes and geometric forms possible.

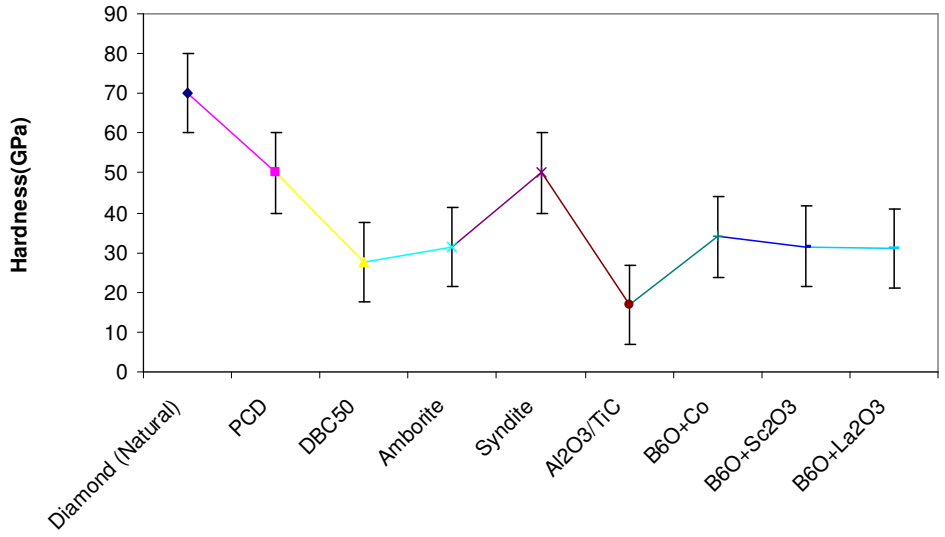

Fig6.1: *Hardness of hard materials in comparison with boron suboxide composites from this study.*

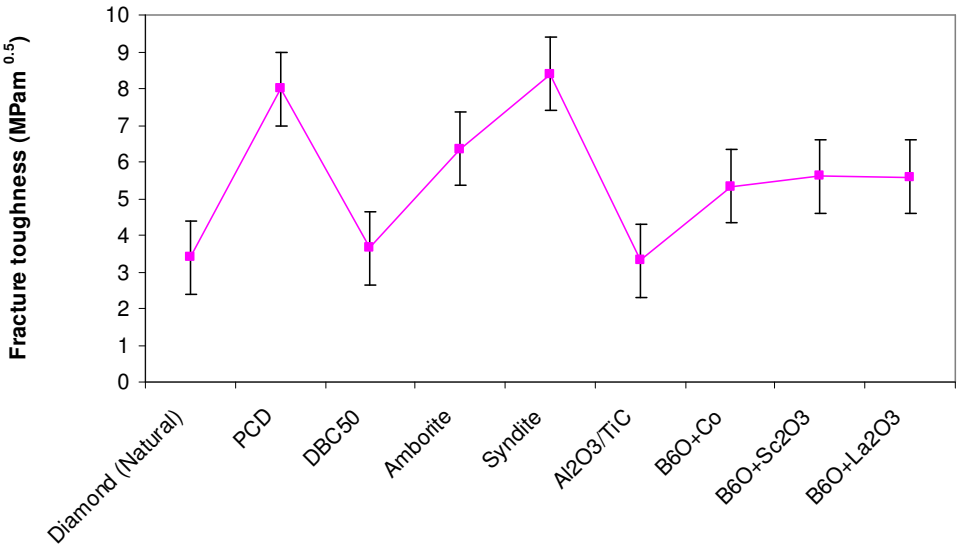

Fig6.2: *Fracture toughness of hard materials in comparison with boron suboxide composites from this study.*

Also, diamond application is somewhat limited at high temperatures owing to its instability, for example, as cutting tool for steel. Furthermore, as the temperature increase, diamond and cBN weaken due to the onset of the transformation to the graphitic structure as well as due to diffusion wear. For these reasons and because of the need to replace expensive diamond and cBN in many other applications, boron suboxide has been of technological interest. More importantly, there are a number of important alloys such as ductile cast iron and ductile steel that cannot be machined by PcBN due to diffusion wear. This diffusion process is enhanced because of the presence of carbon or nitrogen in the cutting tools containing diamond or cBN, such elements are absent in B_6O. Therefore, there is a high likelihood that B_6O-based cutting tools will be less susceptible to diffusion wear when machining these hard to machine but industrially very important work piece materials.

Further optimization of the additive content, composition, and mechanical properties are needed to better understand the microstructure formation and toughening mechanisms existing in the materials. This will allow fabrication of B_6O materials for industrial applications such as cutting tool, drill bits, grinding wheels, abrasives and ballistic armour.

REFERENCES

Andrews, A., Herrmann, M., Shabalala, T.C. and Sigalas, I. (2008): "Liquid phase assisted hot pressing of boron suboxide materials", *Journal of European Ceramics Society.* Vol 28, pp. 1613-1621.

Anstis, G., Chantikul, P., Lawn, B. and Marshall D. (1981): "A Critical Evaluation Indentation Techniques for Measuring fracture Toughness: I, Direct Crack Measurements", *Journal of Ceramic society*. Vol 64, pp. 533-8.

Avril, L., Courant, B. and Hantzpergne, J.J (2006): "Tribological performance of α-Fe (Cr)-Fe2B-FeB and α-Fe (Cr)-h-BN coatings obtained by laser melting." www.elsevier.com/locate/wear. Vol. 260, pp. 351–360.

Badzian, A.R., Gildenblat, G. Sh., Grot, S.A. and Hatfield, C.W (1988): "Superhard Material Comparable in Hardness to Diamond", *Applied Physics Letters*, Vol. 53, pp. 586-588.

Badzian, A.R., Badzian, T. and Pilione, L. (1990): 'Superhard materials and superhard coatings," *Refractory Metals Hard Materials*. Vol. 9, pp. 92-95.

Bairamashvili, I. A., Kalandadze, G. I., Eristavi, A. Jobava, J.S. and Chotulidi, Yu. V. (1979): Boron compounds with group IV elements: boron carbide: further properties. Saloev, *Journal of the Less-Common Metals*, Vol. 67, pp. 455-461.

Bairamashvili, I.A., Kalandadze, G.I., Eristavi, A.M., Jobava, J.S., Chotulidi, V.V. and Saloev, Y.L.(1979): "*An investigation of the physicomechanical properties of* B_6O *and* SiB_4", *Journal of Less Common Metals,* Vol. 67, pp. 461-561.

Bingqiang, L., Chuanzhen, H., Xinyu, L., Meilin, G. and Hanlian, L. (2007): "In situ growth of TiC whiskers in Al_2O_3 matrix for ceramic machine tools." *Ceramics International,* Vol. 33, pp.1475–1480.

Brodhag, C. and Thevenot, F. (1986): "Hot pressing of various boron phases". *Journal of the Less-Common Metals*, vol.117, pg.1-6.

Brookes, C.A. (1986): Mechanical properties of cubic boron nitride- a perspective. *Institute of Physics*, *Conference Series*. Issue 75, pp 207-220.

Campos, I., Palomar, M., Amador, A., Ganem, R. and Martinez, J. (2006): "Evaluation of the corrosion resistance of iron boride coatings obtained by paste boriding process." *Surface & Coatings Technology,* Vol. 201, pp. 2438–2442.

Celebi, G., Ipek, M., Bindal, C. and Ucisik, A.H. (2005): "Some mechanical properties of borides formed on AISI 8620 steel." *Materials forum*. Vol. 29, pp. 456-460.

Chen, Y.A., Guo L. and Wang, E. G. (1997): Experimental evidence for alpha - and beta -phases of pure crystalline C_3N_4 in films deposited on nickel substrates, *Philosophical Magazine Letters*, vol.75, No. 3, pp. 155-162.

Clarke, D.R. and Faber, K.T. (1987): "Fracture of ceramics and glasses." *Journal of Physics and Chemistry of Solids,* Vol. 48, pp. 1151-1157.

Cote, M. and Cohen, M. L. (1997): "Carbon nitride compounds with 1:1 stoichiometry ", *Physical Review B,* vol. 55, pp. 5684 -88.

Duanwei, H., Yusheng Zhao, Daemen, L., Qian, J. and Shen, T.D (2002): Boron suboxide: As hard as cubic boron nitride. *Applied Physics Letters*. vol. 81, No. 4, pp. 643-645.

Dubrovinskaia, N., Solozhenko, V.L., Miyajima, N., Dmitriev, V., Kurakevych, O.O. and Dubrovinsky, L (2007): Superhard nanocomposites of dense polymorphs of boron nitride: noncarbon material has reached diamond hardness. *Applied Physics Letters*, Vol. 81, pp. 101912-101914.

Ellison- Hayashi, C., Morteza, Z., Murray, Frank, J.S. and Shih-Yee K (1992): Boron suboxide material and method for its preparation. *United State Patent*, US 5135892.

Endo, T., Sato, T. and Shimada, M. (1987): "High-Pressure Synthesis of B_2O with Diamond-Like Structure," *Journal of Material Science Letter,* vol. 6, pp. 683-85.

Evans, A.G. (1972): The Strength of Brittle Materials Containing Second phase dispersions, *Philosophical Magazine*. Vol .26, pp. 1327-1344.

Evans, A.G. (1988): High Toughness Ceramics. *Materials Science and Engineering*, A105/106, pp. 65-75.

Gal'Chenko, G.L. and. Matkovich, V.I. (1977): "VIII Borides of Group VI b elements", *Boron and Refractory Borides*, pg. 331-333.

Garvie, L.A.J., Hubert, H., William, T. P., McMillan, P. F. and Buseck, P.R. (1997): "High-Pressure, high- Temperature Syntheses in the B-C-N-O System." *Journal of Solid State Chemistry,* vol. 133, pp 365-371.

Goosey, B.F. (1974): Method of fabricating boron suboxide articles. *United State Patent*- US 3816586.

Hall, T. and Compton, L.A. (1965): "Group IV Analogs and high Pressure, High Temperature Synthesis of B_2O," *Inorganic Chemistry,* vol. 4, pp. 1213-16.

Hansson, T., Warren, R. and Wasen, J. (1993): Fracture anisotropy and toughening mechanisms of a hot-pressed alumina reinforced with silicon carbide whiskers, *Journal of the American Ceramic Society,* vol. 76, pp. 841-848.

Hazen, R.M. and Finger, L.W. (1982): Comparative Crystal Chemistry, *John Wiley*, *Chichester*, pp. 147–164.

Hideaki Itoh, Yamamoto, R. and Iwahara, H. (2000): B_6O-*c*-BN Composites Prepared by High-Pressure Sintering. *Journal of the American Ceramic Society*, vol. 83, pp. 501–506.

Hideaki Itoh (2004): Preparation of Superhard Ceramic Materials and Evaluation of their Mechanical Properties. *Journal of the Ceramic Society of Japan*, vol. 112, pp. 121-129.

Holcombe, C. E. and Ottis, J.H. (1972): method for preparing boron suboxide. *United State Patent*- US 3 660 031.

Hubert, H., Garvie, L., Devouard B., Buseck, P., Petuskey, W. and McMillan, P. (1998): High-Pressure, High-Temperature Synthesis and Characterization of boron suboxide (B_6O). *Chemistry of materials*, vol. 10, pp 1530-1537.

Itoh, H., Maekawa, I. and Iwahara, H. (1998): High pressure sintering of B_6O powder and properties of the sintered compact, *Journals of the Society of Materials Science*, *Japan*, vol. 47, No. 10, pp.1000-1005.

Itoh, H., Maekawa, I. and Iwahara, H. (2000): Microstructure and mechanical properties of B_6O-B_4C sintered composites prepared under high pressure, *Journal of Materials Science, vol.* 35, pg. 693-698.

Jean-Michel Leger and Julian Haines (1997): The search for superhard materials. *Endeavour,* vol. 21, pp.121-124.

Jianxin, D. (2000): Effect of thermal residual stress on the high temperature toughening behaviour of TiB_2/SiC composites." *Journal of Materials Processing Technology*, Vol. 98, pp. 292-298

Kayhan, I. O and. Inal, O. T (1999): Synthesis of aluminium infiltrated boron suboxide drag cutters and drill bits, *Journal of Materials Science,* 34, pg. 4105-4120.

Kharlamov, A.I., Kirillova, N.V., Loichenko, S.V. and Kostyuk, B.D. (2002): "Properties of Boron suboxide $B_{13}O_2$," *Powder Metallurgy and Metal Ceramics*, vol. 41, pp 1-2.

Kobayashi, M., Higashi, I., Brodhag, C. and Thevenot, F. (1993): Structure and Bulk Modulus of High-Strength Boron Compounds. *Journal of Materials Science,* vol 28, pp 2129-2134.

Kleebe, H. J., Lauterbach, S., Shabalala, T.C., Herrmann, M. and Sigalas, I. (2008): B_6O: Correlation between mechanical properties and microstructure evolution upon Al_2O_3 addition during hot pressing, *Journal of the American Ceramic Society*, vol. 91, No. 2, pp. 569-575.

Kulka, M. and Pertek, A. (2008): "Gradient formation of boride layers by borocarburizing." *Applied Surface Science.* Vol. 254, pp. 5281–5290.

Lange, F. F. (1970): Interaction of a Crack front with a Second phase Dispersion, *Philosophical Magazine*, vol .22, pp. 983-992.

Lee, F., Sandlin, M.S. and Bowman, K.J. (1993): Toughness anisotropy in textured ceramics, *Journal of the American Ceramic Society,* vol. 76(7), pp. 1793-1800.

Lee, W.E. and Rainforth, W.M. (1994): Ceramic Microstructures (Property control by processing), *Chapman and Hall*.

Léger, J.M., Haines, J., Schmidt, M., Petitet, J.P., Pereira, A.S. and. Jornada, J.A. (1996): Discovery of hardest known oxide. *Nature,* vol. 383 pp. 401.

Li, D., Cheng, S.C., Lin, W.W., David, V.P. and Chung, Y.W. (1995): Synthesis of superhard carbon nitride composite coatings. *Applied Physics Letters,* vol. 67, pp. 203–205.

Liu, X., Zhao, X., Hou, W. and Su, W. (1995): "A new route for the synthesis of boron suboxide B_7O." *Journal of Alloys and Compounds*, Vol. 223, L3-L9.

Liversage J.H (2005): "An enhancement of the mechanical properties in functionally graded liquid-phase SiC-TiC ceramic composites". *PhD Thesis*, University of Witwatersrand.

Lundstrom, T. (1997): Structure and bulk modulus of high- strength boron compounds. *Journal of Solid State Chemistry*, vol. 133, pp. 88-92.

Lundstrom, T. and Andreev, Y. G. (1996): "Superhard Boron-Rich Borides and Studies of the B-C-N System." *Journal of Material Science &. Engineering A,* vol. 209, pp. 16–22**.**

Lundstrom, T. and Bolmgren, H. (1994): Proceeding of the 11th International Symposium on Boron*, Borides and Related Compounds*, *JJAP Series*, pp 1.

Makarov, V.S. and Ugai, Ya. A. (1986): Thermochemical study of boron suboxide B_6O. *Journal of the Less-Common Metals*, vol. 117, pp. 277-281.

Massalski, T.B., Murray, J.L., Bennett L.H. and Baker, H. (1986): "Binary alloy phase diagrams." Vol 1 Ac-Au to Fe-Rh, *American Society for Metals*, Metals Park, Ohio.

McMillan, P.F., Hubert, H., Chizmeshya, A., Garvie, L., Devouard, B. and Petuskey, W. (1999): "Chemistry of materials under extreme high pressure- high-temperature conditions." *Journal of Solid State Chemistry*, vol. 147, pp. 281-290.

Meguid, S. A. (1996): Mechanics and Mechanisms of Toughening of Advanced Ceramics. *Journal of Materials Processing Technology*, vol. 56, pp. 978-989.

Novak, R. E. (1972): "Structure of Rhombohedral Borides," *doctorate thesis*, University of Illinois, Urbana.

Olofsson, M. and Lundstrom, T. (1997): Synthesis and structure of non-stoichiometric B_6O. *Journal of Alloys and Compounds,* vol. 257, pp. 91-95.

Ozbayraktar, S. and Riedel, R. (2000) : *In Handbook of Ceramic Hard Materials*, ed. R. Riedel (Wiley, Weinheim, 2000).

Pan Y.B., Qiu, J.H., Morita, M., Tan, S.H. and Jiang, D. (1998): "The mechanical properties and microstructure of SiC–AlN particulate composite." *Journal of Material Science,* Vol. 33, pp. 1233–1237

Pasternak, R. A. (1959): "Crystallographic Evidence for the Existence of B_7O" *Acta Crystallography*, vol.12, pp 612-613.

Petrak, D.R., Robert, R. and Atkins, G.R. (1974): Mechanical Properties of Hot- Pressed Boron suboxide and Boron. *Ceramic Society Bulletin*, vol. 53, pp. 569- 573.

Riedel, R., Hegemann, D. and Oehr, C. (1999): Synthesis of a Novel B CN Compound by Pyrolysis of Precursor, *Thin Solid film,* vol.339, pp.154.

Rizzo, H.F., Simmons, W.C. and Belstein, H.O. (1962): The existence and formation of the solid B_6O. *Journal of Electrochemical Society*, vol.109, pp. 1079-1082.

Sasai, R., Fukatsu, H., Kojima, T. and Itoh, H. (2001): High pressure consolidation of B_6O-diamond mixtures. *Journal of Materials Science,* vol. 36, pp 5339-5343.

Seung, K.L. and Chong, H.K. (1994): Effects of α-SiC versus β-SiC starting powders on microstructure and fracture toughness of SiC sintered with Al_2O_3-Y_2O_3 additives, *Journal of the American Ceramic Society,* vol. 77(6), pp. 1655-1658.

Shabalala, T.C., McLachlan, D.S., Sigalas, I. and Herrmann, M. (2007): Hard and tough boron suboxide based composites. *Ceramics International*, in press, available online at www.sciencedirect.com.

Shabalala, T. C. (2007): The preparation and characterization of boron suboxide (B_6O) based composites. *PhD thesis*, University of the Witwaterstand.

Solozhenko, V.L., Andrault, D., Fiquet, G., Mezouar, M. and Rubie, D.C. (2001): "Synthesis of superhard cubic BC_2N." *Applied Physics Letters,* Vol. 78, No. 10, pp. 1385-1387.

Sung, C.M. and Sung, M. (1996): Carbon nitride and other speculative superhard materials, *Materials Chemistry and Physics*, vol. 43, pp. 1-18.

Taniguchi, T., Akaishi, M. and Yamaoka, S. (1999): Sintering of cubic boron nitride without additives at 7.7 GPa and about 2000^{o}C. *Journal of Material Research*, vol. 14, pp 162-169.

Teter, D.M. and Hemley, M.J. (1996): Low-compressibility carbon nitrides, *Journal of Materials Science*, vol. 271, pp. 53-55.

Veprek, S., Zeer, A. and Riedel, R. (2000): *In Handbook of Ceramic Hard Materials*, ed. R. Riedel (Wiley, Weinheim, 2000).

Wachtman, J.B. (1996): Mechanical Properties of Ceramics. *John Wiley and Sons*, New York.

Wahi, R.P. and B. Ilschner, B. (1980): "Fracture behavior of composites based on Al_2O_3–TiC." *Journal of Material Science,* Vol. **15**, pp. 875–885.

Weintraub, E. (1909): "Preparation and Properties of Pure Boron," *Transactions of American Electrochemical Society*, vol.16, pg. 165.

Yoshida, M., Onodera, A., Ueno, M., Takemura, K. and Shimomura, O. (1993): Pressure-induced phase transition in SiC. *Physical Review B, vol.* 48, pp. 10587–10590.

Zerr, A. and Riedel, R. (2000): Introduction: Novel Ultrahard Materials, in Handbook of ceramic hard materials, ed. Ralf Riedel, vol. 1, Weinheim, New York.

Zerr, A., Riedel, R., Sekine, T., Lowther, J. E., Ching, W. And Tanaka, I. (2006); "Recent advances in new hard high-pressure nitrides". *Advanced Materials.* Vol. 18, pp.2933-2948.

Zhongwu, W. and Yusheng, Z. (2005): In situ pressure Raman spectroscopy and mechanical stability of superhard boron suboxide. *Applied Physics Letters,* vol.86. No 041911, pp. 1-3.

www.netzsch-thermal-analysis.com

www.webelements.com

www.memsnet.org

www.b4c.com.tw

APPENDICES

Appendix A.1

Table A.1 gives the full list of all the samples together with the amount of additives, hardness & fracture toughness obtained, Archimedes densities measured, and phases formed before and after sintering of powder.

Table A. 3*: Properties of boron suboxide composites*

Sintered Material	*Additive Ratio (wt %)*	*Hv (GPa)*	*K_{IC} MPa.m.$^{0.5}$*	*Phases (after mixing)*	*Phases (after sintering)*	*Density (g/cm3)*	*Open porosity (%)*
Pure B_6O	-	30.2 ± 1.0	-	-	B_6O	2.46	3.7
B_6O+ Fe	1.17	27.4 ± 1.5	3.2 ± 0.8	B_6O Fe	B_6O FeB	2.53	1.1
B_6O+ FeO	1.50	28.4 ± 1.4	3.1 ±0.2	B_6O FeO	B_6O FeB	2.51	0.9
B_6O+FeB	1.40	27.2 ± 2.2	7.6 ± 1.1	B_6O FeB	B_6O FeB	2.56	0.4
B_6O+Cr	1.07	29.4 ± 2..9	5.5 ± 0.4	B_6O Cr	B_6O CrB_2	2.57	0.7
B_6O+CrO_3	1.40	30.4 ± 2.6	4.8 ± 0.3	B_6O Cr_2O_3	B_6O CrB_2	2.53	1.2

B_6O+ Co	1.33	33.9± 2.2	5.3 ± 0.8	B_6O Co	B_6O CoB	2.53	1.2
$B_6O + Sc_2O_3$	1.50	31.6 ±0.9	5.6±0.2	B_6O Sc_2O_3	B_6O	2.48	1.6
$B_6O + La_2O_3$	2.50	31.0 ± 1.8	5.6 ±0.8	B_6O La_2O_3	B_6O LaB_6	2.47	2.1
$B_6O + Yb_2O_3$	1.50	30.5 ±1.7	3.9±0.8	B_6O Yb_2O_3	B_6O YbB_6	2.51	0.9

Appendix A.2

Calculation of the amount of additives used

1.5*wt%* FeO was used as the basis, added to boron suboxide (B_6O) powder to form composite. The equivalent amount of other additives was calculated to retain the volume percent of the second phase in the mixture.

Amount of Equivalent Fe in the Mixture

56g of Fe = 72g of FeO

Xg of Fe = 100g of FeO

Therefore,

x = 77.78g of Fe

Similarly,

77.78g of Fe = 100g of FeO

y g of Fe = 1.5g of FeO

y = 1.17g of Fe

Amount of Equivalent Cr in the Mixture

Mass of Fe in B_6O = 1.17g, Density of Fe = 7.78g/cm3

Therefore, the volume occupied by Fe in the mixture is;

$$\rho = \frac{m}{V}$$

Volume of Fe $= \frac{1.17}{7.87}$

$= 0.149cm3$

Mixture	
Component	***Amount (g)***
Cr	1.07
B_6O	98.93
Total	**100**

Mass of Cr in B_6O =?, Density of Cr = 7.2g/cm3

Having the same volume in the mixture as Fe:

Mass of Cr = Density x Volume

= 7.2 x 0.149

= 1.07g

Table A.2 gives the result of the calculated amount of additives used, following the examples above.

Table A. 4*: Calculated amount of additives used*

Additive	***Density*** *(g/cm^3)*	***Amount of Additive (g)***	**Vol% of Additives**
Fe	7.78	1.17	0.4
FeO	5.70	1.50	0.7
FeB	7.15	1.40	0.5
Cr	7.20	1.07	0.4
CrO_3	2.67	2.06	2.0
Co	8.90	1.33	0.4
Sc_2O_3	3.86	1.50	1.0
La_2O_3	6.50	2.50	1.0
Yb_2O_3	9.20	1.50	0.4

Appendix A.3

Theoretical density

It is important to estimate the theoretical density of the composites formed after sintering of the admixed powders in order to ascertain the densification obtained from the hot pressing process. It was assumed that all the additives in the powder completely transformed to their respective secondary phase after sintering. The theoretical density is determined from the expression;

$$Theoretical...density = \frac{100}{\left(\frac{wt\%B_6O}{\rho_{B_6O}}\right)+\left(\frac{wt\%A}{\rho_A}\right)+...}$$

The theoretical density of B_6O was assumed to be 2.55g/cm^3

ρ_A= density of the resulting sintered phase

B_6O+ Fe composite

Amount of Fe added = 1.17 *wt%*

Molar mass of Fe = 56 g/mol

Molar mass of FeB =66.8 g/mol

After sintering, all the Fe is converted into FeB with (calculated) density of 6.75g/cm^3 (card no = 01-076-0092).

If X (in *wt %*) is the amount of FeB formed after sintering, then;

$$X = \left(\frac{wt\%\ of\ Fe \times mass\ of\ FeB}{mass\ of\ Fe}\right)$$
$$= 1.40 wt\%$$

Therefore,

Amount of B_6O in the composite = 98.60 *wt%*

$$Theo..density = \frac{100}{\left(\frac{98.60}{2.55}\right)+\left(\frac{1.40}{6.75}\right)} = 2.57$$

Table A.3 gives the result of the theoretical density calculated, following the example above.

Table A. 5*: Calculated amount of additives used*

Composite	***Amount of additive (g)***	***Second phase after sintering***	***Calculated density of the phase*** *(g/cm^3)*	***Theoretical density*** *(g/cm^3)*
B_6O+ Fe	1.17	FeB	6.75	*2.57*
B_6O+ FeO	1.50	FeB	6.75	*2.57*
B_6O+FeB	1.40	FeB	6.75	*2.57*
B_6O+Cr	1.07	CrB_2	5.20	*2.57*
B_6O+CrO_3	2.06	CrB_2	5.20	*2.57*
B_6O+ Co	1.33	CoB	7.37	*2.58*
B_6O + Sc_2O_3	1.50	-	4.00	*2.56*
B_6O + La_2O_3	2.50	LaB_6	4.71	*2.58*
B_6O + Yb_2O_3	1.50	YbB_6	5.54	*2.58*

Appendix B

XRD patterns

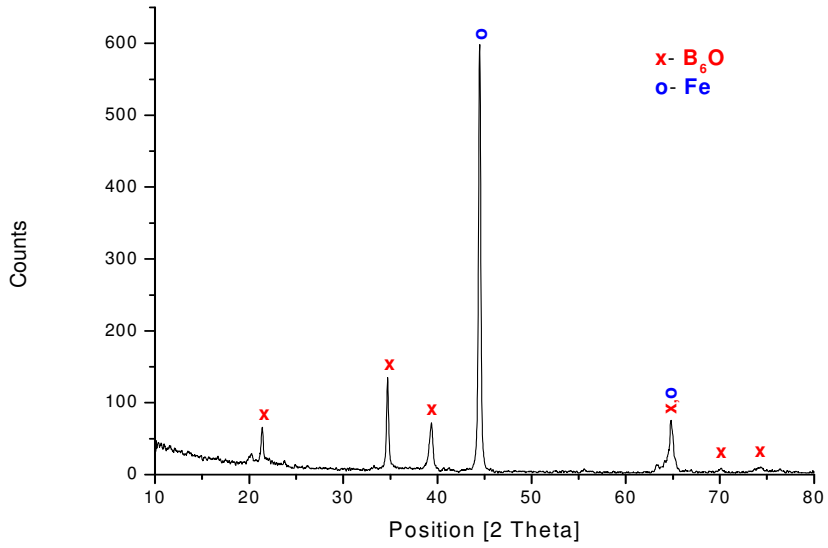

Fig B. 1*: XRD pattern of B_6O and iron powder (00-050-1505, 01-085-1410)*

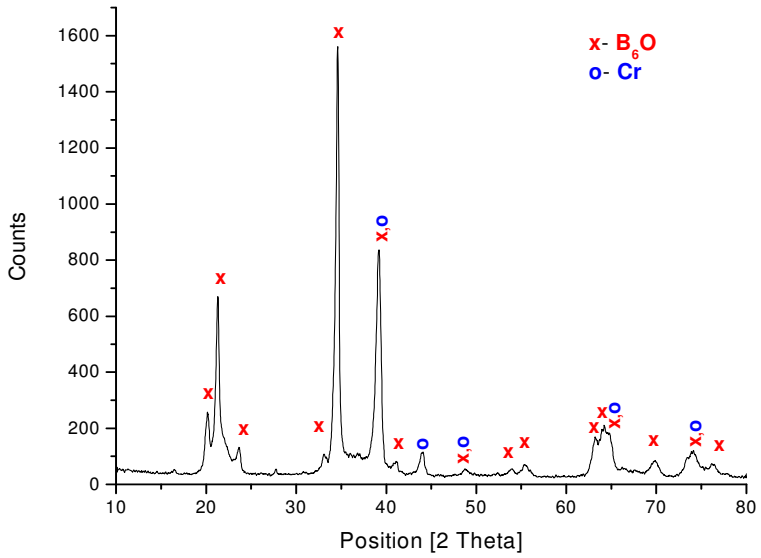

Fig B. 2*: XRD pattern of B_6O and chromium powder (00-050-1505, 01-019-0323)*

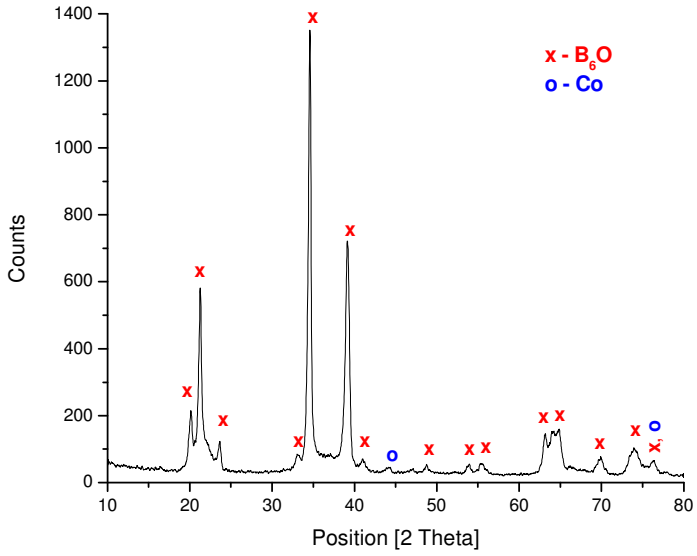

Fig B. 3*: XRD pattern of B_6O and cobalt powder (00-050-1505, 01-089-43037)*

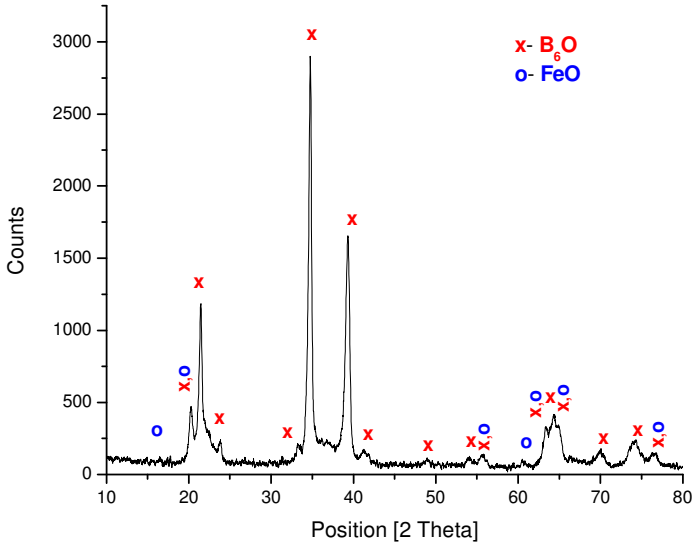

Fig B. 4*: XRD pattern of B_6O and iron oxide powder (00-050-1505, 01-089-0690)*

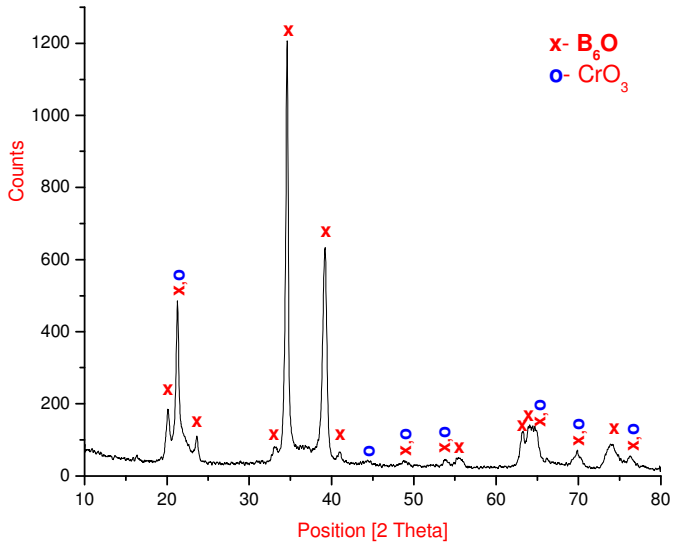

Fig B. 5*: XRD pattern of B_6O and chromium oxide powder (00-050-1505, 01-072-0634)*

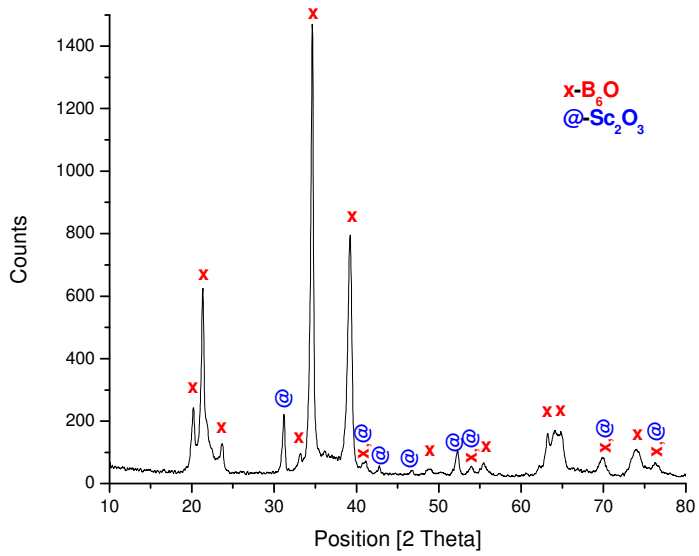

Fig B. 6*: XRD pattern of B_6O and scandium oxide powder (00-050-1505)*

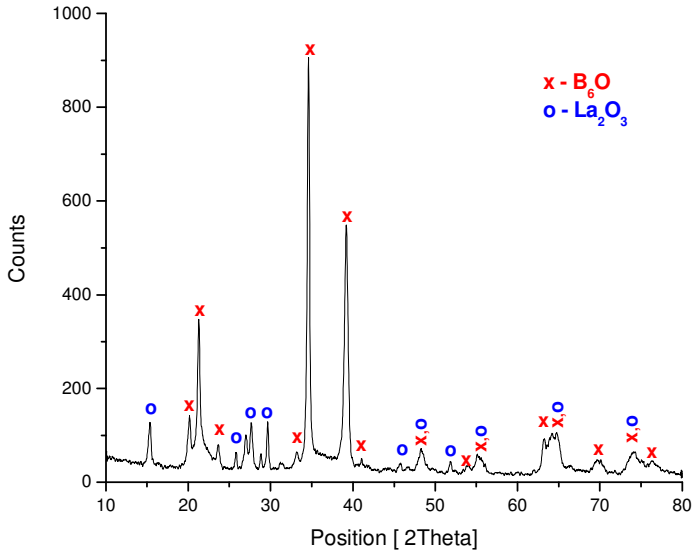

Fig B. 7*: XRD pattern of B_6O and lathanium oxide powder (00-050-1505, 01-065- 3185)*

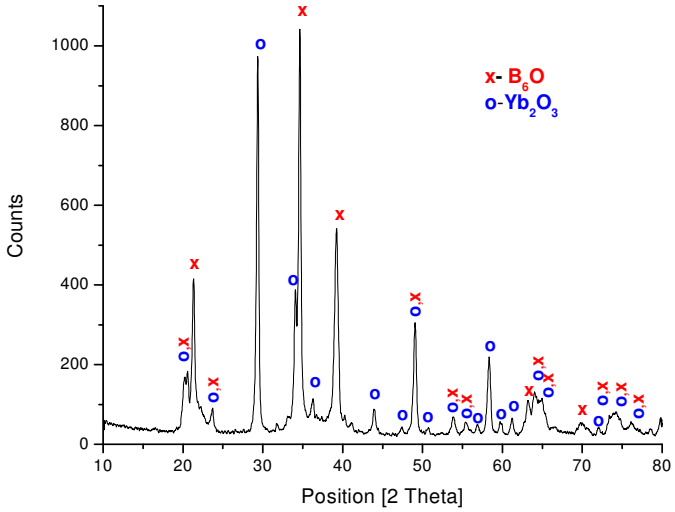

Fig B. 8*: XRD pattern of B_6O and Ytterbium oxide powder (00-050-1505, 01-077-0455)*

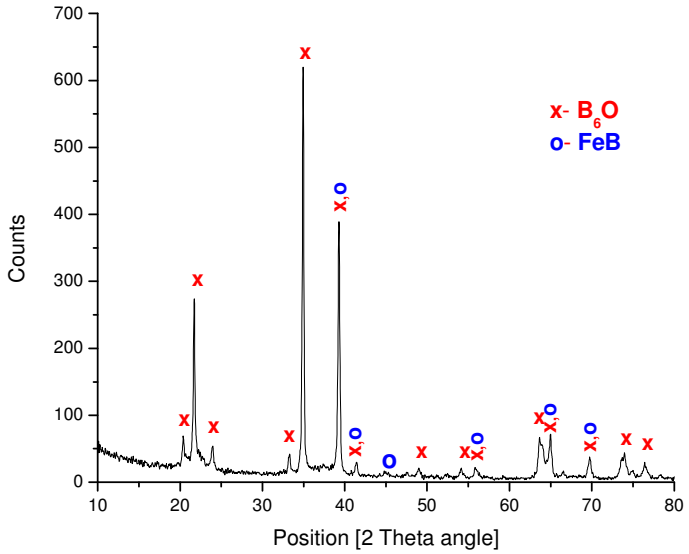

Fig B. 9*: XRD pattern of mixture of B_6O and iron boride powder (00-050-1505, 01-076-0092)*

Appendix C

SEM images

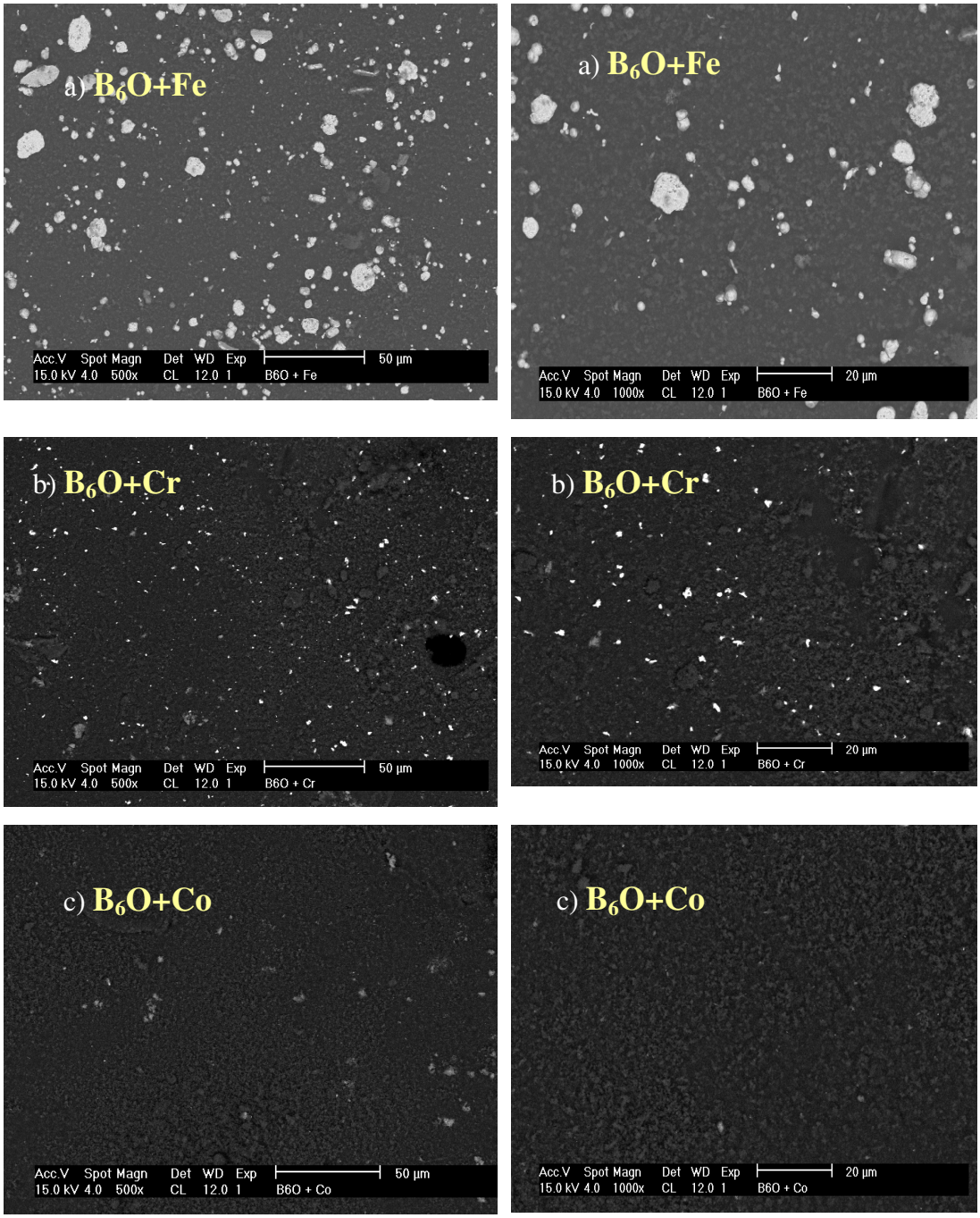

Fig C. 1*: SEM images of the mixed powder (a) B_6O + Fe (b) B_6O + Cr (c) B_6O + Co*

Optical images

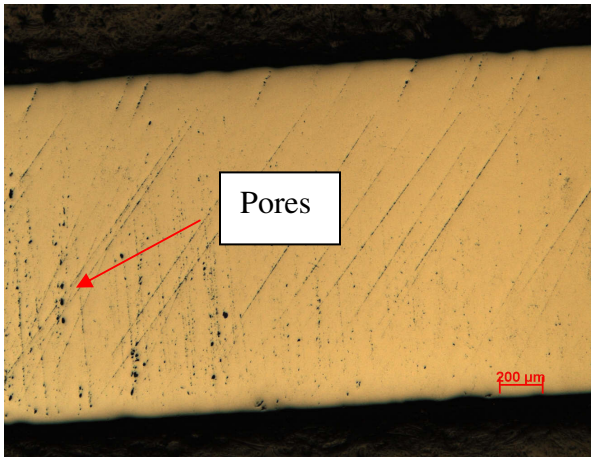

Fig C. 2*: Optical image showing pores at the edge of B_6O material*

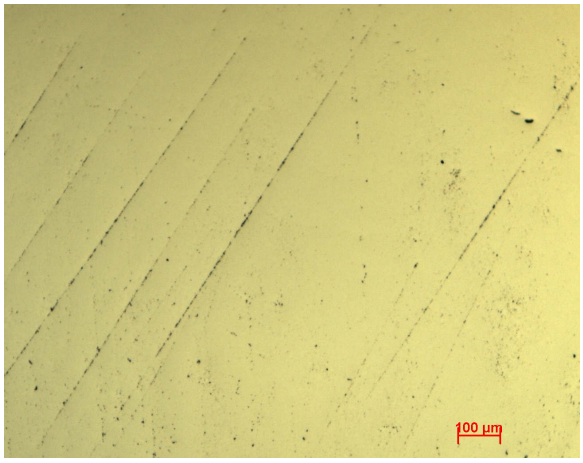

Fig C. 3*: Optical image showing pores at the centre of B_6O material*

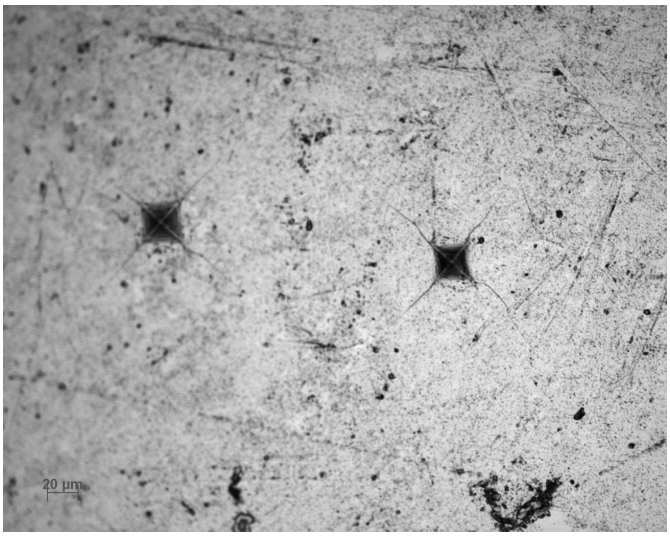

Fig C. 4*: Optical image showing the indentation on the* B_6O+ Sc_2O_3 *material*